UNIVERSITÀ DEGLI STUDI DI MILANO

PhD Course in Experimental Medicine (XXXIII cycle)
Curriculum: Neuroscience and Neuropathology
Department of Medical Biotechnology and Translational Medicine (BIOMETRA)

Epigenetic Homeostatic Mechanism in Neuronal Adaptation

and Metaplasticity to Environmental Stimuli

(BIO/13 – Applied Biology)

PhD thesis of:

Dr. Alessandra LONGARETTI

R12020

Tutor: Prof. Elena BATTAGLIOLI

Supervisor: Dr. Francesco RUSCONI

PhD Coordinator: Prof. Massimo LOCATI

A.A. 2019-2020

INDEX

1 INTRODUCTION

1.1 Focus on stress

1.1.1 What is stress?

For decades scientists tried to define stress. Some of them identified it with the stressor -imminent or perceived challenges to homeostasis-, others with the body's response to the stimulus -an innate, stereotypic, adaptive response to stressors that has evolved to restore the non-stressed homeostatic set point-, others with the neurobiological and psychological substrates between the two [1]. Indeed, defining stress is not an easy task since its effects on individuals depend on different parameters (the nature, intensity and duration of a stressor, the presence of a supporting environment and of efficient physiological coping mechanisms) and therefore stress response is highly subjective since something perceived as stressful by someone, could be neutral to someone else.

Our brain is the first and primary organ to be elicited when a stressful event takes place. It is responsible for the induction of the stress response and of the adaptation to stress thanks to its ability to sense the environment and undergo physiological changes at molecular levels, and subsequently of circuitry networks and macroscopic structures, in order to fit in an everchanging social and physical environment.

Physiologically, the sympathetic and parasympathetic systems, HPA axis, immune system, metabolic hormones and molecular processes within all organs promote adaptation via "allostasis", the reaching of a steady state via activation of these systems. However, the same mediators activated during a physiological stress response have biphasic effects and can promote pathophysiology when overused or when their activity is out of balance with each other causing an allostatic load or overload [2].

Considered all these data, we now know that there is no such a thing as a good stress or a bad stress *per se*. The best way to describe stress and stress response is to think about it as an inverted-U (Fig 1):
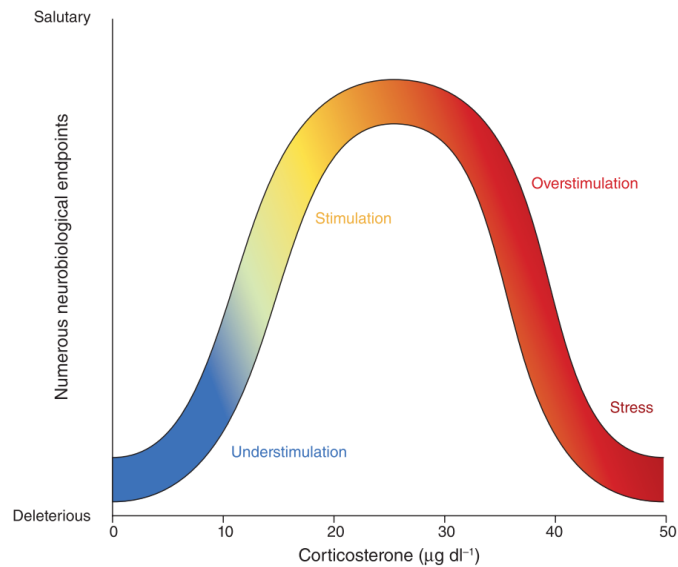
Figure 1. The inverted-U. Scheme representing the various effects of different levels of stimulation on neurobiological endpoints, correlated to the levels of corticosterone [adapted from 3].

Mild to tolerable stress (roughly corresponding to 10–20 µg dl^{-1} of corticosterone, the glucocorticoid of rodents) are considered as salutary inputs for the brain since they are transitory and benefit the brain by stimulating it (among them we can consider taking the driving license test or present a research at a workshop, for example). We are in the yellowish left rising side of the inverted U. In contrast, both the absence of stress (in blue), or a stress that is more severe and/or prolonged than that in the stimulatory range (in red), have detrimental long-lasting effects on our body [3]. It is now clear how perception and management of stress are highly subjective and variable.

1.1.2 Overview of the physiological stress response

The stress response is an innate and stereotypic, adaptive response to stressful stimuli that has evolved in order to restore the non-stressed homeostatic set point. This process comprises the contribution of specific neuroanatomical sites that activate a plethora of cognitive, behavioral and physiological phenomena. Stress mediators are the molecules released upon stress which bind to their receptors on specific neuronal populations resulting in downstream effects promoting stress response. There are many stress mediators, for examples neurotransmitters such as glutamate, noradrenaline and serotonin, peptides like the corticotropin-releasing hormone (CRH), and steroid hormones as corticosterone. The type of molecule and therefore the brain area engaged depends on the stressor. Hemorrhage, freezing or trauma activate the

5

brainstem and the hypothalamic region while exams, the loss of a beloved person and other psychological traumas engage the hippocampus, the prefrontal cortex (PFC) and the amygdala, brain regions that are related to learning, memory, emotional behavior and decision making. Classically stress response is characterized by two phases in which stress mediators act. The first is fast-acting and includes noradrenaline, serotonin, dopamine and CRH. This first wave of stress mediators promotes behaviors involved in facing a stressful condition such as vigilance, evaluation of the situation and decision making to optimally face the challenge. Since the increase, and therefore the actions of fast-acting mediators' levels are brief, this first wave of events is not optimal for provoking the sustained, adaptive components of a stress response, such as the memory consolidation of information associated with the stressor. This is instead fulfilled by other molecules, corticosteroids acting through glucocorticoid receptors, which alter gene expression and cell function, classically considered the second wave. Recent works suggest that this orchestrated stress response could be better described if pictured as a framework of three temporal domains characterized by distinct mechanisms of operation of the stress mediators (Fig 2). Receptor activation by neurotransmitters can, in addition to having rapid synaptic effects, regulate transcription factors within a seconds-to-minutes time frame.

A

B
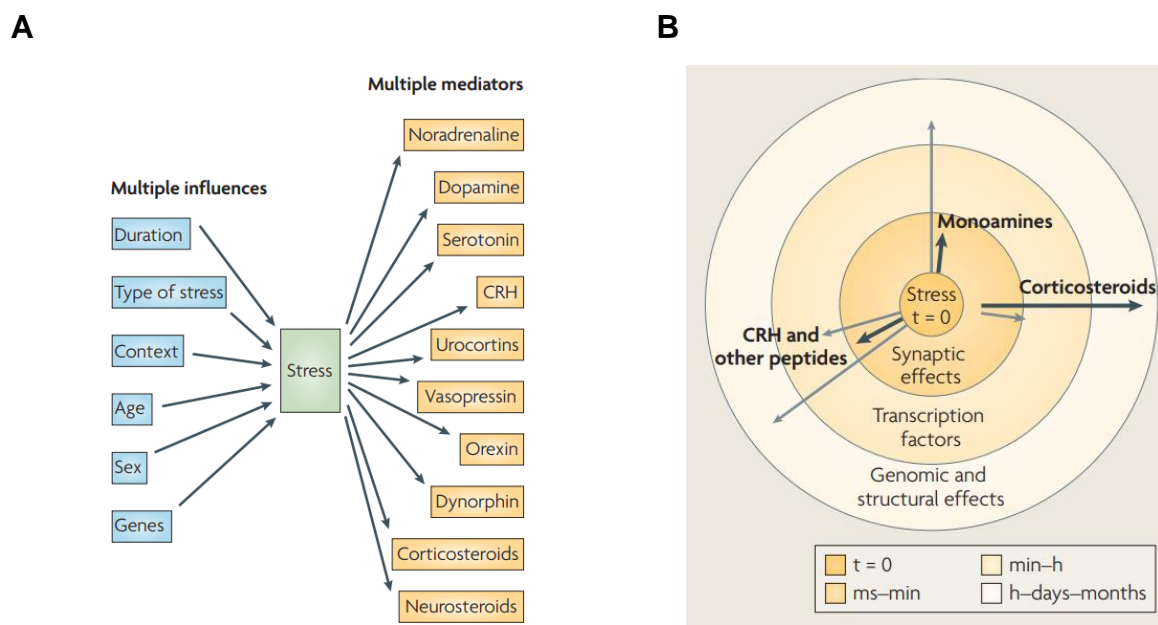
Figure 2. Stress response mediators. (A) Graphic scheme of the factors impacting stress response and stress response mediators. **(B)** Graphic scheme of the timing of stress mediators' effects [adapted from 4].

This rapid activation (or deactivation) of transcription factors support long-lasting genomic changes that help the organism to respond to stressors of different magnitudes and durations, as well as to recurrent stress. Conversely, corticosterone, through non-genomic pathways involving membrane-located mineralocorticoid receptors, can act within minutes [4].

The stress response is complex and different components take part to the process [1] (Fig 3):

1. Behavioral responses.

A) Establishment of a state of mild anxiety: stress induces the inhibition of the PFC, a brain area that exerts emotional and cognitive control over anxiety restraining the activation of the amygdala which on the contrary promotes anxiety.

B) Transient and adaptive modulations of attention and memory function: upon stress, attention shifts away from neutral stimuli towards the threat and this is due in part to a decrease in the activity of the ventrolateral PFC and to the cooperation of many other brain areas such as the anterior cingulate cortex, the dorsolateral PFC and the superior parietal cortex.

C) Anhedonia: the ability of a subject to experience pleasure is reduced upon stress, probably to lower the chances of distraction during stress response. Many brain areas are involved in reward and pleasure, among them there are the nucleus accumbens (NAc) and the ventral tegmental area (VTA). A decreased functionality of the PFC leads to anhedonia since VTA neurons do not increase dopamine release in the NAc.

2. Metabolic, hormonal and neurotransmitter-mediated responses.

CRH and activation of the HPA axis: the principal aim of CRH is the activation of the HPA axis, however this hormone has further roles during a physiological stress response. CRH can be found in the amygdala, the hypothalamus and in sympathetic nerve terminals. CRH directly promotes anxiety and fear-related behaviors. It activates the locus coeruleus to promote arousal and an improved signal-to-noise relationship among the components of the stress response. It activates the sympathomedullary system for the secretion of norepinephrine and epinephrine. At the same time, CRH promotes a negative modulation on the thyroid, gonadal and growth hormone axes to preserve calories to the immediate stressor response. In addition, CRH suppresses appetite and sleep. CRH released from sympathetic nerve terminals activates the innate immune response. CRH stimulation of the anterior lobe of the pituitary gland

leads to the secretion of ACTH which in turn promotes to synthesis of cortisol, glucocorticoids and mineralcorticoids. Cortisol activates the amygdala to promote anxiety, arousal and conditioned fear responses. Cortisol leads to an increase in cardiac contractility and the sensitivity of noradrenergic beta-receptors. By promoting mild, brief insulin resistance, cortisol helps glucose mobilization for the brain and other body sites. Cortisol also activates the renin–angiotensin and endothelin systems in case of possible loss of blood pressure secondary to blood loss. In addition to CRH acting centrally, cortisol directly downregulates the thyroid, gonadal and growth hormone axes in the periphery.

3. Promotion of neuronal integrity in face of extra demands.

A) Brain-derived neurotrophic factor (BDNF): BDNF is expressed in most of the Central Nervous System (CNS) and exerts a neurotrophic function through the activation of the TRKB receptor. In the adult brain, the main function of BDNF is to enhance synaptic transmission, facilitate synaptic plasticity and promote synaptic growth. This molecule is implicated in many stages of neural circuits development for example neurogenesis and neural stem cell survival and differentiation, axon/dendrite differentiation, growth and guidance of axons, synapse formation and maturation and refinement of developing circuits. A eustress, such as physical exercise, increases the activities of BDNF. Other positive experiences, such as early nurturing, also potentiate BDNF activity. On the other hand, chronic stress leads to a significant reduction of BDNF's positive effects on the CNS and produces, instead, potentiation of anxiety. Sustained stress decreases the hippocampal expression of BDNF, while it increases its expression in the amygdala where it promotes dendritic branching promoting anxiety.

B) The role of neuronal neuroplasticity during the normal stress response: the complexity of neuronal dendrites and the number of dendritic spines increase during mild controllable stress to promote new connections among neurons. Synaptogenesis provides the means for processing and including new information that can be used to make appropriate responses to a changing environment.

C) Neurogenesis: several stimuli are known to induce neurogenesis in the dentate gyrus, for example learning, an enriched environment, exercise, long-lasting antidepressants treatment. Acute, mild, controllable stress also induces neurogenesis in the dentate gyrus.

	AUTONOMIC NERVOUS SYSTEM		HYPOTHALAMIC – PITUITARY – ADRENAL AXIS	
	Mediators	**Effects**	**Mediators**	**Effects**
PRIMARY RESPONSE	SNS **Epinephrine Norepinephrine** ↓ Binding to peripheral adrenergic receptors	Promotion of *fight-or-flight* response: • **Metabolic function**: increased hepatic gluconeogenesis and glycogenolysis, increased glucose blood levels • **Cardiovascular function**: increased heart rate and stroke volume, enhanced blood flow in skeletal muscle and brain, constriction of vessels in viscera • **Respiratory function**: increased respiratory rate, dilatation of bronchioles; • **Digestive function**: inhibition of peristaltic movements and gastric secretion • **Sensory function**: pupils dilatation and ciliary muscles relaxation	Hypothalamus (PVN) **CRH** ↓ Pituitary gland **ACTH** ↓ Adrenal gland **Cortisol** (human) **Corticosterone** (rodent) *(Negative feedback)*	Promotion of *fight-or-flight* response: • **Metabolic function**: increased hepatic gluconeogenesis and glucose blood levels, lipolysis and protein degradation • **Cardiovascular function**: increased blood pressure, increased heart rate, increased cardiac output • **Immune function**: suppression of immune system and inflammation • **Reproductive function**: inhibition of reproductive physiology and behaviour • **CNS function**: enhanced memory consolidation, increased cognition, vigilance and focused attention, altered reward processing
SECONDARY RESPONSE	PSNS **Acetylcholine** ↓ Binding to peripheral muscarinic receptors	Promotion of *rest and digest* response: • **Cardiovascular function**: decreased heart rate, dilatation of blood vessels leading to GI tract • **Respiratory function**: decreased respiratory rate, constriction of bronchioles • **Digestive function**: increased peristalsis and secretion by digestive glands • **Sensory function**: pupils constriction and ciliary muscles contraction	Binding to peripheral and central GRs and MRs (*fight-or-flight response*)	*Negative feedback* mechanism: • **Suppression** of the ACTH secretion from the pituitary gland via cortisol/corticosterone actions • **Suppression** of spontaneous glutamate transmission in the hypothalamus via activation of the ECS due to the engagement of membrane-associated GRs • **Alterations** in intrinsic excitability, long-term synaptic plasticity, and neuropeptide synthesis due to activation of cytosolic GRs in hypothalamic neurons

Figure 3. The stress response. Scheme resuming the primary and the secondary stress responses of the autonomic nervous system and in the HPA axis. SNS= Sympathetic nervous system; PSN = Parasympathetic nervous system; PVN= Paraventricular nucleus; CRH= Corticotropin releasing hormone; ACTH= Adrenocorticotropic hormone; GRs= Glucocorticoid receptors; MRs= Mineralocorticoid receptors [adapted from 5].

1.1.3 Overview of the glutamatergic synapse

Excitatory neuronal transmission, predominantly mediated by glutamate, plays a pivotal role in synaptic transmission and neuroplastic processes such as learning and memory. Postsynaptic AMPA receptors are among the first complexes that are engaged upon neurotransmitter release. These receptors are heteromeric tetramers composed by the combinations of GluA1, GluA2, GluA3 and GluA4 subunits. In the adult brain, AMPA receptors are composed mainly of GluA1/GluA2 and GluA2/GluA3 heteromers. Being involved in cognitive processes, AMPA receptors play a major role in synaptic plasticity paradigms such as long-term potentiation (LTP) and long-term depression (LTD). LTP induces AMPA receptors exocytosis, predominantly from endosomal compartments, but also through a process of lateral diffusion of AMPA receptors on the head of the dendritic spine. After exocytosis, receptors diffuse and accumulate at postsynaptic density compartments from extra-synaptic, peri-synaptic sites or near the spines. This process is also necessary to enlarge and stabilize the size of dendritic spines (Fig 4).
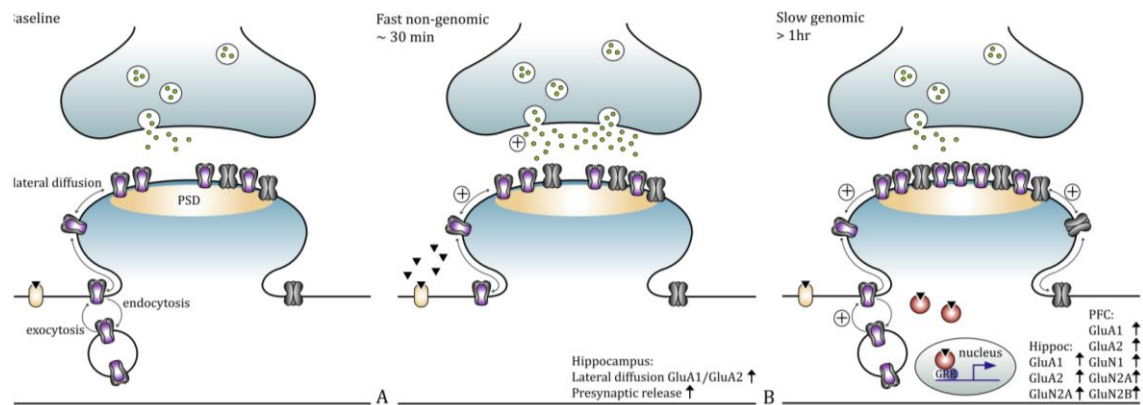
Figure 4. Graphic timeline of the events that lead to AMPAr insertion. Upon excitatory stimulation fast non-genomic events (~30 min) take place such as lateral diffusion of AMPAr at the post synaptic density. Then slow genomic effects (>1h) increase AMPAr levels via de-novo synthesis [adapted from 6].

Another receptor which is fundamental in synaptic plasticity is the ionotropic NMDA receptor. The NMDA receptor is in form of heterotetramer with two GluN1 and two GluN2 subunits; two obligatory GluN1 subunits and two GluN2 (GluN2A and/ or GluN2B) subunits. NMDA receptors are coincident detectors, this means that for them to be activated they require both presynaptic glutamate release and postsynaptic depolarization. NMDA receptors are permeable to Na^+ and Ca^{2+}. The permeability of NMDA receptors to this bivalent cation is mainly modulated by the expression of GluN2A and GluN2B subunits. Whereas GluN2B is predominantly expressed in the developing brain, the number of GluN2A subunits grows along with aging, becoming the preponderant subunit in the adult brain. Being a second messenger, calcium influx in postsynaptic cells via NMDA receptors activates downstream pathways, mainly thought the interaction with several kinases which are crucial for establishing synaptic plasticity [6].

Glutamatergic neurotransmission occurs predominantly within the confines of a tripartite synapse (Fig 5). Several molecular mechanisms within the synapse — including basal and stimulated presynaptic glutamate release, postsynaptic receptor trafficking and function, and transporter-mediated uptake and recycling of glutamate through the glutamate–glutamine cycle — are sensitive to regulation by stress and glucocorticoids. Here a very brief overview of such pivotal physiological processes: glutamate can be either synthesized de novo from glucose in astrocytes in a process that involves the Krebs cycle and the transamination or reductive amination of α-oxoglutarate, or it can be recycled through the glutamate–glutamine cycle. Once

glutamate is loaded in synaptic vesicles, the SNARE presynaptic complex oversees neurotransmitter release. This machinery is formed by the interaction of two synaptic membrane proteins (syntaxin 1 or syntaxin 2 and SNAP25) and a vesicular protein (synaptobrevin 1 or synaptobrevin 2), together they mediate the fusion of synaptic vesicles with the presynaptic membrane [7].
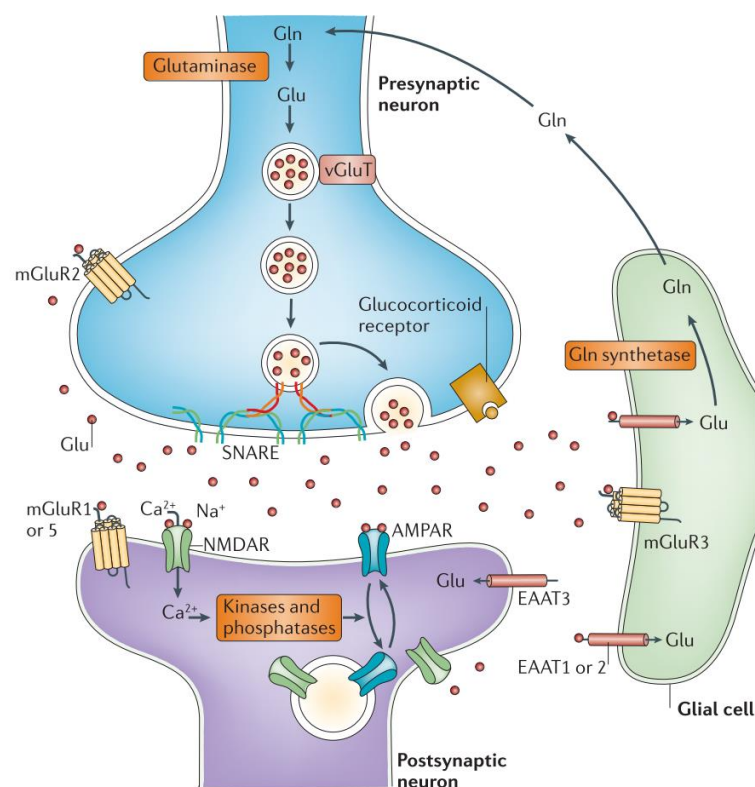
Figure 5. The tripartite synapse. Graphic representation of the tripartite synapse. The presynaptic terminal is shown in blue, the postsynaptic neuron in purple and the glial cell in green. Some pivotal mechanisms are displayed such as glutamate synthesis, vesicles release and glutamate receptor endo- exo- cytosis [adapted from 7]

The number and stability of ionotropic glutamate-activated receptors at the synaptic membrane is an important factor in determining excitatory synaptic efficacy.

Many are the mechanisms that have been proposed to control the surface expression of NMDARs and AMPARs. They include PDZ domain-mediated interactions between channel subunits and synaptic scaffolding proteins, clathrin-dependent endocytosis regulated by phosphorylation, and motor protein-based transport along microtubule or actin cytoskeletons.

Concerning glutamate clearance from the extracellular space is due to the action of high-affinity excitatory amino acid transporters (EAATs), which are located on glial cells (EAAT1 and EAAT2) and, in few amounts, on neurons (EAAT3 and EAAT4). Since the

synapse lacks degradative enzymes, uptake by EAATs is the primary mechanism through which the action of extracellular glutamate is terminated [7].

1.1.4 The effect of stress on the glutamatergic synapse

Glucocorticoids are normally secreted during the diurnal rhythm and upon stress and they affect the basal release of glutamate in several limbic and cortical areas, including the hippocampus, amygdala and PFC. Numerous animal studies suggest that exposure to acute stress or administration of glucocorticoids rapidly increases glutamate release in these brain areas. For example, tail-pinch, forced-swim or restraint stress induce a marked, transient increase of extracellular glutamate levels in rat PFC (Fig 6). In different studies using patch-clamp recordings, application of 100 nM corticosterone to murine hippocampal slices rapidly enhanced the frequency of miniature excitatory postsynaptic potentials (mEPSPs) in CA1 pyramidal neurons and reduced paired-pulse facilitation (PPF which is a form of synaptic facilitation that reflects presynaptic release). Moreover, it has been observed that the acute footshock behavioral test, which entails a strong stress that induces learned helplessness, produces a marked, rapid change in the depolarization-evoked release of glutamate in rats. Authors showed that the increased glutamate release in the PFC and frontal cortex was dependent on glucocorticoid receptor activation [7].
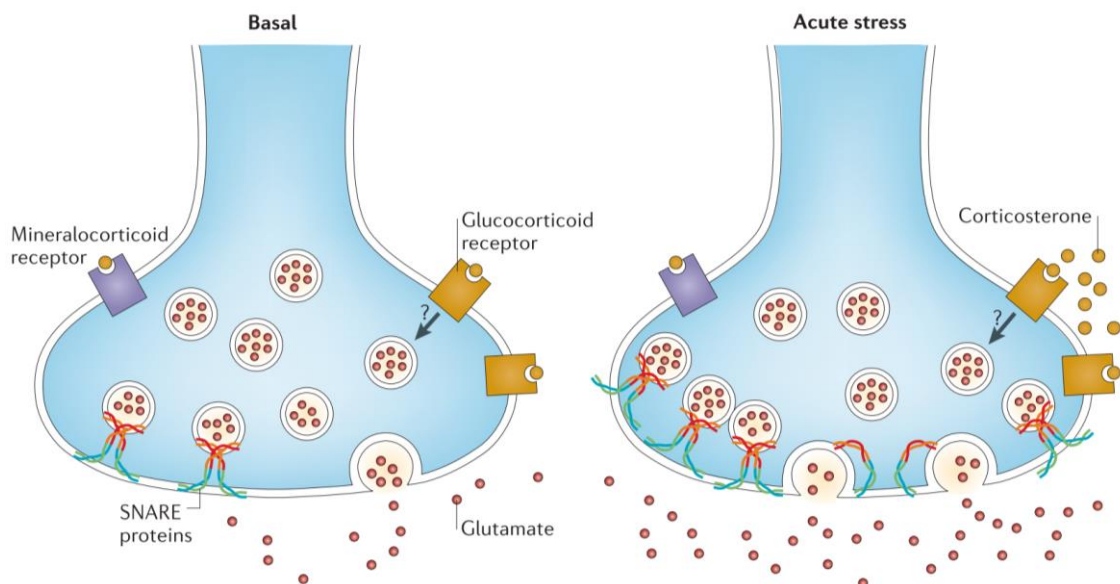
Figure 6. Glutamate release is enhanced upon acute stress. Graphic representation of a glutamatergic presynaptic terminal in basal condition (on the left), and upon acute stress (on the right). Corticosterone binding leads to the fusion of neurotransmitter-filled vesicles and therefore of glutamate release in the synaptic cleft [adapted from 7].

In principle, the enhanced stimulus-evoked release of glutamate induced by acute stress may be achieved through two events: increasing the number of synaptic vesicles in the readily releasable pool (RRP)— or by increasing the probability of release of synaptic vesicles, or both. At the level of presynaptic terminal, footshock stress is able to increase the number of SNARE complexes bound to the presynaptic membrane from PFC neurons, suggesting the implication of least this first mechanism.

There are not many studies that investigate the effects of chronic stress on glutamate release. It has been shown that three repeated tail-pinch stressors (at 2.5-hour intervals) in rats produce transient glutamate effluxes in the hippocampus that remain constant in duration and magnitude, whereas in the PFC they decrease upon subsequent applications. These results suggest a selective adaptation of glutamate release to stress in the PFC. A different study tested the response to an acute stressor in rats subjected to 21-day chronic restraint stress. After a subsequent single stress challenge, extracellular glutamate levels in CA3 remained high in chronically stressed rats compared to naive rats that were subjected to the same acute stressor, suggesting an altered regulation of the termination of glutamate release after chronic exposure to stressful stimuli [7].

Glutamate transmission induces different effects according the brain area, for example, acute stress or corticosterone treatments increase AMPAR and NMDAR responses in a similar way in the PFC, but specifically enhances AMPAR-mediated currents in CA1 neurons, midbrain dopaminergic neurons and NAc shell neurons. As stated, electrophysiological experiments showed that both NMDAR- and AMPAR-mediated synaptic currents are markedly increased in PFC pyramidal neurons in many models of acute stress. This effect becomes visible >1 hour after stress and lasts for 24 hours after the cease of the stress. Interestingly this is mimicked by short-term corticosterone treatment in vitro. The described enhanced basal glutamatergic transmission is due to an increased surface expression of NMDARs and AMPARs at the postsynaptic compartment. The delay in the increment of basal PFC glutamate transmission induced by acute stress or corticosterone treatment is due to the fact that this process is mediated by intracellular glucocorticoid receptors. On the contrary, in the CA1 area of hippocampus the increase of glutamate release occurs faster since it is mediated by membrane-bound mineralocorticoid receptors [7].

In contextual learning paradigms, there is an increase in the number of GluA1 and GluA2 subunits in hippocampal synapses, suggesting that these kinds of tasks are

accompanied by changes in AMPA receptor trafficking. Moreover 24 h after fear conditioning, newly synthesized AMPA receptors are recruited in a selective manner to mushroom-type spines in adult neurons of the CA1 area of the hippocampus. Experiments employing GluA1 deficient mice revealed that the lack of this AMPAr subunit leads to impaired short-term memory processes. Furthermore, GluA2 deficient mice show alterations in a spatial working memory task and elevated Y-maze. Another evidence also confirms GluA1-containing AMPA receptors critical role in the memory formation of emotionally arousing events, since the prevention of the synaptic insertion of GluA1-containing AMPA receptors in the amygdala hampers tone-cue as well as contextual fear conditioning [6].

Since AMPA and NMDA receptors are involved in synaptic plasticity, in the hippocampus and PFC, stress elicits changes in the capability to potentiate or depress the efficacy of glutamate transmission. Acute stress suppresses LTP in the amygdala–PFC pathway, in parallel with the inhibition of hippocampal LTP. Concerning LTD, acute stress enhances mGluR-dependent LTD in the hippocampus but prevents serotonin-facilitated LTD induction in the PFC.

In the hippocampus, LTP induction is hampered after a prolonged period of mild stress or chronic corticosteroid exposure. Actually, it has been observed that long-lasting stress and elevated corticosteroid hormone levels lead to a reduction in the surface expression of glutamate receptors (GluN1 and GluA1). These effects are probably due to an enhanced ubiquitin/proteasome-mediated degradation and loss of synaptic NMDA receptors and AMPA receptors (Fig 7). In addition to increased corticosteroid hormone levels, also CRH is known to mediate the negative effects of prolonged stress on hippocampal function.

At a functional level, LTP in the thalamus–PFC pathway and LTP in the hippocampus–PFC connection is altered in chronic stress, and these effects are associated with the disruption of PFC-dependent tasks, such as working memory and behavioral flexibility that are observed in mice chronically stressed.

Considering these evidences, the disruption of excitatory synaptic transmission after exposure to chronic stress has been implicated in impaired learning and memory and disruption of excitatory synaptic transmission and plasticity [6].
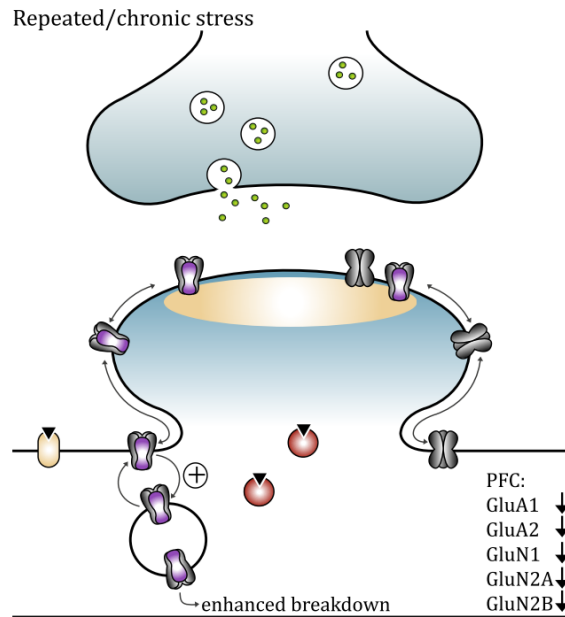
Figure 7. The effect of chronic stress on the glutamatergic synapse. Upon chronic stress, the levels of glutamate receptors on the surface of the post synaptic neurons decrease probably due to an enhanced lateral diffusion and degradation [adapted from 6].

1.1.5 Detrimental effects of stress on the hippocampus, PFC and amygdala lead to the onset of neuropsychiatric disorders

Neuropsychiatric disorders are common and disabling multifactorial illnesses that cause a strong deterioration of life quality. Since 10 to 20% of the general population suffers from these pathologies, including depressive diseases, all forms of anxiety, post-traumatic disorders, schizophrenia, eating disorders, addiction, and autism, they are a widely spread plague for the affected individuals, their beloved ones and society [5].

It is now widely recognized that severe stress exposure is linked to the onset of psychiatric disorders, impairing cognitive function and enhancing emotionality. Many studies employing clinical and neuroimaging data have shown that three brain areas involved in learning and memory—the hippocampus, amygdala and prefrontal cortex— are differentially altered at a structural and functional level in individuals with stress-related disorders (Fig 8) [8].
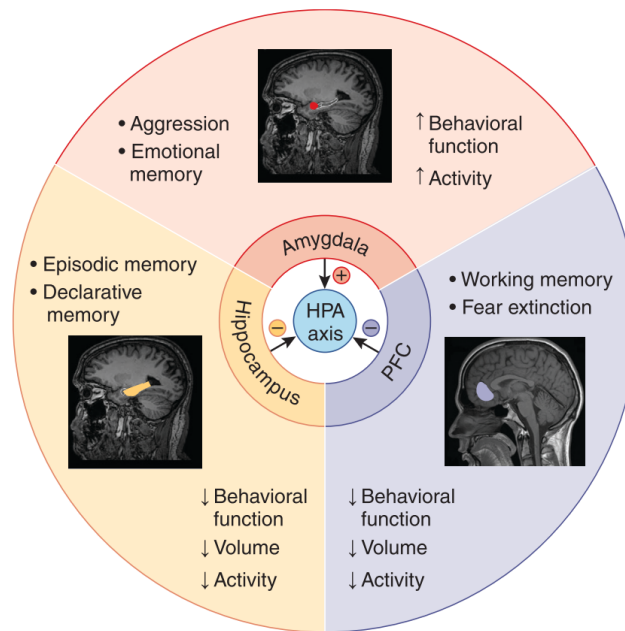
Figure 8. Hippocampus, amygdala and PFC upon stress. Strong or chronic stress induces structural and functional alterations in the hippocampus, amygdala and PFC, impacting higher cognitive functions such as memory and emotional behavior [adapted from 8].
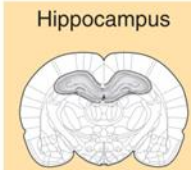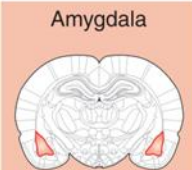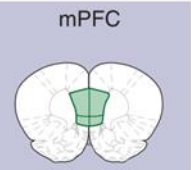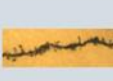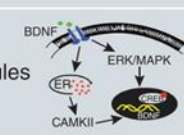
The hippocampus is a brain area located in the medial temporal lobe and is responsible for the formation of stable declarative memory in higher primates, and spatial memory in rodents. This structure is strongly influenced by stress hormones, since it has one of the highest concentrations of receptors for corticosteroids in the mammalian brain. The hippocampus takes part in the important function of terminating the stress response through glucocorticoid-mediated negative feedback that inhibits the HPA axis [9].

Many studies shown how chronic stress has a negative impact on synaptic plasticity. Data show how it leads to the shrinkage of dendrites of hippocampal CA3 and dentate gyrus neurons as well as loss of spines in CA1 neurons. Shorter apical dendrites of CA1 neurons were found in adult rat after chronic neonatal bedding stress. Another evidence is the induction of strong memory defects assessed with NOR in animals that experienced multimodal stress (light, noise, restrain, manipulations). The researchers who conducted these experiments found that CA3 hippocampal synapses were reduced upon this paradigm, together with a decrease in synapse number in the dorsal CA1 region. Another group perform a chronic paradigm of stress, 10 days of immobilization stress, showing that dendrites of short-shaft pyramidal neurons retracts in the CA3 area, together with dendrites of dorsal CA1 pyramidal neurons [10].

Interestingly, in KO mice for NMDAr in CA3 neurons, this chronic stress did not induce any alteration in the considered neurons (Fig 9) [11].

The prefrontal cortex is a brain area involved in cognition and fear extinction that, upon stress, exerts a similar negative feedback function on the HPA axis and stress response. It has been observed that repeated restrain stress or chronic corticosterone injections lead to a reduction in the length of dendrites and to the simplification of their branching in layer II/III pyramidal neurons [11]. Interestingly these modifications are reversible after the cease of the stress in young animals [12,13,14,15] but this process is not as efficient in older and elderly models [16]. Moreover, it has been observed that the distal dendrites undergo the shrinkage but the ones that grow back are the proximal [17]. This seems to suggest that these neurons are different after stress and that probably they display altered connectivity and gene expression [18]. Together with dendrites remodeling, there is also a reduction is spine density on these neurons after 21 days of restrain stress (Fig 9) [8].

The amygdala instead plays its central role in fear and anxiety. Studies performed on chronically immobilized animals (2 hrs/die for 10 days) show that principal neurons in the basolateral complex of the amygdala (BLA) display a more complex dendritic arborization in response chronic stress. Interestingly after 21 days of recovery, animals exposed to chronic stress continue to exhibit enhanced anxiety, in contrast to what happens in the hippocampus and PFC [19]. Concerning spine density, authors observed that acute immobilization stress fails to increase spine density or dendritic arborization a day later, but the same 2-hour stress is able to gradually rise spine density 10 days later, without affecting the dendritic arbors. Concomitantly to the structural changes, animals develop and increase anxiety behaviors [20]. Importantly this model, able to cause a delayed anxiety and formation of dendritic spines in the BLA, has been used to study PTSD (Fig 9).

	Hippocampus	Amygdala	mPFC
Behavior	↓ Spatial memory ↓ Spatial navigation	↑ Fear memory ↑ Anxiety	↓ Working memory ↓ Fear extinction
Networks	↓ Auditory-evoked potential ↓ Place cell	↑ Auditory-evoked potential	?
Neurons	↓ Dendrites	↑ Dendrites	↓ Dendrites
Synapses	↓ Spines ↓ LTP ↑ LTD	↑ Spines ↑ LTP	↓ Spines ↓ LTP
Molecules	↓ BDNF	↑ BDNF	?

Figure 9. Molecular, cellular, circuitry and behavioral alterations in hippocampus, amygdala and PFC upon chronic stress. Repeated stressors lead to functional and structural changes in several brain areas, impacting long-term memory formation, fear extinction and anxiety arousal [adapted from 8].

1.2 A nuclear mechanism to buffer stress response: Lysine-specific Demethylase 1 isoforms

1.2.1 Lysine-specific Demethylase 1 (LSD1)

In 2004 Shi and colleagues showed that the protein KIAA0601, conserved from the yeast Saccharomyces Pombe to humans, is a highly specific flavin dependent demethylase that acts on the lysine 4 of histone H3 when this is mono- or di-methylated. For this reason, they name it Lysine-specific Demethylase 1 (LSD1) [21]. LSD1 human gene maps on the short arm of chromosome 1 (1p36.12) and encodes for a protein of 852 aminoacids (aa) that weights 116kDa. It is composed of three main domains: the SWIRM domain, usually present in many chromatin remodeling proteins and involved in the interaction with other molecules, the Amine Oxidative (AOD) domain and the Tower domain (Fig 10). LSD1 C-terminal is able to bind CoREST, which is a known transcriptional corepressor, via the association between two α-helix of the Tower domain and a helix of CoREST, generating a helix coil. At the AOD domain instead, in proximity to flavin, there is the catalytic pocket of LSD1, in which the N-terminal of the histone H3 (residues 1 to 16) binds [22].
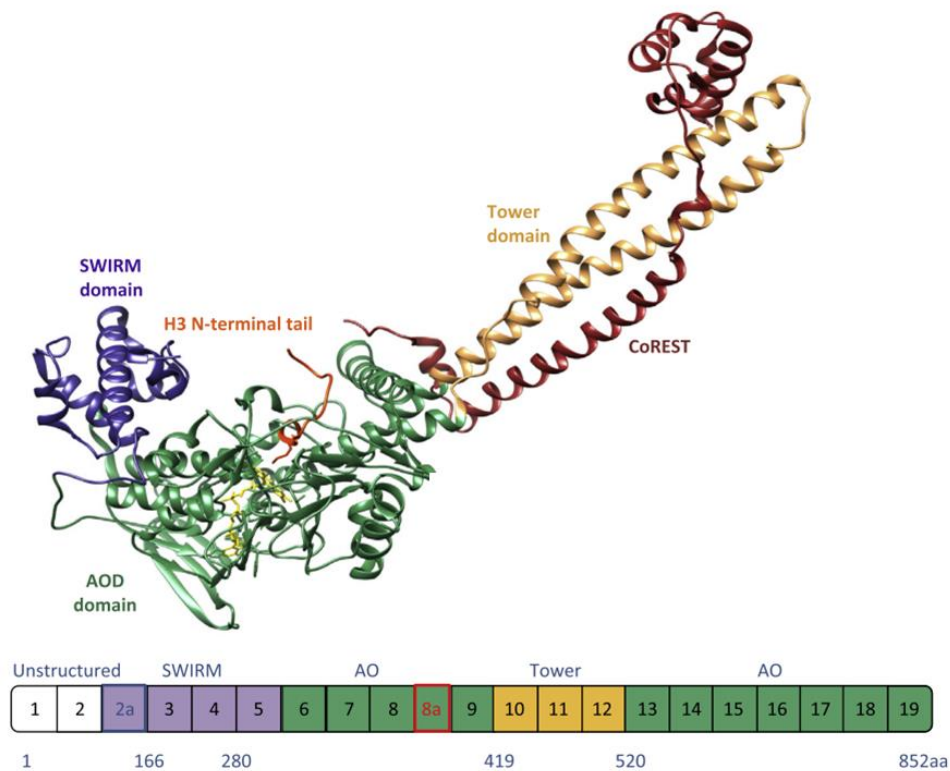
Figure 10. LSD1 crystal and schematic structures. Upper panel, LSD1 crystal structure: SWIRM domain is indicated in purple, the AO domain in green and the Tower domain in yellow. CoREST and the H3 N-terminal tail are in red. **Lower panel,** schematic structure of LSD1 showing the exons composing each domain. Aa are indicated [adapted from 23]

The enzymatic reaction orchestrated by LSD1 occurs in 2 main steps (Fig 11): firstly the histone tail interacts with the enzyme and the methylated lysine is oxidized by FAD, then the imine intermediate product is hydrolyzed generating formaldehyde (HCHO) and the demethylated aa [24].
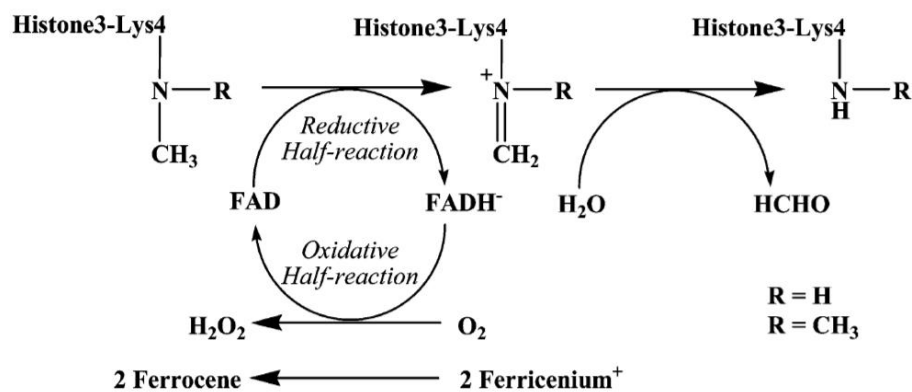
Figure 11. LSD1-mediated enzymatic reaction. The histone 3 tail interacts with the enzyme and the methylated lysine is oxidized by FAD, then the imine intermediate product is hydrolyzed generating formaldehyde (HCHO) and the demethylated lysine 4 [adapted from 24].

Forneris et al. also shown that for the reaction to take place the interaction of at least 21 aa of the histone tail is required and that the acetylation of lysine (K) 9 and the phosphorylation of serine 10 must be removed since they prevent the enzyme-substrate interaction. This last peculiarity is really interesting since it highlights how LSD1 is an epigenetic enzyme able to read the histone code [25]. Due to these constrains, LSD1 does not act alone but it functions in concert with CoREST and HDAC 1 and 2. Since the ultimate outcome of this enzyme is to remove a histone mark of active transcription (H3K4 me1/me2), LSD1 can be considered as a transcriptional corepressor [26]. The transcription factor that gives LSD1 complex the target gene specificity is the Serum Response Factor (SRF), which binds to Serum Response Factor Elements (SRE) on the DNA sequences of a plasticity-related class of genes, the Immediate Early Genes (IEGs), such as Egr1, c-fos, Npas4 and Nr4a1(Fig 12) [27].
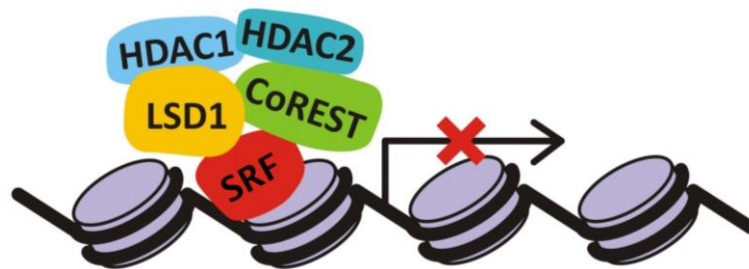
Figure 12. LSD1 corepressor complex. Graphic representation of LSD1 transcriptional corepressor complex: histones, the transcription factor SRF, LSD1, CoREST and HDAC 1 and 2.

1.2.2 NeuroLSD1, a neuronal-specific splicing isoform of LSD1

The annotated LSD1 human gene encodes for a 19-exon-long mRNA. However, the study of the conservation of the sequence between different species allowed the identification of two more exons subjected to alternative splicing, one between introns 2 and 3 and one between introns 8 and 9. The first one is referred to as E2a, and the second as E8a. Exon E2a is long 60 base pairs (bp) while exon E8a is only 12 bp, giving rise to a microexon (Fig 13A) [28]. These 12 nucleotides encode for a tetrapeptide (Asp-Thr-Val-Lys, DTVK) that can be phosphorylated on the second residue [29]. These two alternative exons can be singularly or concomitantly included in mature transcripts and their presence does not alter the reading frame, generating functional proteins. Interestingly E8a-containing isoforms (LSD1 E2a+E8a and LSD1

E8a) are expressed only in neurons and testis, this is why E8a isoforms are named neuroLSD1, while all the other isoforms (LSD1 and LSD1+E2a) are ubiquitous (Fig 13B). Furthermore, microexon E8a can be found only in mammals [28]
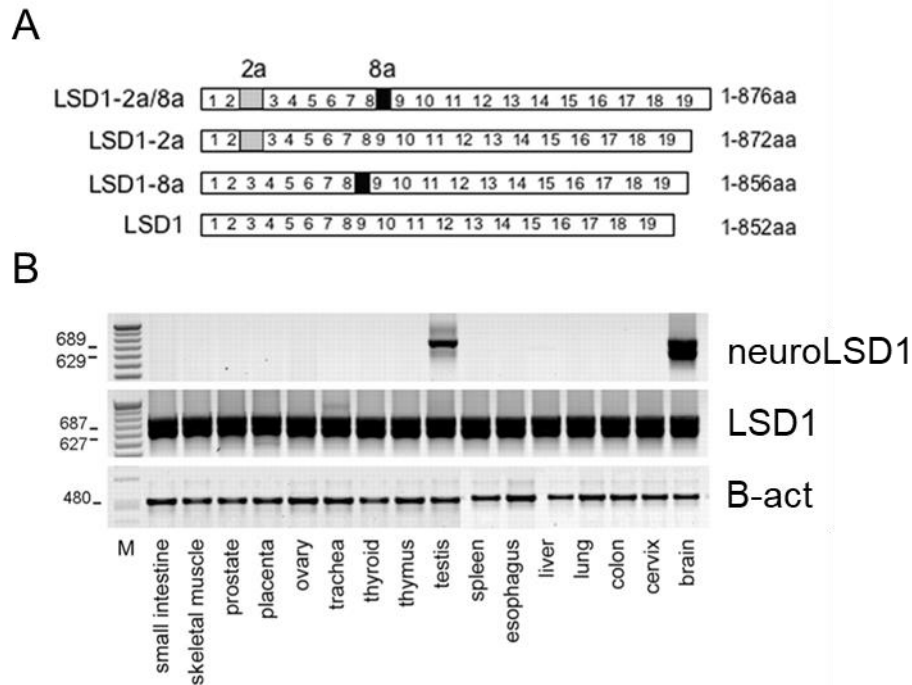
Figure 13. LSD1 isoforms and expression. (A) Scheme of all the possible LSD1 isoforms: LSD1, LSD1-E8a, LSD1-E2a and LSD1-E2a+E8a. **(B)** Expression of LSD1 isoforms transcripts in a panel of human tissues, normalized over β-actin. NeuroLSD1 isoforms are present only in the brain and in the testis [adapted from 28].

From a functional point of view, neuroLSD1 isoforms can be considered as dominant negative of LSD1 since they cannot exert the co-repressor function, lacking the demethylase activity. This is due to the fact that the threonine residue can be phosphorylated, preventing the binding of the other corepressors, including HDAC 1 and 2, which catalyze a necessary step for the demethylase reaction [29]. Moreover, it has been observed that neuroLSD1 expression is developmentally regulated both in vitro and in vivo, something that does not happen for the ubiquitous isoforms. Interestingly, the peak of the expression of neuroLSD1 is between the postnatal day 1 (P1) and P7, a very well-known window of increased neuroplasticity (Fig 14) [28].
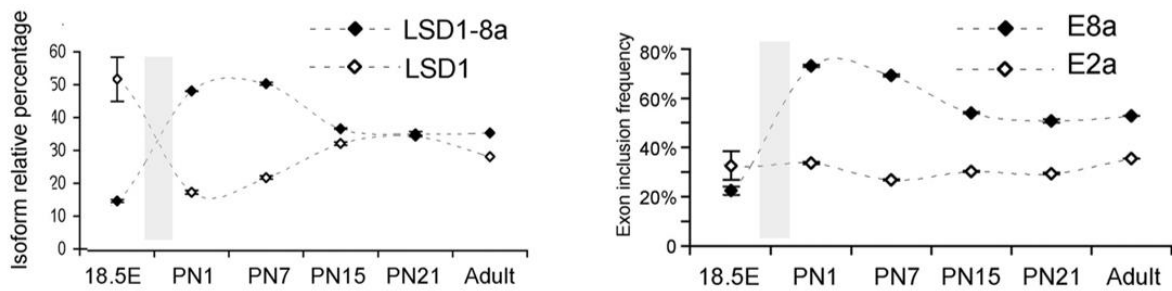
Figure 14. LSD1 isoforms expression during the development. On the left, LSD1 and neuroLSD1 relative percentage follows opposite trends along mice development. **On the right,** LSD1 isoforms expression is steady along with aging while neuroLSD1 isoforms increase in the perinatal window and then decrease and stabilize their levels [adapted from 28]

Further characterization studies led to the identification of regulatory elements of LSD1 isoforms alternative splicing. Two splicing factors have been identified, nSR100, which gives the neuronal expression specificity, and NOVA1, a factor whose levels are influenced by excitatory stimuli, that quantitatively modifies LSD1 splicing.

Besides these in trans regulatory elements, an in cis palindromic sequence has been found 300 bp downstream E8a which exerts a negative role in the micro exon inclusion in mature transcripts. This sequence is a complementary reverse of E8a therefore, binding the microexon, it prevents the formation of neuroLSD1 (Fig 15) [30].
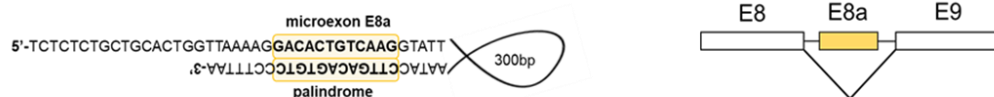
**Figure 15. Mechanism of action of the palindromic sequence.** The palindrome is an in cis negative regulatory element that acts preventing the formation of neuroLSD1 via the binding to E8a since its sequence is a complementary reverse of the microexon. This folding induces exon skipping [adapted from 31].

1.2.3 Molecular processes involving LSD1 and neuroLSD1

LSD1 has been implicated in many processes since it has been described as a co-activator when in complex with androgen and estrogen receptors [23], a pivotal regulator of the oncogenic potential of leukemic cells [32], and it has a role in cellular lineage determination and differentiation [33].

NeuroLSD1 isoforms take part in different cellular processes such as neuronal differentiation and morphogenesis. It has been shown that knocking down neurospecific isoforms in rat cortical neurons neurites fail to mature, while their overexpression lead to an increase in their maturation [28]. Moreover, it has been observed how neuroLSD1, in collaboration with Supervillin, demethylates H3K9me2 and that, when this complex is absent, neuronal differentiation is compromised [34]. But neuroLSD1 is also involved in complex molecular events such as memory formation [35], emotional behavior [36] and neuronal excitability [30]. MG Rosenfeld and colleagues demonstrated that neuroLSD1 has a role in long-term memory formation. In cultured cortical primary neurons derived from their neuroLSD1 constitutive knock out mouse model they observed an impaired activity-dependent transcription of many IEGs (Arc, Btg2, Cyr61, Npas4) upon KCl treatment (Fig 16A). This transcriptional impairment has a behavioral readout, indeed neuroLSD1^{-/-} mice display significant memory defects in the Barnes maze and in the Novel Object Recognition tests (Fig 16B) [35].
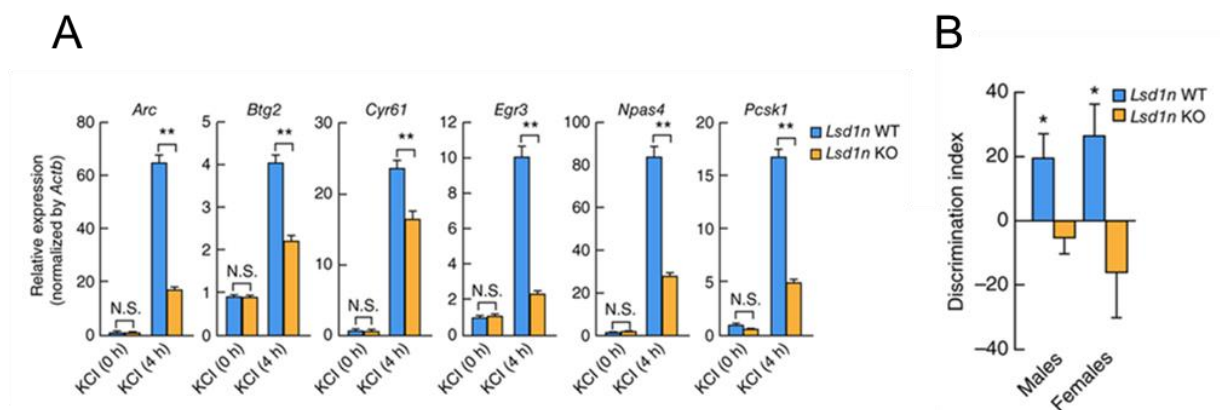
Figure 16. Lack of neuroLSD1 impairs activity-dep gene transcription and memory formation. (A) KCl-induced IEGs transactivation in wild-type (blue) and neuroLSD1^{-/-} (blue) cortical neurons. **(B)** Discrimination index of a NOR test showing a long-term memory impairment in neuroLSD1^{-/-} mice [adapted from 35].

Other studies, performed in the laboratory of Prof. Battaglioli on a neuroLSD1^{-/-} mouse model in which only the 12 nucleotides of microexon E8a have been removed, allowed to uncover another altered plasticity-related phonotype. This mouse model indeed displays a reduced anxiety measured with the Elevated Plus maze, the Marble Burying test and the Novelty Suppressed Feeding test (Fig 17). These data suggest that neuroLSD1 is implicated in shaping a correct emotional behavior [36].
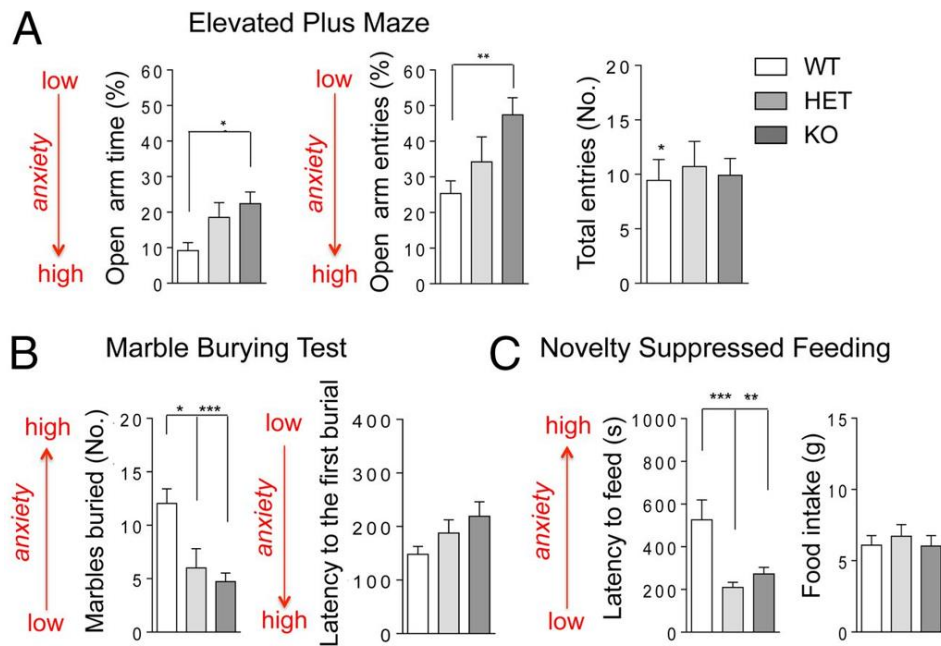
Figure 17. NeuroLSD1^{-/-} mice display reduced anxiety. **(A)** Elevated Plus Maze showing open arm time, open arm entries and total entries of WT, neuroLSD1 HET and KO mice. **(B)** Marble Burying Test showing buried marbles and latency to first burial in WT, neuroLSD1 HET and KO mice. **(C)** Novelty Suppressed Feeding showing latency to feed and food intake of WT, neuroLSD1 HET and KO mice [adapted from 36].

Concerning neuronal excitability, it has been observed that neuroLSD1^{-/-} mice display a higher excitability threshold upon the injection of the chemoconvulsant drug pilocarpine compared to WT. NeuroLSD1^{-/-} mice treated with the drug show a higher latency to the first seizure compared to wild-type littermates. At the same time the display reduced mortality and less seizures (Fig 18) [30]. Interestingly, in the same work, the authors show that in the Rett Syndrome mouse model (Mecp2[y/-]), which is characterized by a high susceptibility to seizures, neuroLSD1 is upregulated in several brain areas since one of its master regulators, NOVA1 is increased due to the lack of MeCP2, further corroborating the implication of LSD1 and neuroLSD1 in neuronal excitability [30].
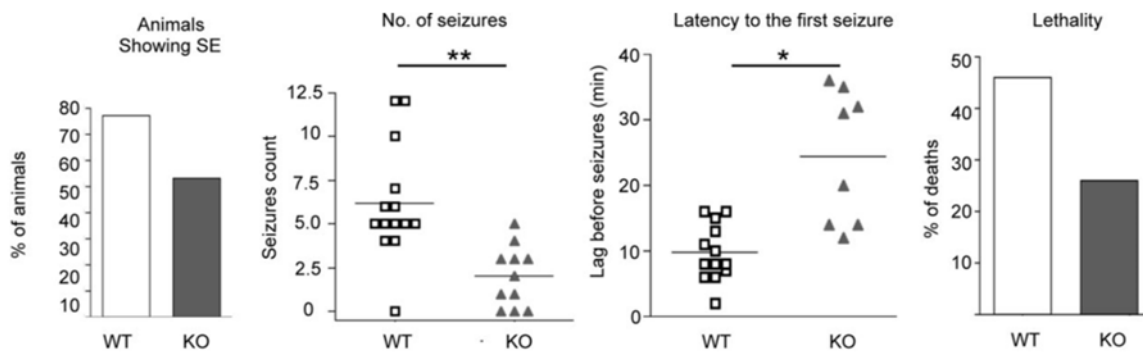
Figure 18. NeuroLSD1$^{-/-}$ mice are hypoexcitable. Panel of histograms comparing WT and neuroLSD1$^{-/-}$ mice upon PISE. Histograms evaluate percentage of animals showing seizures, number of seizures, latency to first seizure and lethality [adapted from 30].

1.2.4 LSD1/neuroLSD1: a dynamic ratio

As it has already been pointed out in the development experiment, the relative ratio between LSD1 and neuroLSD1 splicing isoforms is dynamic. However, it has been discovered that also in adulthood this balance can be altered, upon several paradigms of neuronal activation. This phenomenon has been observed for the first time upon Pilocarpine-induced Status Epilepticus (PISE), which is a pharmacological paradigm, but it happens also upon Acute Social Defeat Stress (ASDS), which is a behavioral test that mimics bullying. In the laboratory of Prof. Battaglioli, the changes in the relative ratio between LSD1 isoforms have been observed mainly in the hippocampus, a brain region where they are highly expressed, and that takes part to high cognitive functions. Seven hours after an intraperitoneal injection of pilocarpine in two-month-old wild-type male mice, LSD1 isoforms have been analyzed and it has been observed that neuroLSD1 isoforms are downregulated with a concomitant increase of LSD1. This means that also the repressive potential of LSD1 is augmented. At the 24 hrs timepoint the balance between LSD1 isoforms goes back to basal levels suggesting that it is a transient modulation (Fig 19) [30]
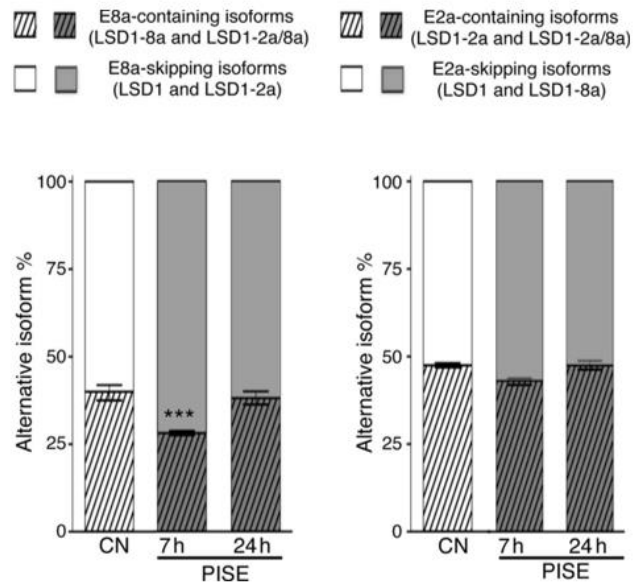
Figure 19. PISE induces neuroLSD1 downregulation. Histograms showing alternative isoform percentage 7 hrs and 24 hrs after the beginning of the PISE. **On the left** are represented neuroLSD1 isoforms, which significantly decrease upon PISE. **On the right**, unchanged LSD1 isoforms [adapted from 30]

As already stated, the ASDS is a behavioral paradigm that induces a physical and psychological stress on experimental animals. In brief, wild-type mice are put in physical contact with aggressor mice for 5 minutes then they are divided inserting a transparent and holed plexiglas divider that allows visual and olfactory interaction. LSD1 isoforms have been analyzed 7 hrs after the beginning of the stress and, as it happens with the PISE, neuroLSD1 isoforms decrease while LSD1 increase (Fig 20) [36].
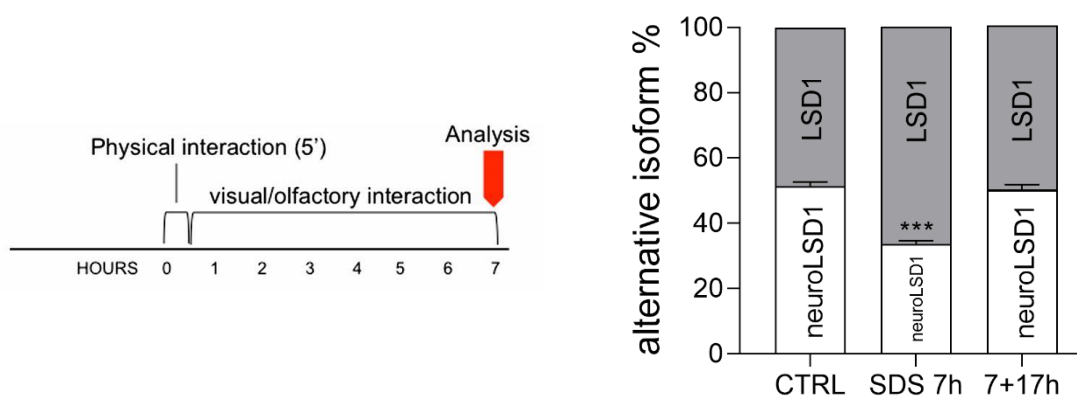
Figure 20. ASDS induces neuroLSD1 downregulation. On the left, schematic representation of ASDS. **On the right,** histograms showing alternative isoform percentage 7 hrs and 24 hrs after the beginning of the ASDS. NeuroLSD1 isoforms significantly decrease upon ASDS [adapted from 36].

On these same animals also other molecular assays have been performed in order to check for possible alteration in mRNA and protein levels of target genes. The IEGs Egr1 and c-fos increase their mRNA and protein levels upon ASDS in wild-types. The ASDS experiment have been performed on heterozygous animals for neuroLSD1and as expected, Egr1 and c-fos levels are similar to control levels, suggesting an impaired response to the stressful stimulus (Fig 21).

A   B
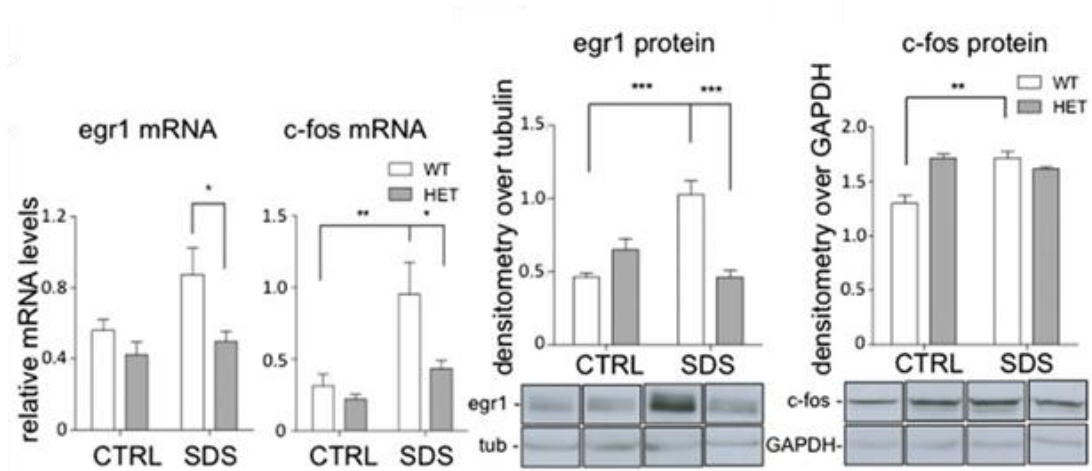
Figure 21. Lack of neuroLSD1 impairs stress-induced IEGs increase. (A) Heterozygous animals for neuroLSD1 display an impaired induction of the transcription of egr1 and c-fos upon ASDS compared to wild-type animals. **(B)** Heterozygous animals for neuroLSD1 display an impaired induction of egr1 and c-fos proteins upon ASDS compared to wild-type animals [adapted from 36].

All these data show how the lack of the dominant negative isoform neuroLSD1 leads to a negative modulation of several plasticity-related phenotypes (memory, anxiety, excitability), probably through the repression of the IEGs operated by LSD1. But it is important to notice that the alteration of the ratio between LSD1 and neuroLSD1 upon acute excitatory stimuli is transient. This mechanism has been indicated as part of the epigenetic homeostatic stress responses that are ultimately aimed at turning off the IEGs transcriptional activation, and restraining their induction, increasing the threshold of their transcriptional activation, for a limited time window (Fig 22) [37].

EPIGENETIC RESPONSE TO ACUTE STRESS IN THE HIPPOCAMPUS

PRIMARY RESPONSE
IEGs transcription

1st episode **STRESS**

no long-term behavioral effect

SECONDARY RESPONSE

Adaptive stress-coping epigenetic mechanisms

Global increase of H3K9me3 and Suv39h2[19,20]

IEG-specific increase of H3K9me2 and DNA methylation[41]

IEGs DNA methylation and increase of DNMT3A[21]

Increase of LSD1 H3K4me1/2 demethylase activity[22]

Figure 22. LSD1 isoforms modulation takes part to stress-induced epigenetic homeostatic mechanisms. Upon stress, the primary event that takes place is the transactivation of the IEGs. Subsequently a secondary response acts buffering the primary response. Several epigenetic events concur to this mechanism, among them neuroLSD1 decrease/ LSD1 increase [adapted from 37].

1.3 A synaptic mechanism to buffer stress response: the Endocannabinoid System (ECS)

1.3.1 Overview of the ECS

The endocannabinoid system is based on lipidic ligands that exert a neuromodulatory action through the binding to the cannabinoid receptors 1 and 2 (CB1r and CB2r). These are Gi/o proteins and, among their functions there are inhibiting adenylyl cyclase activity and voltage-gated Ca^{2+} channels and activating K^+ channels. The two principal endogenous ligands are the N-arachidonylethanolamine or anandamide (AEA) and the 2-arachidonoyl glycerol (2-AG). These are retrograde messengers that are synthetized "on demand" in the post-synaptic compartment starting from phospholipids precursors placed in the membrane via Ca^{2+}-dependent and -independent mechanisms. The synthesis of 2-AG is dependent on the activity of phospholipase C (PLC) which generates diacylglycerol, that is then rapidly converted to 2-AG by the enzyme diacylglycerol lipase (DAGL). Less is known about AEA synthesis, but it seems to be performed by at least three pathways, none of which have been verified as the primary

source of AEA within the brain, that involve N-acyltransferase (NAT) and a phospholipase D (NAPE-PLD).

Since CB1r is located on the pre-synaptic neuron, AEA and 2-AG exert a negative modulation on synaptic activity suppressing neurotransmitter release. Many are the neuronal subtypes subjected to the ECS neuromodulation, indeed CB1r are the most abundant class of G-protein-coupled receptors (GPCR) in the CNS but they can be found also in peripheral tissues. Within the brain, CB1r are expressed on GABAergic, glutamatergic, serotonergic, noradrenergic, and dopaminergic terminals, but since GABAergic and glutamatergic neurons are the most abundant, they act predominantly on these synapses. After the endocannabinoids are released in the synaptic cleft, they are uptaken and degraded by hydrolytic enzymes. Some enzymes are involved in these processes but the main are the fatty acid amide hydrolase (FAAH), which is placed post-synaptically and acts on AEA, while two different enzymes degrade 2-AG: the monoacylglycerol lipase (MAGL), positioned in close proximity of CB1r, in presynaptic terminals, and the post-synaptic alpha-beta hydrolase (ABHD) class of enzymes, specifically ABHD6 and ABHD12 (Fig 23) [38,39].
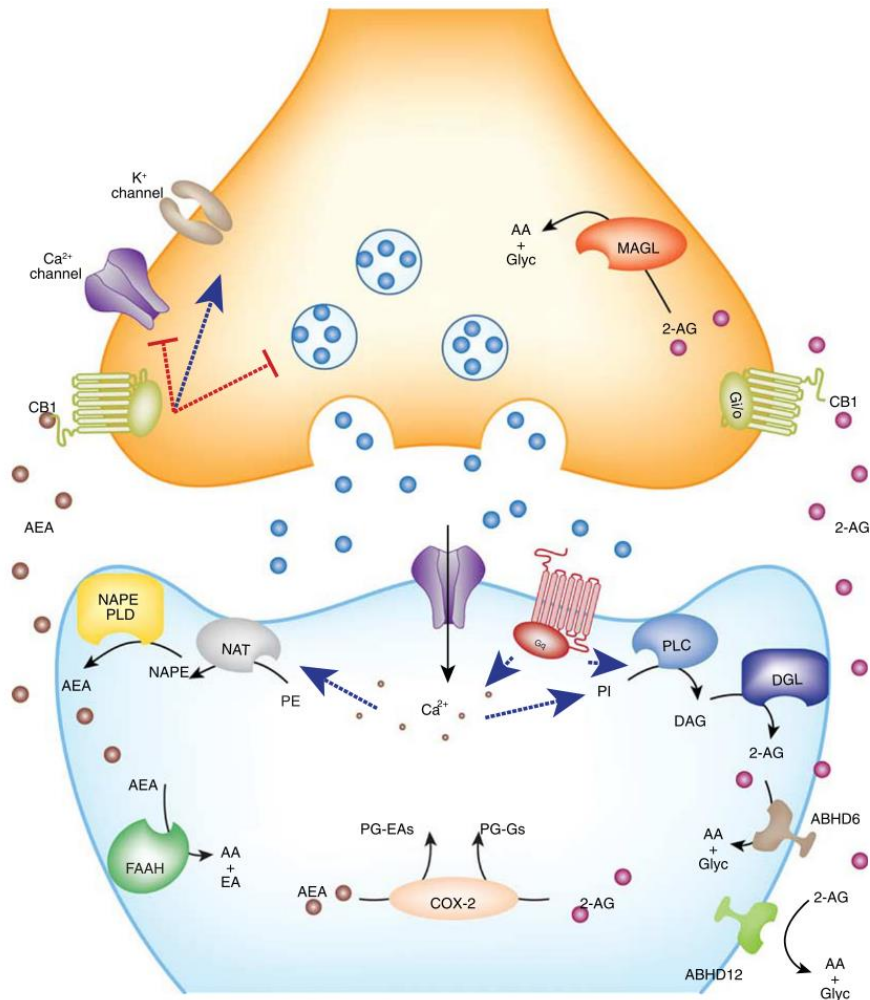
Figure 23. The endocannabinoid system. In blue the postsynaptic terminal: upon depolarization-induced calcium entry AEA and 2-AG are synthetized by NAPE-PLD and DAGL, respectively. These endocannabinoids retrogradely diffuse and bind to the CB1r on the presynaptic terminal (in yellow) inhibiting neurotransmitter release. MAGL ABHD6 and FAAH are the degradative enzymes of 2-AG and AEA, respectively [adapted from 38].

1.3.2 Molecular processes involving the ECS with a focus on 2-AG

Many are the evidences that suggest a role of the ECS in stress response. First of all, cannabis users report a reduction of perceived stress, an increase in relaxation, and a dampening of feelings of anxiety after its consumption [40]. Since Δ9-THC, which is the active principle of the cannabis, binds to the CB1r, it is thought that these buffering effects of stress response might actually be also the ones played by the endocannabinoids. Secondly, these observations are correlated to many experimental data that show how pharmacologically or genetically disrupting the ECS, the outcome is the induction of the stress response with activation of the HPA axis, increased anxiety, suppressed feeding behavior, reduced responsiveness to rewarding stimuli,

hypervigilance and arousal, enhanced grooming behavior, and impaired cognitive flexibility [41-50].

All together these data strongly suggest a pivotal stress-inhibitory role of the ECS. However different functions are played by the two main endocannabinoids. Upon stress AEA seems to be involved in the arousal of stress response. Upon stress, AEA is rapidly degraded by FAAH contributing to the activation of the HPA axis.

On the contrary, 2-AG effects are delayed and its levels increase upon stress, promoting stress termination. More in details, it has been shown that acute restrain stress leads to a moderate increase of 2-AG concentration in mPFC [51], hippocampus [52] and hypothalamus [53] after 1 hr from the beginning of the stress and that this different kinetic seems to be mediated by corticosterone (Fig 24).
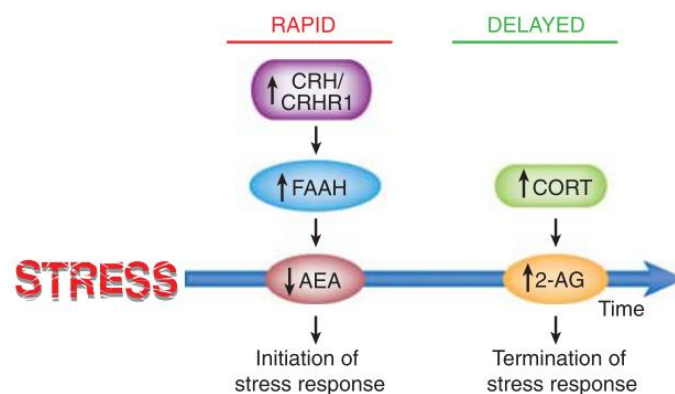
Figure 24. Timing and actions of stress-induced AEA and 2-AG production. Upon stress, AEA concentration rapidly decreases promoting the initiation of stress response. Subsequently 2-AG levels increase, by the action of corticosterone, cooperating in stress response termination [adapted from 38].

Conversely, upon chronic stress, in particular homotypic stress, 2-AG levels increase in the amygdala, something that does not happen upon acute stress. Mixed evidences come from heterotypic stress experiments; however it seems that upon chronic unpredictable stress there is a reduction in 2-AG content [38] probably mediating HPA habituation.

Some experimental evidences confirming ECS involvement in negatively modulating stress response, in particular anxiety arousal, come from the pharmacological or genetic disruption of CB1r signaling in which animals, in basal condition, already display a moderately increased anxiety but this dramatically enhances when a stress paradigm is applied [54-58].

The same outcome can be achieved through the induction of a central genetic 2-AG deficiency [48]. Conversely, if 2-AG levels are increased, pharmacologically blocking MAGL, basal but especially under high stress conditions, anxiety is reduced.

Concerning fear responses, global genetic deletion and pharmacological blockade of CB1r impair the ability to decreases the freezing behavior after repeated or prolonged conditioned stimulus-alone presentations [59,60].

In mice lacking DAGLα, the enzyme in charge of 2-AG synthesis, there are no impairments in fear acquisition but there is an altered fear extinction process [48]. Indeed stress-induced glucocorticoid signaling impairs memory retrieval. Rising hippocampal 2-AG levels systemically injecting corticosterone 1 h before retention testing, impairs the retrieval of a contextual fear memory; an effect which is reversible by pharmacological blockade of hippocampal CB1 receptors [61]. All these evidences point out a strong involvement of the ECS in terminating stress response and in promoting fear extinction.

2 AIM OF THE PROJECT

It is widely known that environmental stress represents a driving factor for the onset of mental illnesses. These are common multifactorial disorders that cause a strong deterioration of the quality of life. Since a wide range (10 to 20%) of the general population suffers from these pathologies -depressive diseases, anxiety, post-traumatic disorders, schizophrenia, eating disorders, addiction, and autism- it is fundamental to study the physiological molecular mechanisms aimed at preventing such diseases and their possible application as new therapeutic interventions.

Upon a stressful event the glutamatergic system is strongly engaged in many brain areas, in particular the hippocampus. Upon acute stress glutamatergic transmission is boosted in order to promptly respond to the incoming threat and to allow the consolidation of stressful memories in order to be prepared to respond to similar future events. However, thanks to homeostatic synaptic plasticity mechanisms devoted to cope with stress, no long-term negative consequences occur. A different scenario is represented by chronic stress. Upon a continuous unpredictable series of stresses, glutamatergic transmission is altered since stress-coping mechanism might fail. This could result, in vulnerable individuals, in the development of neuropsychiatric disorders.

The aim of my PhD work was to investigate the function of an epigenetic enzyme named LSD1 and its brain-specific dominant negative isoform neuroLSD1 in transcriptional mechanism underlying neuronal plasticity and impacting complex emotional and cognitive behaviors. In particular I focused on the role of these enzymes in stress response, a process that entails memorization of the traumatic event but that, at the same time, requires homeostatic mechanisms to avoid a too vivid memorization of the stressful event.

We hypothesize that the modulation of the ratio of LSD1 isoforms is implicated in this process, with the aim of buffering stress response and the consequent memory consolidation of the traumatic event. More in detail, if on one hand the transcription of neuroplastic genes is required to memorize a stressful event to engage protective behaviors in response to a future similar threat (primary stress response), on the other hand memory consolidation should not be excessive risking to lead to pathological fear and anxiety. According to this hypothesis neuroLSD1 downregulation, which occurs upon stress, might represent an epigenetic homeostatic stress response that is

ultimately aimed at temporarily turning off the transcriptional activation of neuroplastic genes engaged by stress-induced glutamate release.

Through molecular, biochemical, ultrastructural, electrophysiological and behavioral approaches I studied how neuroLSD1 modulation could impact on glutamatergic synapses and transmission.

Moreover I focused on another player which is implicated in this homeostatic process, the endocannabinoid system. This system is composed by lipidic neuromodulatory mediators and correlated enzymes and receptors, and is implicated in stress response termination preventing glutamate release from presynaptic neurons.

The aim of this second part of my work was to investigate a possible implication and crosstalk among LSD1 isoforms and the endocannabinoid system in restraining glutamatergic neuroplasticity in response to stress-induced glutamate release as converging homeostatic mechanisms aimed at preventing maladaptive plasticity. In particular, the study focused on the identification of endocannabinoid-related genes as new LSD1 transcriptional targets.

3 MATERIALS AND METHODS

3.1 Experimental animals

Animals were housed in a specific pathogen-free animal facility. 3-month-old male CD1(RRID:IMSR_ CRL:22) and nine to ten-week-old male C57BL/6N (RRID:IMSR_CRL:027), neuroLSD1 heterozygous and neuroLSD1 knock-out (neuroLSD1$^{-/-}$) littermates, derived either from our colony or from Charles River facility (ad hoc back up colony), were housed at controlled temperature (20–22°C) with free access to food and water in a 12-hr light/dark cycle (lights on at 7:00 a.m.). Mice were kept in an enriched environment and individually caged only during testing periods. Animals killed (decapitation) without anesthetic drugs to limit molecular interference with the processes analyzed. No exclusion criteria were applied, nor animals died during the experiments; death did was not an experimental end point in any case. Animals did not experience excessive pain during behavioral tests, which is why we did not use pharmacological strategies to reduce animal suffering (see below). In the investigation of the of LSD1 isoforms in the process of memory consolidation, we used a total number of 232 mice including 8 CD1 (ex-breeder) 224 C57BL/6N (wild type and neuroLSD1 HET and KO). Among C57BL/6N we used 54 naïve mice and 178 manipulated mice. Concerning the study of the crosstalk between LSD1 and the ECS, we used a total number of 126 mice including 24 CD1 mice and 102 C57BL/6N (wild type and neuroLSD1$^{-/-}$). Among C57BL/6N we used 28 naïve mice and 74 manipulated mice including 17 controls and 57 stressed animals.

All experimental procedures involving animals followed the Italian Council on Animal Care guidelines (Legislative Decree no. 26, March 2014) and European regulations (2010/63/ UE) and were approved by Italian Ministry of Health (no. 275/2015 and 322/2018). Every effort was made to accomplish to the "3R" regulations, that is, Reduction of animal number, Refinement of experimental procedures, Replacement with simpler research models, which has been not possible during this study. All current rules and regulations regarding animal usage were strictly adhered to.

3.2 Total RNA extraction, qRT-PCR analysis, and rqfRT-PCR

Total RNA isolation from hippocampal extract was performed using TRIzol reagent (15596026; Invitrogen) [62]. Residual RNA was treated with RNase-free DNase set

contained in the retrotranscription reaction kit Maxima™ H Minus cDNA Synthesis Master Mix with dsDNase (M1682; Thermo Scientific) to remove any residual DNA. qRT-PCR analysis was performed as described elsewhere [63]. Target genes expression was normalized on RPSA or RPL13. We used rqfRT-PCR to measure exon E8a splicing inclusion in mature LSD1 endogenous transcripts, as described in [30] Primers are indicated in table 1.

Table 1 Primers used for splicing and mRNA quantification

Primers for splicing quantification
mLSD1_FW
5'-CTACCATTTCATCTTTTTCTTTTGG-3'
mLSD1_REV
[6FAM] 5'-AGTGAGCCGGAAGAGCCGTCTG-3'
hLSD1_Ex2_fluo_FW
[6-FAM]5'-GTGAGCCTGAAGAACCATCG-3'
hLSD1_Ex9_REV
5-'CTACCATTTCATCTTTCTCTTTAGG-3'

Primers for mRNA quantification
mRPSA_FW
5'-ACCCAGAGGAGATTGAGAAGG-3'
mRPSA_REV
5'-TGGGGAACTGCTGAATGGGC-3'
hRPL13_FW
5'-GTCCGGAACGGTCTATAAGAAG-3'
hRPL13_REV
5'-GTCCTTTTTGCCCGTATGCC-3'
mLSD1_FW
5'-GCCTCAGCAGACACAGAAGG-3'
mLSD1_REV
5'-TGTTGTAAGGCGCTTCCAGC-3'
hLSD1_E15_ FW
5'-GCTAATGCCACACCTCTCTCA-3'
hLSD1_E16_ REV
5'-CCTGTCGCACTGCTGTATTCA-3'
hmLSD1_E8a_real_ FW
5'-AGCTGACACTGTCAAGGTTC-3'
hLSD1_Ex9_real_ REV
5'-GGACACAGGCTTATTATTGAGG-3'
mGRIN2A_FW
5'-CTGGAAGAGGCAGATTGACC-3'
mGRIN2A_REV
5'-CGTAAGCCACAGTGTCTCCA-3'
mGRIN2B_FW
5'-ATTCCCAACATGCGCTCTCCC-3'
mGRIN2B_REV
5'-GAGGATGACAGCGATGCCGAT-3'
mGRIA1_FW
5'-GTACCACTACATCCTCGCCAA-3'
mGRIA1_REV
5'-CTGTCACATTGGCTCCACTCT-3'
mPSD95_FW
5'-CAAGATCCTGGCGGTCAAC-3'
mPSD95_REV
5'-CGTCATATGTGTTCTTCAGGG-3'
mABHD6_FW
5'-AGTTCTGTTACTCCTTCCGGG-3'
mABHD6_REV
5'-CTTCGGAAGGAACTTGACCAC-3'
mMGLL_FW
5'-CCTGGTCAATGCAGACGGACA-3'
mMGLL_REV
5'-GCTCCATGGGACACAAAGATG-3'
mDALG_FW
5'-GCCCACATACTTTGCCATCTG-3'
mDALG_REV
5'-CTCCAGCACCTTATTGAGCC-3'
mCB1_FW
5'-CCTCTAACTTCCTTCAGGGGT-3'
mCB1_REV
5'-TGGTTGTGTCTCCTGCTGGAA-3'

3.3 Golgi Staining

After deep anesthesia with 5% chloral hydrate (dose 10ml/kg), animals were perfused with 4% paraformaldehyde in 0.1 M phosphate buffer (pH 7.4). Whole brains were kept for 2 weeks in the dark at room temperature in Solution A/B. Brains were then transferred in solution C for 5 days. Whole brains were cut in 400 μm slices using a vibratome (Leica VT1000S). Slices were stained and dehydrated following manufacturer procedures. Apical dendrites were acquired with a 63x/1.4 oil objective and analyzed with Stereo Investigator software (MBF Bioscience).

3.4 Transmission Electron microscopy (TEM)

Mice were anesthetized by intraperitoneal injection of 5% chloral-hydrate (10ml/kg) and transcardially perfused with 2.5% glutaraldehyde, 2% paraformaldehyde in 0.15 M sodium cacodylate buffer (pH 7.4). Dissected brains were post-fixed for additional 24 h at 4°C. Coronal sections (100 μm thickness) where obtained with a vibratome (Leica VT1000S) and *hippocampi* were manually dissected. After washing, samples were post-fixed with 2% osmium tetroxide, rinsed, *en bloc* stained with 1% uranyl acetate in water for 45 min, dehydrated and embedded in Epon-Spurr's epoxy resin that was baked for 48 h at 60°C. Thin sections (70-90 nm) were stained with a saturated solution of uranyl acetate in ethanol 20% and 1% lead citrate. Grids were observed in a Philips CM10 transmission electron microscopy (TEM) (FEI, Eindhoven - Netherland). For quantitative analyses, images were acquired at a final magnification of 25,000–46,000x using a Morada CDD camera (Olympus, Munster - Germany). Quantitative measurements were performed with ImageJ 1.51 as described [64]. Evaluation of synapse density from 2D TEM images was performed according to the size-frequency stereological method as described in [65].

3.4.1 Serial block face scanning electron microscopy (SBF-SEM) – Sample preparation

Primary tissue fixation was performed as described and the coronal sections (100 μm thickness) where obtained with a vibratome (Leica VT1000S) and *hippocampi* were manually dissected from these sections. After washing with cold cacodylate buffer 0.1 M, samples were fixed in a reduced osmium solution containing 3% potassium ferrocyanide in 0.3 M cacodylate buffer combined with an equal volume of 4% aqueous osmium tetroxide, for 1 h, on ice. At the end of the first heavy metal incubation the tissues were washed with ddH$_2$O at room temperature and are then placed in the 0.22

μm-Millipore-filtered 1% thiocarbohydrazide (THC) in ddH$_2$O solution for 20 min, at room temperature. Tissues were then rinsed again in ddH$_2$O and incubated in 2% osmium tetroxide in ddH$_2$O for 30 min, at room temperature. After several washed at room temperature in ddH$_2$O they are then placed in 1% uranyl acetate (aqueous), and left overnight at 4°C. Samples were washed, and were than immersed *en bloc* in 0.02M lead nitrate dissolved in 0.003 M aspartic acid solution, pH 5.5 at 60°C for 30 min. The tissues were washed, and dehydrated using ice-cold solutions of freshly prepared ethanol series ethanol, then placed in anhydrous ice-cold acetone for 10 min and embedded in Epon hard resin cured at 60°C for 48 h. Resin blocs were mounted on aluminium specimen pins using cyan acrylic glue and trimmed with a glass knife to a rectangle ~0.5 x ~0.75 mm with the tissue exposed on all four sides. Silver paint was used to electrically ground the edges of the tissue block to the aluminium pin (unless otherwise indicated, all reagents were purchased from Electron Microscopy Science, Hatfield PA).

3.4.2 SBF-SEM – Image acquisition

Serial block-face images were collected using an APREO Volume Scope SEM (Thermofisher Scientific) operating at an accelerating voltage of 1.8 kV with high vacuum. Data were collected with a pixel size of 10 nm along the x,y-axis and 40 nm along the z-axis.

3.4.3 Data visualization and measurements

The resulting datasets were assembled into volume files aligned using Imagej, and then manually segmented into 3D models. Three-dimensional structures in image stacks containing hundreds or thousands of 2D orthoslices are traced individually in each plane and surface rendered.

3.4.4 Statistical analyses for EM data

For EM analyses, 3 adult mice for each genotype were used, all data are presented as mean ± SEM. For each group of data, two-tailed unpaired Student's *t* test was used. Unless otherwise indicated all statistical analyses were performed with PRISM 5.00

3.5 Preparation of Protein Extracts and Western Blot Analyses for LSD1 role in synaptic homeostatic plasticity

Wild-type and neuroLSD1$^{-/-}$ mice (n=8/group) were sacrificed and hippocampi (including both ventral and dorsal parts) were grossly dissected from the whole brain. Tissues were immediately frozen on dry ice and stored at -80 °C.

Proteins of whole homogenate and post-synaptic density fraction were analyzed as previously described [66] with minor modifications. Briefly, hippocampi were homogenized in a teflon-glass potter in cold 0.32 M sucrose buffer pH 7.4 containing 1 mM HEPES, 1 mM $MgCl_2$, 1 mM $NaHCO_3$ and 0.1 mM PMSF, in presence of commercial cocktails of protease (Roche, Monza, Italy) and phosphatase (Sigma-Aldrich, Milan, Italy). Each homogenate was centrifuged at 800 g for 5 min; the obtained supernatant was then centrifuged at 13000 g for 15 min, obtaining a pellet. This pellet was re-suspended in a buffer containing 75 mM KCl and 1% Triton X-100 and centrifuged at 100000 g for 1 h. The resulting supernatant, referred as Triton X-100 soluble fraction (TSF, extra-synaptic fraction), was stored at -20°C; the pellet, referred as PSD or Triton X-100 insoluble fraction (TIF, post-synaptic density), was homogenized in a glass–glass potter in 20 mM HEPES, protease and phosphatase inhibitors and stored at -20°C in presence of glycerol 30%. Total proteins have been measured in the homogenate and TIF fractions according to the Bradford Protein Assay procedure (Bio-Rad, Milan, Italy), using bovine serum albumin as calibration standard.

Equal amounts of proteins of the homogenate (10 ug) and of TIF fraction (8 ug) were run on a sodium dodecyl sulfate-8% polyacrylamide gel under reducing conditions and then electrophoretically transferred onto nitrocellulose membranes (GE Healthcare, Milan, Italy). Blots were blocked 1 h at room temperature with 10% non-fat dry milk in TBS + 0,1% Tween-20 buffer and then incubated with antibodies against the proteins of interest. Primary antibody conditions are indicated in table 2.

Results were standardized using β-actin as control protein, which was detected by evaluating the band density at 43 kDa. Immunocomplexes were visualized by chemiluminescence using the Chemidoc MP Imaging System (Bio-Rad Laboratories). Gels were run 3 times each and the results represent the average from 3 different western blots.

3.5.1 Data analysis and statistics

Molecular changes produced by genotype were collected in individual animals (independent determinations), presented as means and standard errors and analyzed by an unpaired Student's t-test. Statistical significance was assumed at $p < 0.05$.

3.6 Western blot analyses for the analysis of ECS components

Protein extraction from mouse hippocampus was performed as in [62]. Immunodecoration methods to comparatively quantify protein levels in the different experimental groups is described elsewhere [67]. Hippocampal protein extracts were analyzed by a blind experimenter who received stressed and control hippocampi both from wild type and KO animals with a labeling whose code was only disclosed at the end of the analysis. Primary antibody conditions are indicated in table 2. Proteins were visualized by ECL detection (1705061; Bio-Rad) and bands were detected with a G:BOX Chemi XT4 camera and captured with GeneSys software (RRID:SCR_015770). Optical density of the bands was quantified using Image Pro Plus 7.0 software (RRID:SCR_016879), normalized and expressed as arbitrary units.

Table 2 Primary antibody conditions

Name	Diliution	Brand	RRID
GluN1	1:1000	Invitrogen, Carlsbad, CA, USA	RRID: AB_2533060
GluN2B	1:1000	Santa Cruz Biotechonology, Santa Cruz, CA, USA	RRID: AB_670229
GluN2A	1:1000	Invitrogen, Carlsbad, CA, USA	RRID: AB_ 2536209
GluA1	1:2000	Santa Cruz Biotechonology, Santa Cruz, CA, USA	RRID: AB_ 641040
GluA2	1:2000	Cell Signaling Technology Inc.	RRID: AB_10622024
PSD-95	1:4000	Cell Signaling Technology Inc.	RRID: AB_2292883
SAP102	1:1000	Cell Signaling Technology Inc.	RRID: AB_2092180
SAP97	1:1000	AbCam, Cambridge, UK	RRID: AB_2091910
Arc/Arg3.1	1:500	BD Transduction Laboratories, San Jose, CA, USA	RRID: AB_399886
anti β-Actin	1:10000	Sigma-Aldrich	RRID: AB_476697
CB1r	1:1000		RRID:AB_327840
NAPE-PLD	1:3000		RRID:AB_1962525
FAAH	1:2000		RRID:AB_327842
DAGLα	1:1000		RRID:AB_1658310
MAGL	1:1000		RRID:AB_10079049
ABHD6	1:1000	Novus Biologicals, NBP2-57800	
β Tubulin	1:2000		RRID:AB_10000656

3.7 Cell culture and transfection

Rat primary hippocampal neurons were prepared from Sprague Dawley rat embryos of either sex at embryonic day (E)18. Neurons were plated on coverslips coated with poly-D-lysine at a density of 75.000/well in 12 wells culture plates. Neurons were grown in Neurobasal Medium (Life technologies, Italy) supplemented with homemade B-27, 0.25% L-glutamine, 1% penicillin/streptomycin and 0.125% Glutamate (Sigma Aldrich) and maintained at 37°C, 5% CO_2. Hippocampal neurons were transfected with standard calcium phosphate method at days in vitro (DIV) 8 and imaged at DIV18.Neurons were transfected with pEFGP plus either HA-pCGN vector (control) or HA-neuroLSD1 (neuroLSD1). Images of pyramidal neurons were acquired with a Zeiss

LSM510 confocal microscope (Carl Zeiss, Italy; gift from F. Monzino) by using a 63x/1.4 oil objective. Images were obtained from the z-projection (maximum intensity) of approximately 6-10 stacks taken at 0.75 µm depth intervals at 1024 x 1024 pixel resolution. Analysis of spine density was done with NeuronStudio software.

3.8 Chromatin immunoprecipitation

Hippocampi of 10-weeks-old mice were dissected and cut in 400 µm slices using a chopper (McIlwain tissue chopper; Ted Pella). Slices were rapidly incubated in 1% formaldehyde (F8775; Sigma Aldrich) for 8 min at 4°C for cross-linking purposes then transferred in 0.125 M glycine (AC04021000; Scharlau) for 15 min and homogenized in lysis buffer: 10 mM Tris-HCl pH 8 (BP153; Fisher Bioreagents), 1 mM EDTA (AC09650500; Scharlau), 0.5 mM EGTA (E3889; Sigma Aldrich), 100 mM NaCl (131659.1211; PanReac AppliChem), 0.1% Na-deoxy-cholate (30970; Sigma Aldrich) 0.5% N-laurylsarcosine (L9150; Sigma Aldrich) containing protease and phosphatase inhibitors (Pierce protease and Phosphatase Inhibitors Mini tablets, EDTA free A32961; Thermo Scientific). Lysates were sonicated twice with a Bandeline Electronic Sonicator for 30 s at 30% power to generate fragments with an average length of ~500–200 bp, as determined empirically by agarose gel electrophoresis of the fragmented chromatin sample. Immunoprecipitation was performed overnight with 40 µg of sonicated chromatin in 600 µl of lysis buffer containing Triton 1% (10789704001; Sigma Aldrich), PMSF 0.2 mM (93482; Sigma Aldrich) and 1.5 µg of rabbit monoclonal anti-LSD1 mAb, (RRID:AB_2070132). A sample with pre-immune IgG (mock) normal rabbit IgG antibody (RRID:AB_1031062) was included as a control. The samples were then incubated with Dynabeads protein G (10003D; Invitrogen) at 4°C for 2 hr. After immunoprecipitation, the mock supernatant was kept apart as input sample. The beads were washed sequentially at 4°C (for 5 min each) with 1 ml of low salt buffer: 0.1% SDS (2811; J.T. Backer), 2 mM EDTA, 1% Triton X-100, 20 mM Tris-HCl pH 8, 150 mM NaCl twice, and high salt buffer: 0.1% SDS, 2 mM EDTA, 1% Triton, 20 mM Tris-HCl pH 8, 500 mM NaCl and TE buffer: 10 mM Tris-HCl pH 8, 1 mM EDTA pH 8.0. At the end the beads were washed with TE-NaCl buffer: 10 mM Tris-HCl, 1 mM EDTA, 50 mM NaCl. Elution was performed in 100 µl of fresh elution buffer: 1% SDS, 50 mM Tris-HCl pH8, 1 mM EDTA. Cross-linking was reversed overnight at 65°C. After cross-link reversal, RNAsi A (R4642; Sigma Aldrich) was added to each sample to eliminate the RNA and the samples were incubated for 40 min at 37°C. The samples were then

digested with proteinase K (EMR023100; EuroClone) for 1 hr at 56°C and DNA was obtained using a phenol:chlorophorm extraction protocol. DNA was recovered by standard methods in 40 µl of 10 mM Tris-HCl pH 8. Promoters were analyzed by quantitative real-time PCR carried out using Power SYBR Green PCR Master Mix (A25742; Applied Biosystem) with a QuantStudio 5 Real-Time PCR System (A28575; Applied Biosystem) according to the manufacturer's instructions.

The primers used in the PCR real-time reaction are listed in table 3. ChIP experiment data result from at least three independent experiments, and all quantitative real-time PCR experiments were performed in duplicate. Data were then plotted as fold enrichment over mock. The experimenter was unaware of sample type, assignment code was disclosed following CT analyses.

Table 3 Primers used for ChIP analyses

Primers for ChIP analyses
mABHD6_FW
5'-CCAGGCAAACAGTAGATGCTC-3'
mABHD6_REV
5'-GCCAAGCCGAATCATCCCTTT-3'
mABHD6_FW (ChIP-seq)
5'-CCATTCCTACGACCTGACCAC-3'
mABHD6_REV (ChIP-seq)
5'-TATCCCTGGGTTTAAGGAGGC-3'
mMGLL_FW
5'-TGCCTACACCTGTGCATCTG-3'
mMGLL_REV
5'-GCACAGTCGAGAACACAGACC-3'
mMGLL_FW (ChIP-seq)
5'-CGTCAACTGCATCTTCCCAGA-3'
mMGLL_REV (ChIP-seq)
5'-AGCAAAGTCACCCCGATTCTC-3'
mUnRelCTR_FW
5'-CGGCATGGGTGGTTATCTTGA-3'
mUnRelCTR_REV
5'-GGGTGTCATTGGTGTTCTGTG-3'

3.9 LSD1 ChIP-seq analyses

LSD1 ChIP-seq analyses were performed within a previous publication [68]. We loaded available ChIP-seq data, retrievable at the annotated link: Gene Expression Omnibus GSE63271 (ftp://ftp.ncbi.nlm.nih.gov/geo/sampl es/GSM15 44nnn / GSM15 44937

/suppl /GSM15 44937 %5FLsd 1%5FKCl minus %5Fhs6 0l3 %5F3%2Eucs c%2Ebed Graph %2Egz) on UCSC genome browser (https://genome.ucsc.edu).

3.10 Pharmacological treatments

DIV 14 rat primary neurons were treated with Bicuculline 40 µM (Sigma-Aldrich) for either 30 minutes or 8 hours. NMDA 50 µM (Sigma-Aldrich) was left 10 minutes in cell medium and then washed out with conditioned medium. Analyses were performed 30 min, 2, 3, 7 and 8 hours after the beginning of the experiment. APV100mM and MK-801 10 µM were added to cell medium and left for 6 hrs. A backbone of 2'-O-Methyl Phosphorothioate (2'-O-MePS) was used to generate a 21nt-long antisense oligonucleotide with the same sequence of the palindromic complementary-reverse endogenous element (AON-21-E8a) or a scrambled AON control (AON-21-SCRA) and purchased from Consorzio Futuro in Ricerca, Università degli Studi di Ferrara (Ferrara, Italy). A fluorescent version of AON was made conjugating OTF (Mediteknology S.r.l, Italy). AON were transfected at 10nM, 25nM and 50nM concentration for minigene reporter assay or directly added to the medium of primary neuronal cultures at 0,5µM, 2,5µM, 15µM and 25µM 48 hours prior molecular or electrophysiological experiments.

3.11 AON synthesis

AONs used in this study are listed in table 4. All AONs contain 2'-O-methyl modified RNA and full-length phosphorothioate backbone. Oligonucleotide syntheses and purifications were carried out at Università degli Studi di Ferrara (Ferrara, Italy), using Äkta instruments and following a well-established protocol [69]. Fluorophore-labeled oligonucleotides were synthesized by reacting the commercial succinimidyl derivative of oligothiophene fluorophore OTF (Mediteknology S.r.l, Italy) with the primary amine group of the ssH-linker, previously attached to the 5'-end AON-21-E8a and AON-21-SCRA. Several thiophene fluorophores have been reported for the selective labeling of intracellular proteins and the fluorescence behavior of several AON-oligothiophene conjugates has been explored in model studies [70]. Nevertheless, to the best of our knowledge, this is the first study considering the use of oligothiophene fluorophore OTF as fluorescent marker of AONs in live cells. To support our choice, absorption and photoluminescence spectra of OTF were in agreement with the required experimental conditions, OTF also showed good fluorescent properties and stability to bleaching even under prolonged irradiation. Finally, but not less important, OTF was non-

sterically hindered, nontoxic to the cells, chemically stable, easy to handle and cost-effective when compared to other widely known oligonucleotide labeling, thus enabling its use for large-scale applications. The purity of full-length desired products was evaluated by HRMS, 31P-NMR and RP-HPLC analyses. OTF molecular structure is shown in figure 25.

Table 4 Antisense oligonucleotides used in this study

Oligonucleotide	Chemistry	Sequence (5' > 3')
AON-21-E8a	2'-OMe PS	AUACCUUGACAGUGUCCUUUU
AON-21-SCRA	2'-OMe PS	GCUGAUAUUUCGCUCAUUCUA
OTF- AON-21-E8a	2'-OMe PS	OTF- AUACCUUGACAGUGUCCUUUU
OTF- AON-21-SCRA	2'-OMe PS	OTF- GCUGAUAUUUCGCUCAUUCUA

AON: antisense oligonucleotide; 2'-OMe: 2'-*O*-methyl; PS: phosphorothioate; SCRA: scramble;

OTF: oligothiophene fluorophore
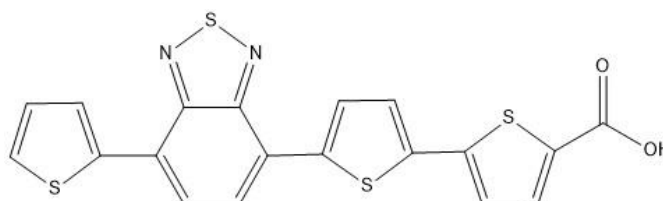
Figure 25. Molecular structure of the fluorophore OTF

3.12 Hybrid Minigene Constructs and Minigene Reporter Assay

Human genomic DNA was amplified to generate fragments containing the exon E8a along with its intronic flanking regions MG-800 (chr1:23392283–23393062) and cloned into pBS-Splicing [71]. Deletion of this 21nt string from the minigene was performed to generate MG800-Δpal as previously described [30] The splicing assay was performed as described [7] in Neuro2A cells. 200×10^3 Neuro2A cells were seeded in 6-well plates in order to extract total RNA. The cells were transfected 24 h after seeding with (2'-O-MePS), using Lipofectamine 2000 (Thermo Fisher Scientific, Waltham, MA, USA) transfection reagent according to the manufacturer's instructions. Cell extracts were prepared for analysis 48 h after the transfection.

3.13 In vitro electrophysiological recordings

13 DIV high density hippocampal neurons in cultures were treated with antisense oligonucleotide AON-E8a-21 or scramble molecule at the concentration of 15 μM and 36 hours later electrophysiological experiments have been performed. Excitatory and inhibitory post synaptic currents in miniature (mEPSCs and mIPSCs) have been measured by patch-clamp recordings in the whole-cell voltage clamp modality using the Axopatch 200B amplifier and the pClamp-10 software (Axon Instruments). To this end, neurons were held respectively at -70 mV or +10 mV in the presence of TTX 1μM. Each patched neuron was tested to record both mEPSCs and mIPSCs in order to calculate the E/I ratio (frequency of mEPSCs/frequency of mIPSCs cell-by-cell) and evaluate the balance between these two inputs on the same neuron in our three conditions (untreated/ scramble/ AON-E8a-21). Recordings were performed in Krebs'-Ringer's-HEPES (KRH) external solution (NaCl 125 mM, KCl 5 mM, MgSO$_4$ 1.2 mM, KH$_2$PO$_4$ 1.2 mM, CaCl$_2$ 2 mM, glucose 6 mM, HEPES-NaOH pH 7.4 25 mM). Recording pipettes were fabricated from glass capillary (World Precision Instrument) using a two-stage puller (Narishige); they were filled with the intracellular solution cesium-gluconate (CsGluc 130 mM, CsCl 8 mM, NaCl 2 mM, EGTA 4 mM, HEPES 10 mM, MgATP 4 mM, GTP 0.3 mM) and the tip resistance was 3-5 MΩ. Recordings were performed at room temperature and currents were sampled at 10 kHz and filtered at 2 kHz. The recorded traces have been analyzed using Clapfit-pClamp 10 software, after choosing an appropriate threshold.

3.14 Ex-vivo electrophysiological recordings

3.14.1 Slice preparation

Mice were anesthetized with isofluorane and decapitated, and their brains were transferred to ice-cold dissecting modified-artificial cerebrospinal fluid (aCSF) containing 75 mM sucrose, 87 mM NaCl, 2.5 mM KCl, 1.25 mM NaH2PO4, 7 mM MgCl2, 0.5 mM CaCl2, 25 mM NaHCO3, 25 mM D-glucose, saturated with 95% O2 and 5% CO2. Coronal sections (350 µm thick for field recordings or 250 µm thick for patch-clamp recordings) were cut using a Vibratome 1000S (Leica, Wetzlar, Germany), then transferred to aCSF containing 115 mM NaCl, 3.5 mM KCl, 1.2 mM NaH2PO4, 1.3 mM MgCl2, 2 mM CaCl2, 25 mM NaHCO3 and 25 mM D-glucose and aerated with 95% O2 and 5% CO2. Following 20 min of incubation at 32°C, slices were

kept at 22-24°C. During experiments, slices were continuously superfused with aCSF at a rate of 2 ml/min at 28°C.

3.14.2 Extracellular field recordings

Extracellular recordings of field postsynaptic potentials (fPSP) were obtained in the CA1 stratum radiatum, using glass micropipettes filled with artificial Cerebral Spinal Fluid (aCSF). Stimuli (50–160 µA, 50 µs) to excite Shaffer collaterals were delivered through a bipolar twisted tungsten electrode placed ≈400 µm from the recording electrode. Long-Term Potentiation (LTP) was induced using the following theta burst stimulation protocol (TBS): 10 trains (4 pulses at 100 Hz) at 5 Hz, repeated twice with a 2-min interval. Long-Term Depression (LTD) was induced using a Low-frequency stimulation protocol (LFS) consisting of 900 pulses at 0.5Hz. The magnitude of LTP or LTD was evaluated by comparing the fPSP normalized slopes from the last 5 min of baseline recordings with those 40–50 min after TBS or LFS.

3.14.3 AMPA/NMDA ratio

For patch-clamp experiments, whole-cell recordings were made under direct IR-DIC (infrared-differential interference contrast) visualization of neurons in the hippocampal CA1 stratum pyramidale region. Excitatory postsynaptic currents (EPSCs) were evoked in the presence of the $GABA_A$ receptor antagonist gabazine (10 µM) by stimulation of stratum radiatum by using a theta glass electrode (20 µsc–80 µsc, 0.02 mA–0.1 mA) connected to a constant-current isolation unit (Digitimer LTD, Model DS3) and acquired every 10 seconds. The glass of theta electrode, composed by two isolated channels, was pulled to produce the tip for microstimulation and each channel of the glass tip was filled with a normal aCSF used during recordings. Voltage clamp experiments were performed on CA1 pyramidal neurons using borosilicate patch pipettes (3–4 MΩ) filled with a solution containing (in mM): 135 CsMeSO3, 5 CsCl, 5 NaCl, 2 MgCl2, 0.1 EGTA, 10 HEPES, 0.05 CaCl2, 2 Na2-ATP, 0.4 Na3-GTP (pH 7.3, 280–290 mOsm/kg). Each CA1 pyramidal neuron was voltage-clamped at −70 mV and at +40 mV to evoke AMPA and NMDA receptor-mediated EPSCs respectively. AMPA and NMDA EPSCs were recorded before and after blocking AMPA mediated currents by bath applying 20 µM NBQX disodium salt. Access resistance was monitored throughout the experiment. Signals were sampled at 10 kHz filtered at 2.4 kHz. Series resistance (range 10–20 MΩ) was monitored at regular intervals throughout the recording and presented minimal variations (≤20%) in the analyzed cells. Data are reported without corrections for liquid junction potentials. Data were acquired using a

Multiclamp 700B amplifier controlled by pClamp 10 software (Molecular Device), with a Digidata 1322 (Molecular Device). AMPA/NMDA ratio of each neuron was calculated as the ratio between AMPA EPSC peak amplitude (pA) of the subtracted current and the NMDA EPSC peak amplitude (pA).

3.15 Acute Social Defeat Stress

30 minutes prior the stress paradigm, experimental animals were intraperitoneally injected either with sterile NaCl 0.9% solution (VEH) or with MK-801 0.3 mg/kg (Sigma-Aldrich). CD1 aggressor mice were used to defeat 2-month-old C57BL/6N wild-type mice in a 7-hour-long session of psychosocial stress. The experimental mouse and the CD1 aggressor interacted for 5 minutes and were kept in visual and olfactory for 7 hours. Experiments were performed at 8:30 a.m. Experimenters checked the health of stressed animal throughout the test to reduce animal suffering and physical interaction time. In this way there has been no need to administer analgesics and further medications. After the contact, mice were divided through a perforated plexiglas divider to allow the psychological stress phase through visual and olfactory interactions. Control mice were manipulated by experimenters housing them in the opposite sides of a plexiglas divider in cages identical to the one used to perform the test. Importantly, control mice were roomed in a different place to avoid control conditioning. After 7 hr (ASDS 7 hr) from the beginning of the stress, both control and stressed mice were analyzed.

3.16 Chronic social defeat stress

We employed a modified protocol of chronic social defeat stress (CSDS), validated to induce enduring depression-like phenotypes as anxiety and social-avoidance behaviors. Briefly, aggressive CD1 ex-breeder mice were used to defeat 8/9 weeks old C57BL/6 mice. C57BL/6 mice were exposed to a novel CD1 aggressor for 5 min/day, at 8:30 a.m. over 10 consecutive days. After the 5 min physical contact, experimental mice and CD1 aggressor were separated by a perforated Plexiglas divider to allow sensory interaction for 7 hr, after which mice were brought back to their home cage. Note that our CSDS protocol has been modified compared to the original method described in [72], and in our version, animals are allowed to recover, returning to their home cages between each 7-hr long stress session. This measure should be included within our procedures to refine the use of animals limiting their suffering.

3.17 Novel Object Recognition Test

Novel Object recognition test was conducted as previously described [73]. The apparatus consisted of an open plastic arena (38 cm x 30 cm x 18 cm) illuminated by a fluorescent lamp placed centrally above it (75 W). The animals were first habituated to the test apparatus for 10 minutes on Day 1 and 24 hour later they were subjected to the familiarization trial (T1). In order to study the short and long-term memory, after an inter-trial of 5 min, 120 min and 24 hours animals were tested in a novel object recognition trial (T2). Each trial was 20 min long. The objects consisted of orange plastic cones, green plastic tubes, and colored plastic Lego stacks of different shapes. During T1, the mouse was placed in the center of the arena between two objects and allowed to explore. During T2, one of the objects was changed for a novel object. To reduce innate object preference, the nature of the stimuli (familiar or novel) was counterbalanced. Time exploring the object was defined as the animal directing the nose towards the object within<0.5 cm of the object. Sitting on, or leaning to, an object was not considered as exploratory behavior. A video camera mounted above the arena recorded the behavior which was evaluated off-line by two experimenters blind to genotype. The discrimination index [(time spent exploring novel object − time exploring familiar object)/(time spent exploring novel object + time exploring familiar object)] was calculated as described elsewhere [74].

3.18 Human hippocampal samples

Postmortem hippocampal tissues from subjects of both genders were collected and immediately frozen during. Postmortem hippocampal samples derived from aged individuals (≥80-year-old people) were obtained from MRC London Neurodegenerative Diseases Brain Bank and associated brain banks, The Netherlands Brain Bank and BrainNet Europe, for all the others we collected samples from a dedicated study. Experimental protocols were approved by University of Milan Ethic Committee (n.40-18) and Territorial Ethic Committee AUSLR, (n. 2019/0004645). RNA integrity numbers assessed, between 4.6 and 7.5 using RNA 6000 Nano Chips on Agilent 2100 bioanalyzer, were suitable for analyses [75]. Not all the 30 human hippocampal samples were available for all the performed analyses. We used RPL13 as housekeeping gene to normalize gene expression. RPL13 expression stability along aging was analyzed using the Microsoft Excel-based tool BestKeeper [76].

4 RESULTS

In the following pages I will discuss the results obtained from two different projects on which I worked on during my PhD - one related to the role of LSD1 and neuroLSD1 in hippocampal plasticity-related processes such as memory consolidation and one related to the crosstalk between LSD1 and the endocannabinoid system in terminating stress response. Despite different molecular mechanisms of action, these two projects are strongly entangled from a functional point of view since both take part to convergent homeostatic synaptic plasticity mechanisms aimed at restraining glutamatergic neuroplasticity in response to stress-induced glutamate release.

4.1 LSD1, an environment and aging-sensitive negative modulator of the glutamatergic synapse

### 4.1.1 Structural analyses reveal a reduced neuroplastic potential of the glutamatergic synapse

Behavioral data collected from the analyses of neuroLD1$^{-/-}$ mice highlighted altered plasticity-related phenotypes such as hypoexcitability upon chemoconvulsant drug injections and reduced anxiety [30,36]. These evidences seem to suggest a possible default activation of homeostatic synaptic mechanisms aimed at decreasing glutamatergic competence. We therefore decided to investigate the dendritic spine morphology of the CA1 hippocampal neurons since we know that there LSD1 and neuroLSD1 actively exert their role in controlling plasticity-related transcriptional programs [36]. Two-month-old WT and neuroLSD1$^{-/-}$ littermates (C57BL/6N strain) were analyzed with transmission electron microscopy (TEM) approaches in resting condition - peculiar behavioral alterations can already be appreciated - thanks to a collaboration with Prof. Maura Francolini of the University of Milan. We considered different parameters both at the pre- and post-synaptic compartments. We examined length, thickness, volume and abundance of PSDs. From our analyses it emerges that neuroLSD1$^{-/-}$ mice have significantly shorter PSDs since WT animals have a mean PSD length of about 250 nm while neuroLSD1$^{-/-}$ mice of about 235 nm (FIG 26A). Moreover, our knockout model displays thinner PSDs (mean of 41,32 nm) in comparison with WT littermates (mean of 43,99 nm) (FIG 26A). Then we plotted the PSD lengths to obtain a distribution graph in which it can be appreciated that the curve

representing neuroLSD1$^{-/-}$ mice is shifted leftwards, indicating an increased frequency of smaller PSDs (FIG 26A). Subsequently, reconstructing dendrites in 3D thanks to the Serial Block Face – Scanning Electron Microscopy (SBF-SEM) technique, we evaluated spine head volumes (FIG 26B). We were able to score a tendency towards a reduced spine head volume in neuroLSD1$^{-/-}$ mice. Despite the non-significant result, these results are not in contrast since evaluated parameters about the PSD dimensions and dendritic spine volume can follow different trends [77].

A
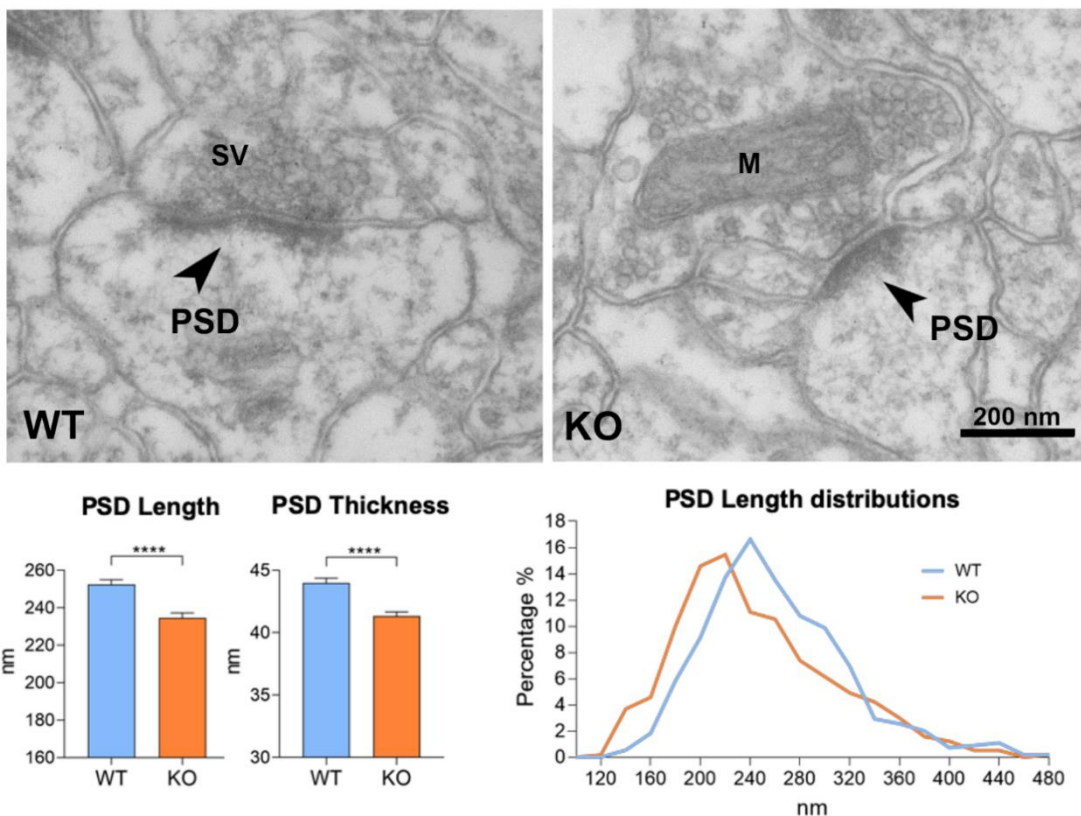
B
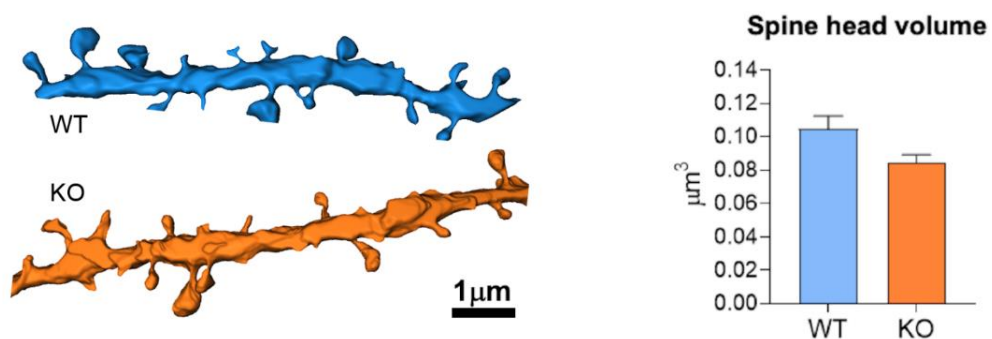
Figure 26. NeuroLSD1 ablation results in an impoverishment of glutamatergic dendritic landscape in the CA1 area of the murine hippocampus. (A) TEM analyses of the CA1 region of neuroLSD1$^{-/-}$ mouse hippocampus compared to WT littermates. Black arrows highlight the post synaptic density length of representative dendritic

spines (image scale bar 200 nm). **Lower Panel,** mean thickness, length and PSD length distribution in WT and neuroLSD1$^{-/-}$ adult mice. Data were acquired from 3 mice/genotype, around 550 spines/genotype. Data are presented as means ± SEM. ****p<0.00001, with Mann Whitney test. **(B)** 3D dendritic reconstruction from SBF-SEM acquisitions showing a comparison between representative dendritic branch of neuroLSD1$^{-/-}$ mice CA1 region. **On the left**, a representative 3D image of PSDs. **On the right**, the histogram shows the PSDs volumes obtained with SBF-SEM technique on WT versus neuroLSD1$^{-/-}$ mice (image scale bar 1 µm). Data are presented as means ± SEM.

Next, we evaluated the number of excitatory PSDs - corresponding to their density (n°/µm^3) - exploiting two different electron microscopy-based techniques. We found a trend in the reduction of PSDs in neuroLSD1$^{-/-}$ mice compared to wild-type littermates with SBF-SEM (1.38 ± 0.05 PSD/µm^3 in neuroLSD1$^{-/-}$ mice vs 1.47 ± 0.06 PSD/µm^3 in wild-type mice FIG. 27A). A similar result was obtained with stereological analysis performed on TEM images (z-stack) (1.23 ± 0.06 synapses/µm^3 in neuroLSD1$^{-/-}$ mice vs 1.35 ± 0.06 synapses/µm^3 in wild type FIG. 27B).

A
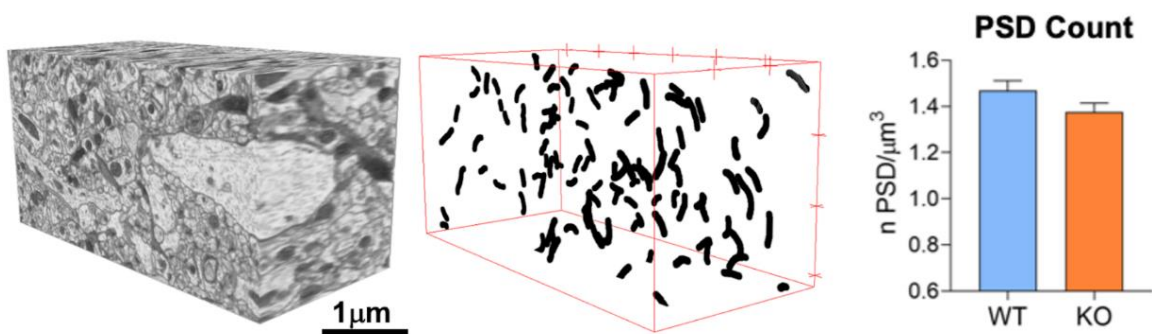
B
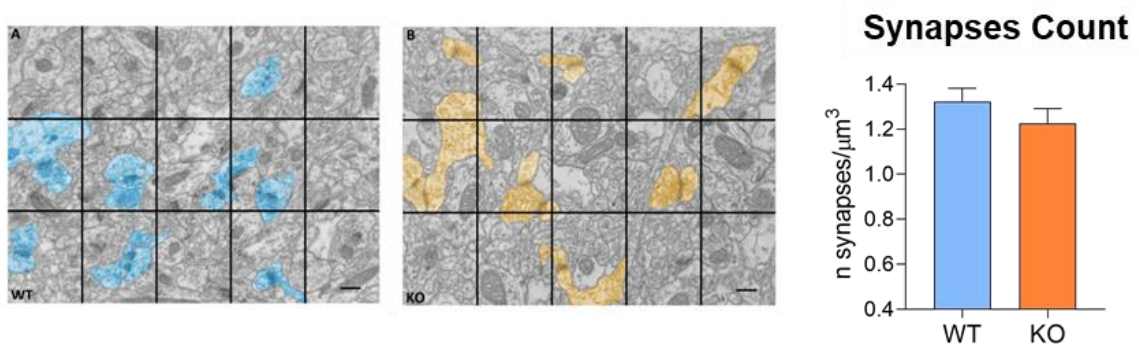
Figure 27. Lack of neuroLSD1 negatively impacts dendritic spines. (A) Representative 3D EM image with digitally reconstructed PSDs. **On the right**, the histogram shows the PSDs count obtained with SBF-SEM volumetric approach comparing the number of PSDs per µm^3 in WT and neuroLSD1$^{-/-}$ mice (image scale bars 1 µm). Data are presented as means ± SEM, unpaired Student's *t* test. **(B)** Stereological approach based on bidimensional projections of z-stack TEM images with stereological tool. **On the right,** the graph shows the density of excitatory synapses in WT and neuroLSD1$^{-/-}$ mice (image scale bar 50 nm). Data are presented as means ± SEM, unpaired Student's *t* test.

Alongside with ultrastructural analyses, we analyzed CA1 dendrites with optical microscopy techniques. With the Golgi-Cox staining we highlighted a statistically significant decrease of 12% in spine density in secondary and higher order dendrites of two-month-old neuroLSD1$^{-/-}$ mice compared to wild-type littermates (FIG 28A). We hypothesize that this significant reduction might be due to the resolution limit of optical microscopy (200 nm) since we pointed out that neuroLSD1$^{-/-}$ mice have more smaller spines than wild-types that are probably not detected with such technique. Furthermore, cotransfecting rat primary hippocampal neurons with EGFP and HA-neuroLSD1 or the empty vector at DIV 4, we scored a significant increase in mean spine density in HA-neuroLSD1 transfected neuron at DIV 18 (FIG 28B). These results support a possible role of LSD1 and neuroLSD1 in the molecular mechanisms that control the shape and number of dendritic spines.

A
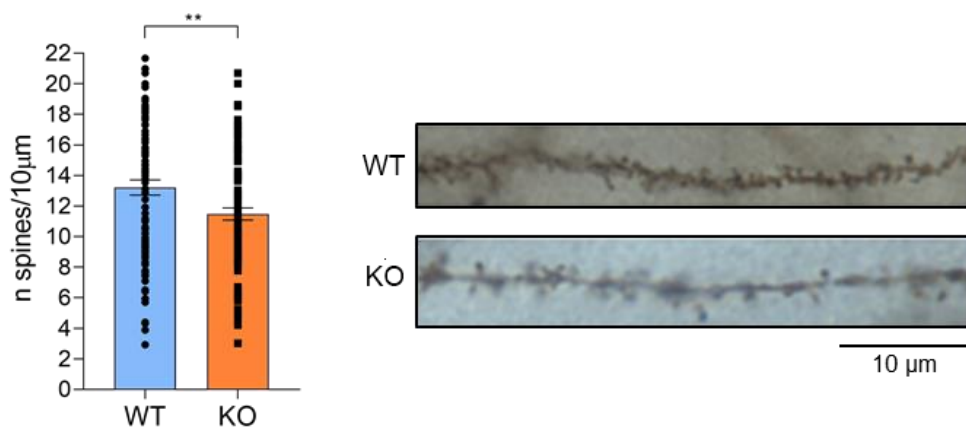
B
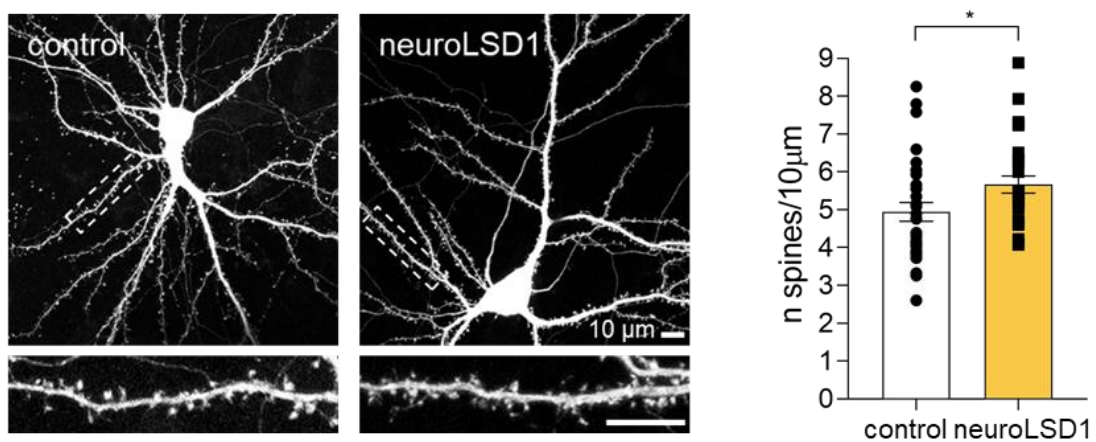
Figure 28. NeuroLSD1 modulation has an impact on the number of dendritic spines in the mouse hippocampus (A) Golgi-Cox staining experiment evidences differences in secondary dendritic segments in the CA1 hippocampal region of neuroLSD1$^{-/-}$ mouse compared to WT littermates. The graph shows mean spine density

(n° of dendritic spines per 10 μM length). Image scale bars 10 µm. N=3 mice/genotype were analyzed. **(B)** Confocal microscopy analysis performed on DIV 18 primary rat hippocampal neurons cotransfected at DIV4 with EGFP and HA-neuroLSD1 or empty vector (image scale bars 10 µm). Data are presented as means $\pm$ SEM. *p<0.01; **p<0.001, Student's *t* test.

For what concerns the presynaptic compartment of excitatory hippocampal synapses, electron microscopy was used to evaluate the presynaptic area, mean diameter and density of the ready releasable pool of synaptic vesicles (FIG 29A) and their distribution expressed as distance (nm) from the active zone of two-month-old neuroLSD1$^{-/-}$ mice compared to wild-type littermates (FIG 29B). As shown in figure 29, these parameters do not undergo any change in absence of neuroLSD1.
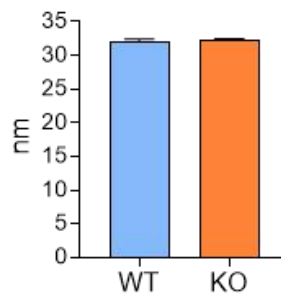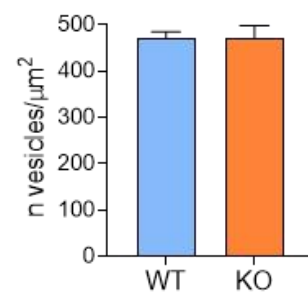
A

B
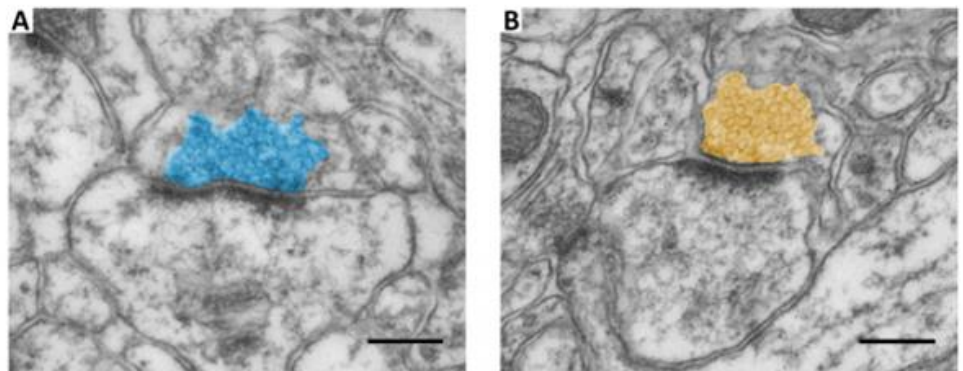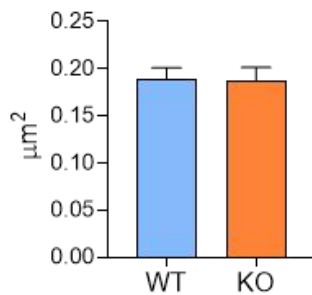
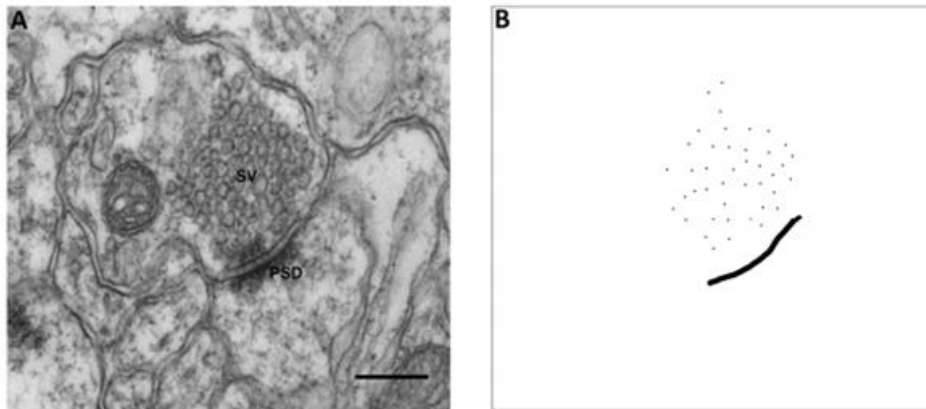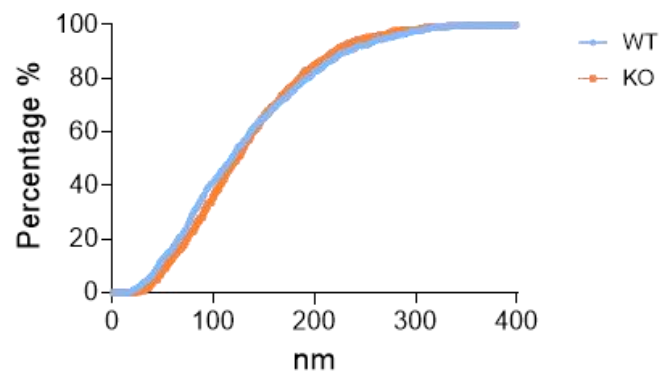**Figure 29. Lack of neuroLSD1 does not affect excitatory presynaptic structural parameters. (A)** A stereological approach based on TEM images was used to analyze the presynaptic area, glutamate vesicles diameter and their density (n°/ μm^2) in wild-type to neuroLSD1$^{-/-}$ mice (image scale bar 50 nm). **(B)** A stereological approach based on TEM images was used to evaluate vesicle distribution (nm from the active zone), the graph shows the percentage of vesicles within a specific distance.

Altogether these data suggest that the lack of neuroLSD1 impacts on the biology of dendritic spines in terms of hypotrophy, unaffecting the presynaptic compartment.

4.1.2 Biochemical evaluation of the postsynaptic compartment confirms a role for LSD1 and neuroLSD1 in dendritic spine biology

To couple the structural data with a biochemical analysis of the excitatory postsynapses, we employed a fractionation technique able to resolve the protein composition of the PSD comparing it with the whole hippocampal homogenate of wild-type and neuroLSD1$^{-/-}$ mice. We selected few pivotal excitatory postsynaptic proteins such as scaffolding proteins of AMPA and NMDA receptors (PSD-95, SAP97,

SAP102), ionotropic glutamate AMPA and NMDA receptor subunits (GluA1, GluA2 and GluN1, GluN2A, GluN2B), and the immediate early protein Arc/Arg3.1. The western blot data from the total hippocampal homogenates highlight a statistically significant common trend in the reduction of all analyzed factors in neuroLSD1$^{-/-}$ mice (FIG 30A). A different picture emerges when the PSD-enriched fraction is considered. PSD-95, GluA1 and GluA2 share the same decrease that was observed in the homogenate. For what concerns all the other analyzed protein, we scored an increase in their levels in the PSD fraction (FIG 30A). Among these proteins it is interesting to notice Arc/Arg3.1, which is a known LSD1 target and that is modulated in the brain of neuroLSD1$^{-/-}$ mice [35]. Concerning the different trends in the homogenate and in the PSD-enriched fraction, we hypothesized that this local increase of protein content at the PSD might be due to an enhanced efficiency of local translation, decreased protein degradation, or increased mRNA transport at the synapse. Concomitantly we analyzed the transcript levels of PSD-95, Grin2A, Grin2B and Gria1 by qRT-PCR to check whether neuroLSD1 ablation could have an impact on their transcription. We found no differences in PSD-95 transcript levels while we observed a significant reduction, in accordance with the total homogenate protein data, of NMDAr and AMPAr subunits (FIG 30B).

A
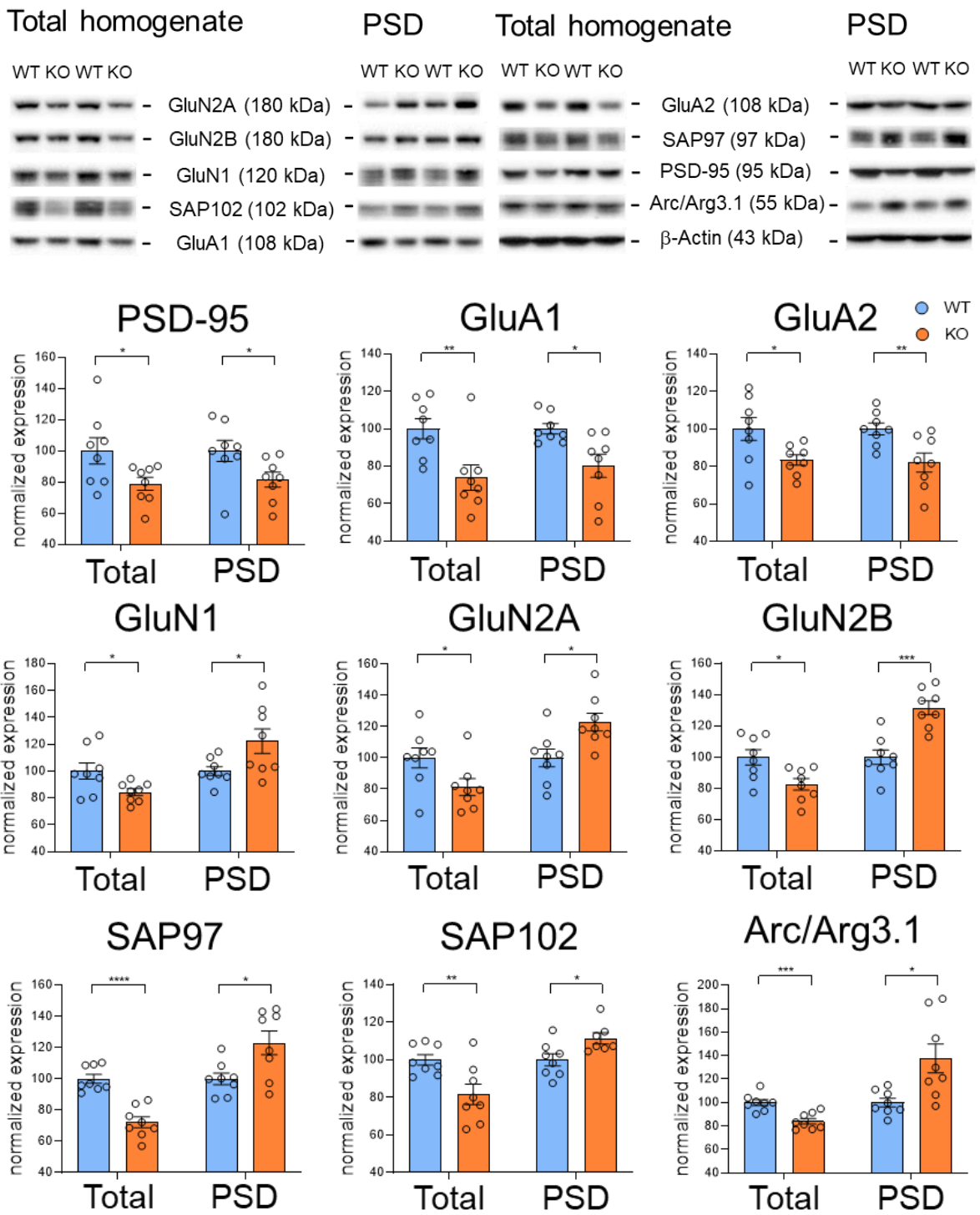
**B**
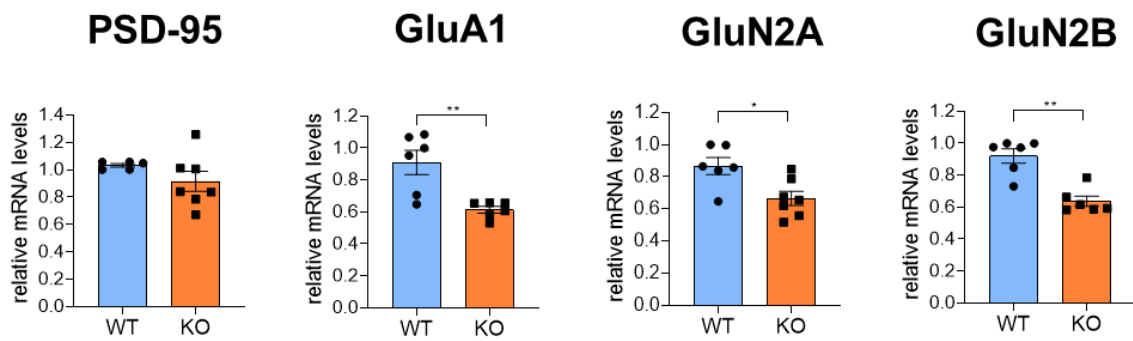
Figure 30. Lack of neuroLSD1 alters the protein composition of the PSD. **(A) Upper panel,** western blot analysis performed on hippocampal homogenates (Total) or PSD enriched fractions (PSD) (two representative lanes from wild type and neuroLSD1^{-/-} mice are shown). **Lower panel,** histograms showing the amount of proteins normalized over β-actin of indicated proteins showing a comparison of wild-type and neuroLSD1^{-/-} littermates. N=8 mice/genotype. Data are presented as means ± SEM. *p<0.01; **p<0.001, ***p<0.0001, ****p<0.00001, one-way ANOVA Tukey *post hoc* test. **(B)** Histograms show the relative mRNA levels of PSD-95, GluA1, GluN2A and GluN2B normalized over RPSA measured by qRT-PCR. N=6-7 mice/genotype. Data are presented as means ± SEM. *p<0.01; **p<0.001, Student's *t* test.

4.1.3 Functional analyses highlight an altered long-term memory formation in neuroLSD1^{-/-} mice

In order to verify whether the observed changes at the PSD might lead to an altered functional readout, we performed an electrophysiological analysis on acute ex vivo hippocampal slices from wild-type and neuroLSD1^{-/-} mice in order to measure AMPAr- and NMDAr-mediated currents with the help of the laboratory of Raffaella Tonini of the Istituto Italiano di Tecnologia. We observed a decreased AMPA/NMDA ratio (FIG 31) which is consistent with the biochemical data obtained from the fractionation technique. The protein asset and this electrophysiological result suggest that in the absence of neuroLSD1, mice have CA1 hippocampal depressed synapses in resting condition.
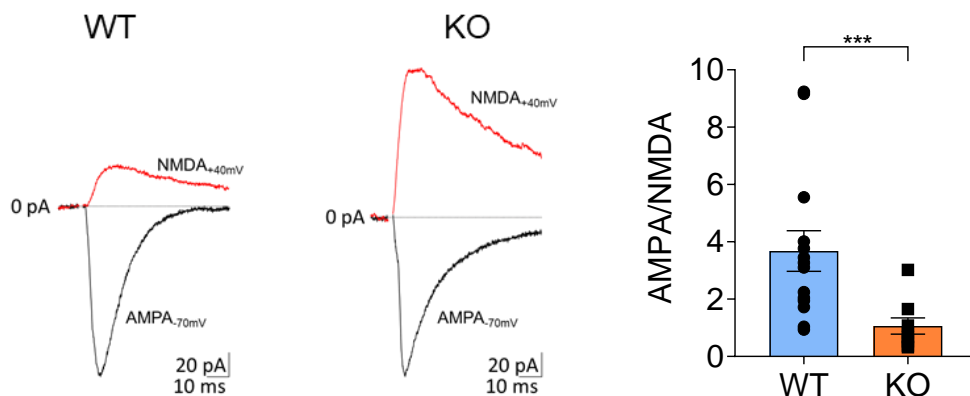
Figure 31. NeuroLSD1 ablation leads to depression of excitatory synapses. Electrophysiological analysis of AMPA/NMDA ratio of acute ex vivo hippocampal slices from wild type and neuroLSD1 [-/-] two-month-old littermates. **On the left,** two example traces of AMPA and NMDA EPSCs recorded at -70mV (black traces) and +40mV (red traces) respectively. **On the right**, the histogram shows distribution and averaged ratio for each genotype. n=8-12 mice/genotype. Data are presented as means ± SEM, ***p<0.0001 assessed with Mann-Whitney test.

We then tested whether neuroLSD1^{-/-} mice might have long term memory impairments. To do so we employed electrophysiological field approaches on ex vivo acute hippocampal slices of both wild-type and neuroLSD1^{-/-} mice. With a theta burst protocol we measured LTP induction as fEPSPs normalized slopes. As we expected from our previous results, we found that neuroLSD1^{-/-} mice less efficiently undergo LTP after theta burst stimulation - with a reduction of about 50% of synaptic potentiation - (FIG 32A) [78].

The ultrastructural and biochemical analyses of neuroLSD1^{-/-} mice evidenced a negative modulation of dendritic spines which correlates with a reduction in AMPAr subunits at a protein level. Actually, these data well fit with a diminished AMPA/NMDA ratio and an impaired LTP. Since a reduction in spine volume and number [79] and AMPA removal from the PSD are pivotal processes to sustain LTD, we employed a low frequency stimulation (0.5Hz for 30 min) on ex-vivo acute hippocampal slices of both wild-type and neuroLSD1^{-/-} mice to verify whether we could score a facilitated LTD in our model. With our protocol on resting condition animals we could not find any differences between control and neuroLSD1^{-/-} mice (FIG 32B).
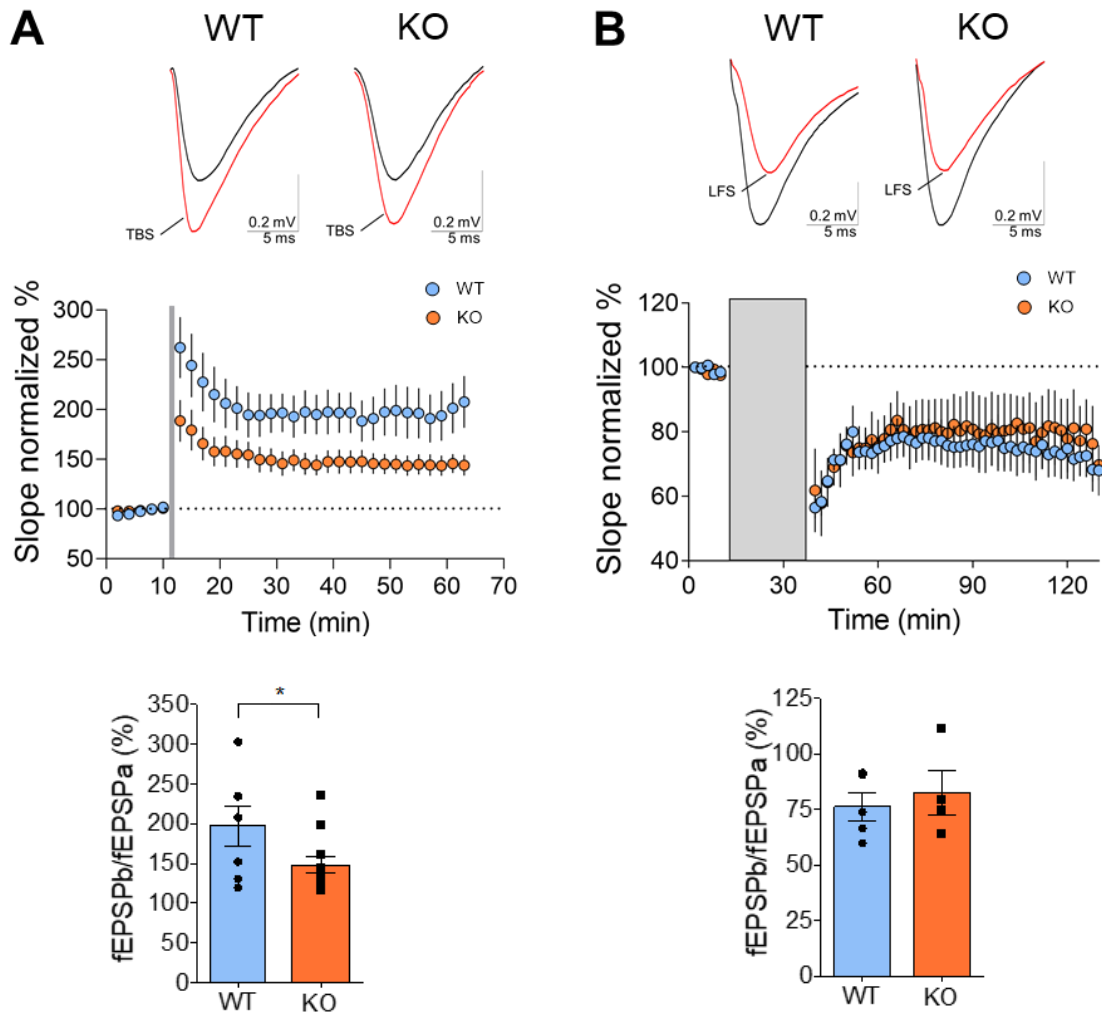
Figure 32. NeuroLSD1$^{-/-}$ mice display altered long-term memory. (A) Top panel, an example of LTP trace. **Middle panel,** time course of the normalized fEPSPs recording. **Lower panel,** ratio between WT an KO traces 35 e 45 minutes post-conditioning. LTP was induced by theta burst stimulation of hippocampal acute ex-vivo slices of 2-month-old male neuroLSD1$^{-/-}$ mice compared to wild type littermates (n=7 wild type mice, n=12 neuroLSD1$^{-/-}$ mice). **(B) Top panel** an example of LTD trace. **Middle panel,** time course of the normalized fEPSPs recording. **Lower panel,** ratio between WT an KO traces 35 e 45 minutes post-conditioning. LFS-induced LTD in hippocampal acute ex-vivo slices of two-month-old male neuroLSD1$^{-/-}$ mice compared to wild type littermates (n=5 mice per genotype). Data are presented as means $\pm$ SEM. *p<0.01, Student t test.

To associate a behavioral readout to the electrophysiological-tested memory defects, we performed a Novel Object Recognition test (NOR) on 2-month-old male wild-type and neuroLSD1$^{-/-}$ mice. We analyzed three different time points in order to check for short-term or long-term memory impairments. At all analyzed time points - 5 min, 120 min and 24 hrs after the switch of the familial object with the novel one - we were able to score reduced memory in neuroLSD1$^{-/-}$ mice, shown as a statistically significant reduced discrimination index (N-F/N+F) compared to wild-type animals in FIG 33A. Also the sniffing time parameter was checked (FIG 33B). Interestingly, long-term

memory defects can already be appreciated in neuroLSD1^{+/-} mice, which have half of the amount of neuroLSD1 compared to wild-types. This genetic condition resembles a more physiological modulation of neuroLSD1 and gives us important insight on what might happen at a behavioral level for example during an acute stress, where we know neuroLSD1 is transiently downregulated, and that might lead to an altered memory consolidation [81].

A
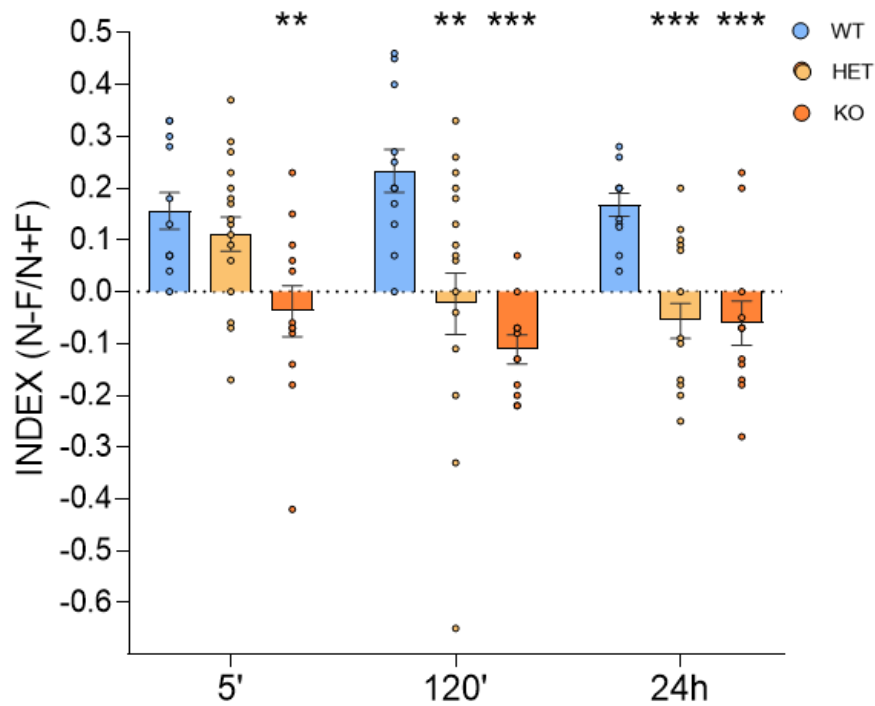
B
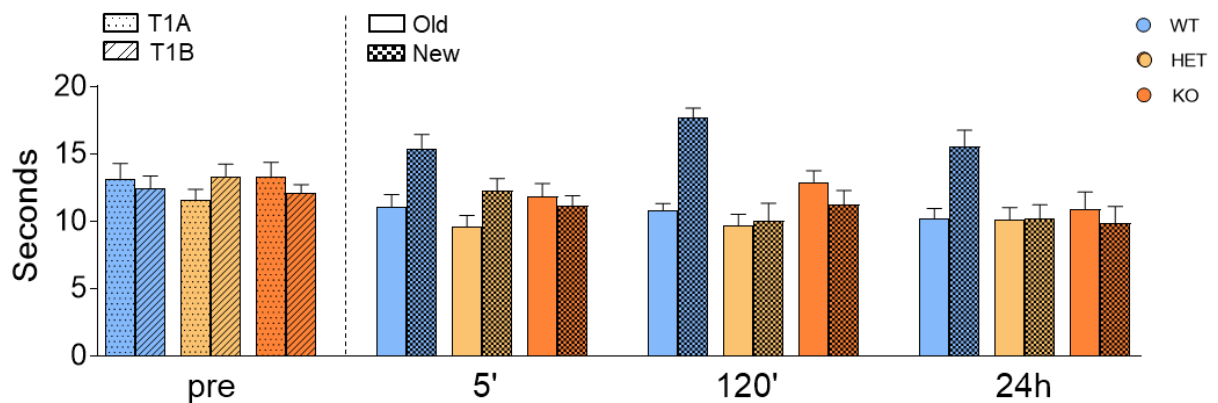
Figure 33. NeuroLSD1^{-/-} mice display impaired long-term memory. (A) Novel Object Recognition test performed at 5 min,120 min and 24 hrs time points in 2-month-old male neuroLSD1^{-/-} and neuroLSD1^{+/-} mice (n=12 mice per genotype). Data are presented as means ± SEM. *p<0.01, **p<0.001, ***p<0.0001, two-way ANOVA coupled to Tukey *post hoc* test. **(B)** Sniffing time in the NOR test performed at 5 min,120 min and 24 hrs time points in 2-month-old male neuroLSD1^{-/-} and neuroLSD1^{+/-} mice (n=12 mice per genotype).

4.1.4 Changes in LSD1/neuroLSD1 balance are dependent from glutamatergic transmission

Data from our laboratory show how the ratio between LSD1 splicing isoforms is modulated upon acute social defeat stress [36, 23] with a reduction of neuroLSD1 and a concomitant increase of LSD1. It is known that stress elicits the activation of glutamatergic neurotransmission in the hippocampus, this is the reason why we decided to pharmacologically induce glutamate release in primary hippocampal neuronal cultures to better understand the pathway that leads to the modification of the ratio between LSD1 and neuroLSD1 splicing isoforms. We treated DIV 14 rat primary hippocampal neurons with bicuculline (bic), a competitive antagonist of the $GABA_A$ receptor, which induces depolarization via disinhibition of the neuronal network. Bic-induced glutamate release is able to stimulate both synaptic and metabotropic glutamate receptors [82]. We treated DIV 14 primary hippocampal neurons with bic 40µM for 30 min. We performed a wash-out and then neurons were analyzed 8 hrs after the beginning of the experiment with a rqfRT-PCR. This particular time window was chosen since splicing modulation is a phenomenon that can be appreciated some hours from the initial stimulus (from 2 hrs from the beginning of the ASDS) [83]. With this kind of stimulation however, we were not able to see any modulation in LSD1 isoforms, probably because this treatment, which engages synaptic glutamate receptors [82], is not sufficient to elicit a chance in the ratio (FIG 34A). Knowing that stress is able to downregulate neuroLSD1 and that is able to facilitate LTD induction stimulating extrasynaptic NMDAr because of glutamate spillover [84], we decided to treat neurons with an NMDA bath. NMDA 50µM was added for 10 [80] min in DIV 14 primary hippocampal cultures. After the wash out, neurons were analyzed at different time points (30 min, 2 hrs, 3 hrs, 7 hrs and 8 hrs) with a rqfRT-PCR. As shown in FIG 34B, along the time course neuroLSD1 markedly decrease, almost disappearing at later time points. The total mRNA levels of LSD1 isoforms were studied and we concluded that there are no changes in its levels indicating that the modulation that we observe might be due to post-transcriptional mechanisms rather than mRNA degradation (FIG 34C). We then decided to further investigate the involvement of the NMDAr by treating primary neuronal cultures with NMDA and, concomitantly, with either APV 100mM or MK-801 10µM. APV is a competitive antagonist of the NMDA receptor while MK-801 is a non-competitive antagonist which blocks the pore impeding

ion flux through the channel. We found that in presence of these drugs, NMDA bath application does not lead to any modification of the splicing ratio (FIG 34D). Thanks to these in vitro experiments we could identify the involvement of both synaptic and extrasynaptic NMDAr as primary event that leads to the downregulation of neuroLSD1.
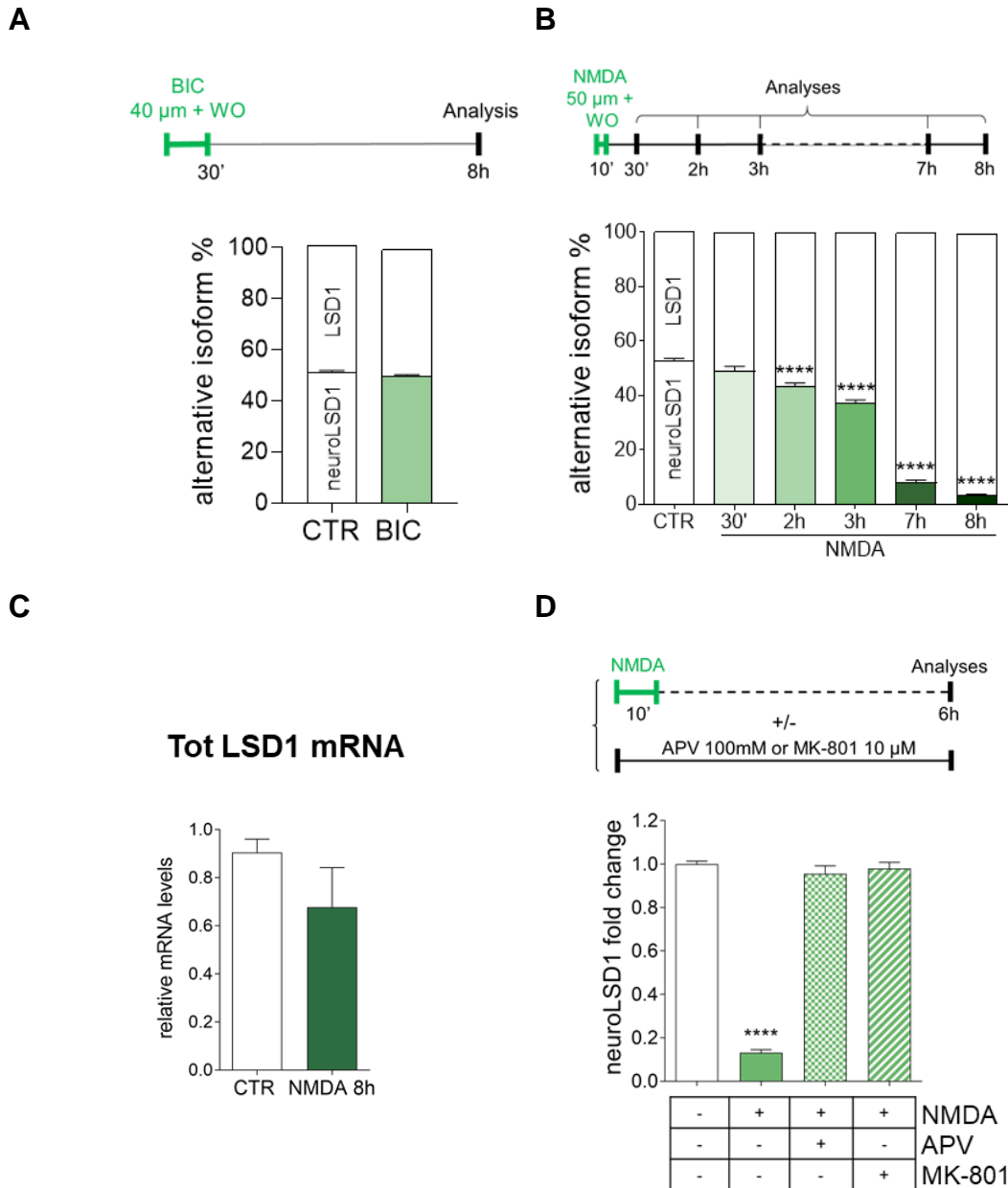
Figure 34. LSD1 isoforms splicing modulation is dependent on the engagement of the NMDA receptor in vitro. (A) LSD1 isoforms of DIV 14 primary rat hippocampal neurons treated with bicuculline 40 µM for 30 min (+ wash out) and analyzed after 8 hours. **(B)** Time course analysis showing LSD1 isoforms of DIV 14 primary rat hippocampal neurons treated with NMDA 50 µM for 10 min (+ wash out) and harvested 30 min, 2 hrs, 3hrs, 7 hrs and 8 hrs from the beginning of the treatment. **(C)** qRT-PCR analysis showing total LSD1 isoforms mRNA levels of DIV 14 primary rat hippocampal neurons treated with NMDA 50 µM for 10 min (+ wash out) harvested at 8 hrs. **(D)** DIV 14 primary rat hippocampal neurons treated with NMDA 50 µM for 10 min (+ wash out) and APV 100mM or MK-801 10 µM. Data are presented as means $\pm$ SEM. ****$p<0.0001$, one-way ANOVA. * relative to controls.

Our next step was to check whether also in vivo we could impede the modulation of the splicing by injecting mice with MK-801 prior a 7-hour-long ASDS session. Two-month-old male wild type mice were intraperitoneally injected with MK-801 0.3mg/kg or vehicle 30 minutes before the start of the ASDS. If naïve and vehicle treated mice exposed to ASDS undergo neuroLSD1 downregulation, MK-801-injected mice do not display any modulation upon stress (FIG 35). This in vivo data strongly supports the involvement of the NMDAr in the splicing modulation.
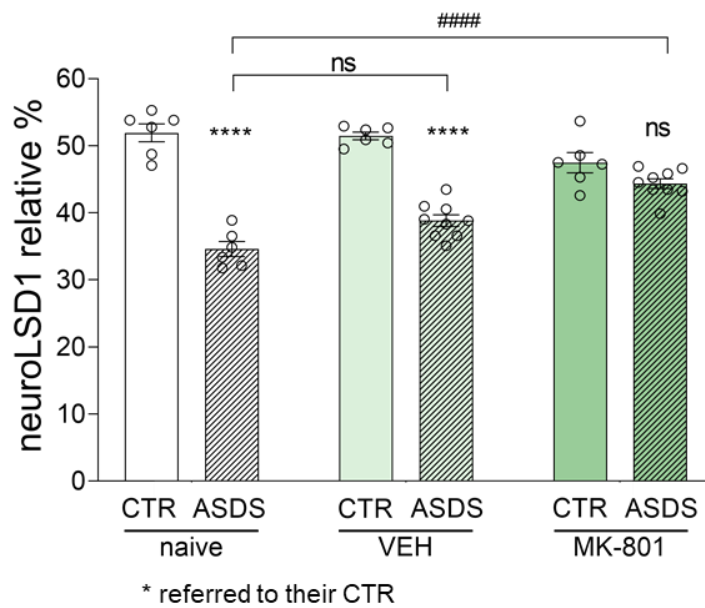
Figure 35. LSD1 isoforms splicing modulation is dependent on the engagement of the NMDA receptor in vivo. Analysis of LSD1 splicing isoforms in the hippocampi of wild-type naïve or treated with vehicle or MK-801 mice that underwent a 7-hour-long session of social defeat stress. N=6-9 mice for each condition. *Relative to controls. #Relative to naïve ASDS. Data are presented as means ± SEM. ****p<0.00001, ####p<0.00001, two-way ANOVA coupled to Tukey *post hoc* test.

4.1.5 Basal synaptic glutamate transmission is negatively modulated by AON-mediated neuroLSD1 downregulation

From the data we collected - the glutamate-induced neuroLSD1 downregulation through the NMDAr, the hypotrophic dendritic spines in neuroLSD1$^{-/-}$, and the reduced AMPA/NMDA ratio probably due to a lower AMPAr protein expression and to an increase of NMDAr at the PSD - a picture emerges of a possible role as a synaptic homeostatic process for LSD1 transient modulation that occurs upon acute stress.
To test the hypothesis that neuroLSD1 transient downregulation might have an impact on synaptic excitability we designed a pharmacological tool able to modulate LSD1

isoforms in a more physiological way. We produced, with the help of the laboratory of Prof. Daniela Perrone of the University of Ferrara, an antisense oligonucleotide (AON) that mimics what happens physiologically with the palindromic sequence - a negative in cis regulator of microexon 8a inclusion in mature transcripts - in neurons [30]. A 21-nt-long AON with a 2'OMe-phosphorothiotate backbone, in order to reduce the vulnerability to endonucleases, was designed to be able to anneal to neuroLSD1 sequence and induce exon skipping (FIG 36).
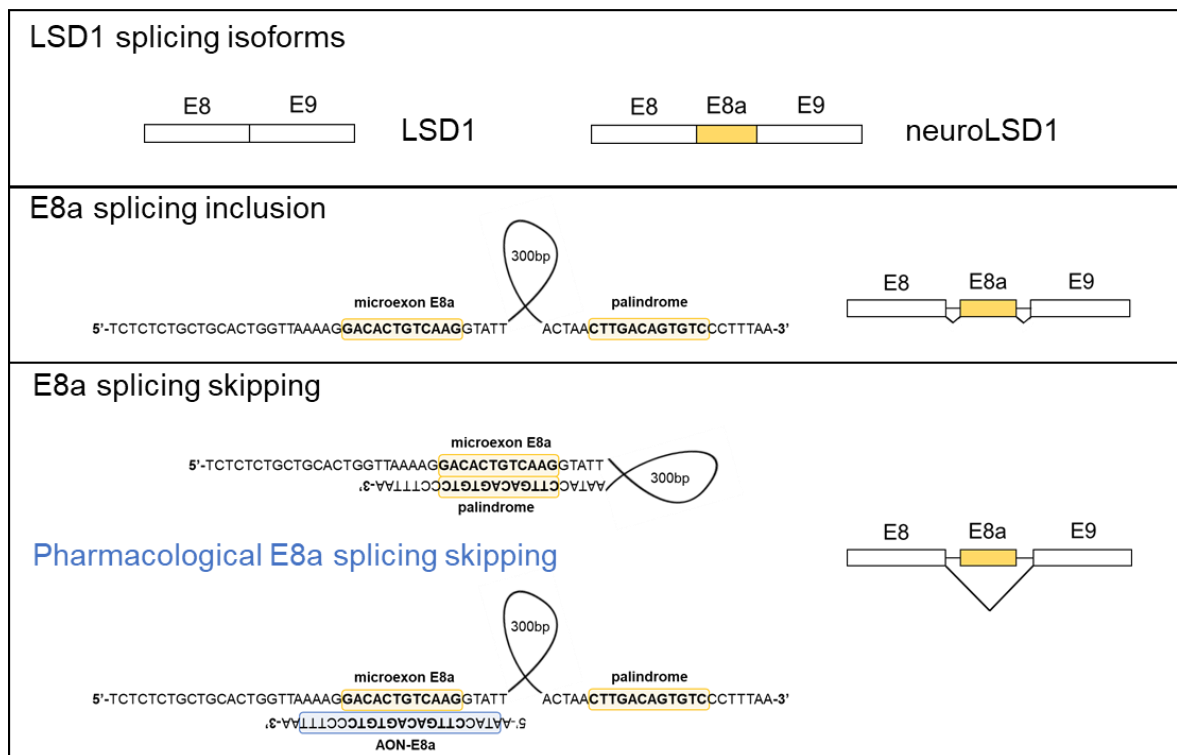
Figure 36. Schematic representation of AON rational. **Top panel,** inclusion of microexon E8a in mature transcripts leads to the formation of neuroLSD1. **Middle panel,** microexon E8a is included in mature transcripts when the negative regulatory palindromic sequence is not annealed to its sequence. **Bottom panel,** endogenous and exogenous splicing skipping mechanisms. The palindromic sequence is highlighted in yellow while the AON-E8a in blue.

In order to check the ability of the AON-E8a to downregulate neuroLSD1 we performed in vitro experiments in cell lines and in primary neuronal cultures. We transfected Neuro2a cells with the MGΔpal construct, that lacks the palindromic sequence allowing a high inclusion of microexon E8a in the transcripts. We transfected these cells with different concentrations of the AON (10,25,50nM) ad we found that microexon-E8a inclusion is drastically reduced upon treatments (FIG 37A). We also treated rat primary neuronal cultures, just adding the compounds to the medium, with the SCRAMBLE at 25 μM and with the AON-E8a at 0,25-2,5-15 and 25 μM for 36 hrs. We then collected

the samples and performed a rqfRT-PCR. We found that the AON leads to a dose dependent decrease of neuroLSD1 isoforms (FIG 37B). However, neurons treated with the 25 µM dose showed signs of toxicity, we therefore decided to use the 15 µM dose for functional experiments.
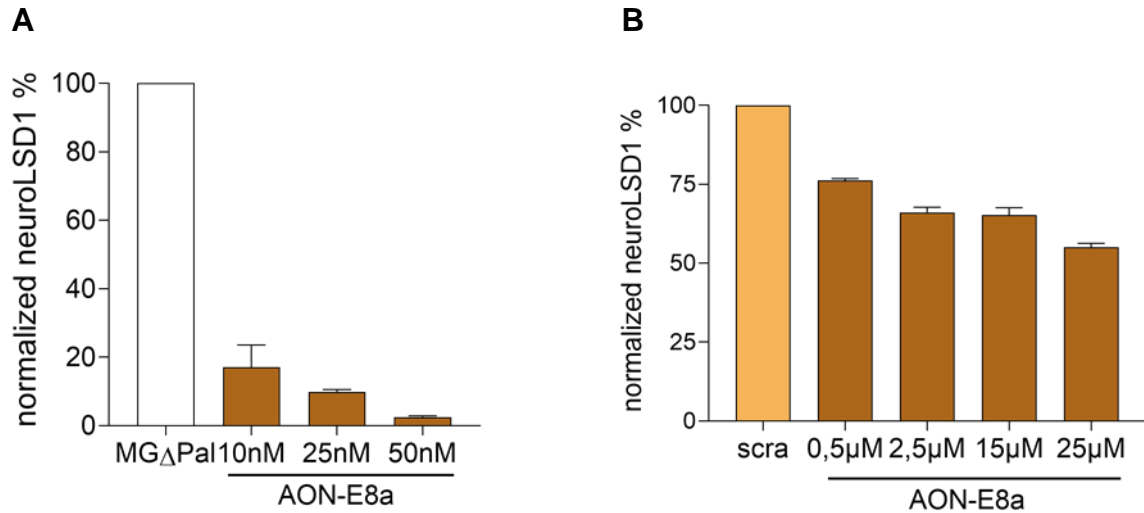
Figure37. AON in vitro treatment induces neuroLSD1 isoforms downregulation. (A) Neuro2A transfected with MGΔpal cells treated with AON-E8a at 10,25,50 nM. **(B)** Primary rat neuronal cultures treated with AON-E8a at 0,25-2,5-15 and 25 µM for 36 hrs. Both experiments were analyzed by rqfRT-PCR.

In collaboration with Prof. Perrone, we also developed a fluorescent version of the AONs. We gave the SCRAMBLE and the AON-E8a at 15 µM marked with a very small fluorescent molecule, a thiophene fluorophore (Mediteknology S.r.l, Italy) -in order to avoid interference with the neuronal uptake- to SHSY-5Y for 36 hrs and acquired microscopy images to see the uptake. As shown in FIG 38 the AONs signals are present in almost all the cells.
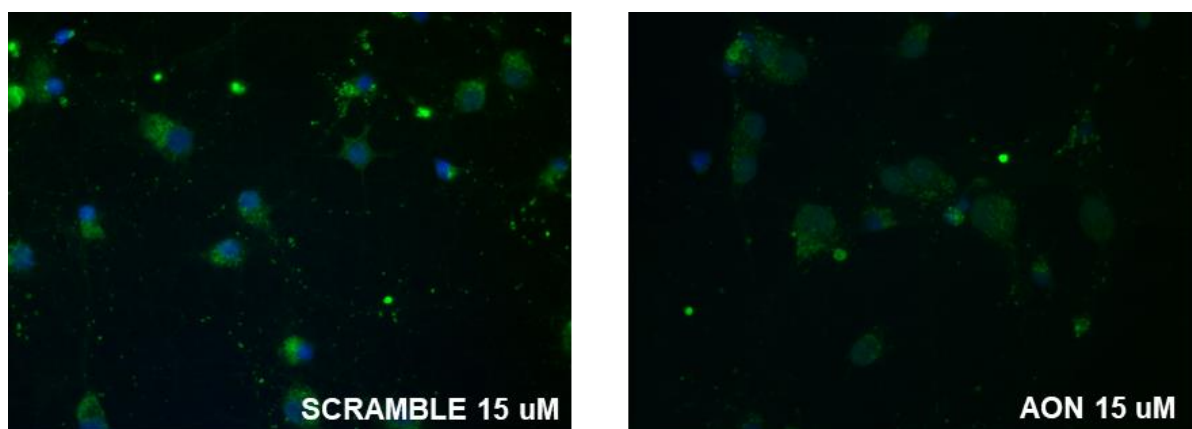
Figure 38. Fluorescent AONs are present in cultured cells. SHSY-5Y treated with fluorescent SCRAMBLE and AON-E8a 15 µM for 36 hrs. Images are acquired with a 20x objective at on the Eclipse Ni (Nikon) microscope.

In order to better understand the impact of the transient neuroLSD1 downregulation on the glutamatergic system we decided to check the effect of the AON on the spontaneous synaptic transmission in terms of mEPSCs and mIPSCs with an in vitro electrophysiological approach. We treated primary rat hippocampal neurons for 36 hrs with either the SCRAMBLE or the AON-E8a 15 µM. We could observe a decrease both in amplitude and frequency of mEPSCs when cultures are treated with the AON-E8a while mIPSCs are unaltered by the compound (FIG39A). In parallel we checked the efficiency of the AON on treated cultures with the rqfRT-PCR and found a significant downregulation of neuroLSD1 (FIG 39B).

A
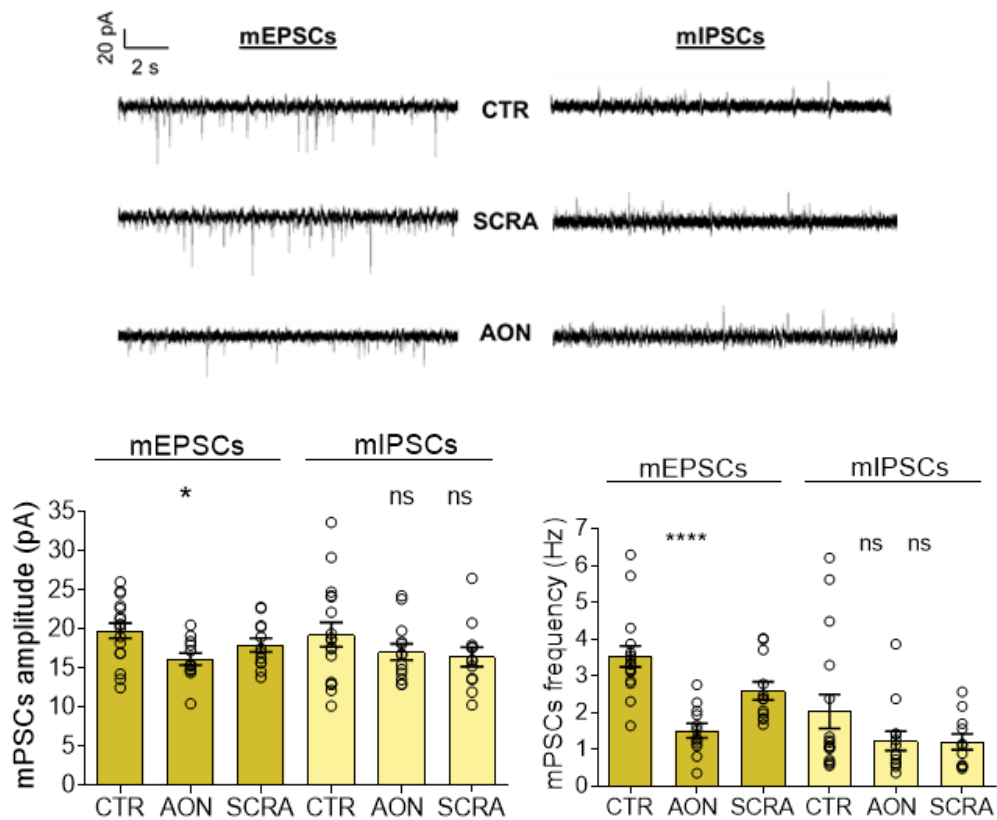
B
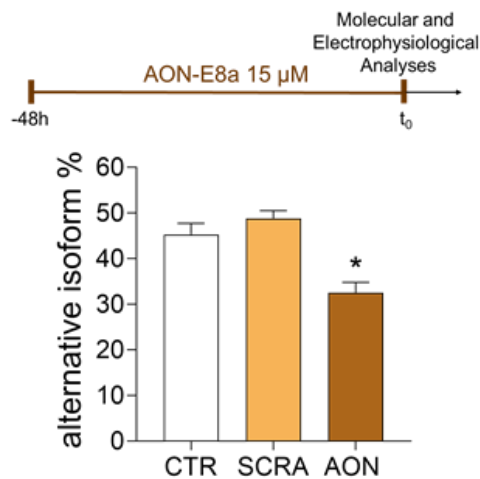
Figure 39. AON-E8a treatment negatively modulates basal glutamatergic transmission. (A) DIV 13 rat primary hippocampal neurons treated with AON-E8a and SCRAMBLE 15 µM for 36 hrs. Amplitude and frequency of mEPSCs and mIPSCs were analyzed. Example traces are shown. **(B)** Primary rat neuronal cultures treated with AON-E8a and SCRAMBLE 15 µM for 36 hrs. Samples were analyzed by rqfRT-PCR. Data are presented as means ± SEM. *p<0.05, ****p<0.00001, one-way ANOVA. All experiments were repeated at least three times.

These results highlight how the exogenous neuroLSD1 decrease induced by the AON-E8a in this in vitro system -therefore uncoupled from receptors activations which occur upon NMDA bath or environmental stress- negatively impacts the glutamatergic transmission in a similar way that can be obtained by eliciting homeostatic synaptic plasticity upon a sustained glutamate tone [85]. Furthermore, these data help to better understand that neuroLSD1 downregulation upon ASDS might by aimed at fine tuning the glutamatergic system, specifically reducing synaptic excitability.

4.1.6 Setting of in vivo hippocampal injections of AON-E8a in wild-type mice

Since in vitro experiments gave promising results, we decided to test the AON-E8a efficacy also in vivo. With the neuroLSD1 heterozygous and knock out mouse models we observed a memory impairment scored with the NOR. Therefore, we tried to recapitulate the alterations in memory consolidation using the AON-E8a in two-month-old wild-type mice. Mice were bilaterally stereotaxically injected in the dorsal hippocampus, since defects in this brain area are well evidenced with the NOR [81], with 50µM of either SCRAMBLE or AON-E8a. On the fifth day from the surgery we performed the familiarization, on the sixth the habituation and 24 hrs later the test – seven days after the surgery. We decided to evaluate the 24 hrs time point since we

wanted to check for possible long-term memory issues. We were not able to see any difference in memory consolidation between the two groups (SCRAMBLE vs AON-E8a) as reported in FIG 40A. We analyzed neuroLSD1 levels in the injection site (distal dorsal hippocampus) and also in the adjacent area, the medial dorsal hippocampus with a rqfRT-PCR. We did not observe any significant change in neuroSLD1 levels in the considered brain regions (FIG 40B).

A   **B**
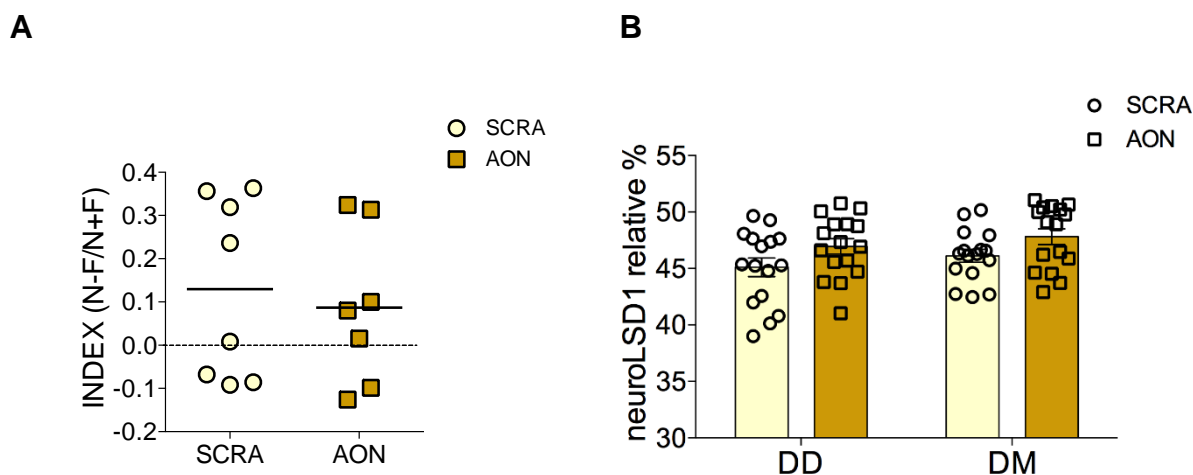
Figure 40. Setting of in vivo hippocampal injections of AON-E8a in wild-type mice. (A) The graph shows the discrimination index (N-F/N+F) of the NOR test performed 24 hrs after the exposure to the objects in the familiarization trial on 2-month-old male wild type mice stereotaxically injected in dorsal hippocampi with AON-E8a 50 µM or SCRAMBLE 50 µM. **(B)** Histogram showing neuroLSD1 relative percentage in the distal (DD) and medial (DM) dorsal hippocampus of 2-month-old male wild type mice stereotaxically injected with AON-E8a 50 µM or SCRAMBLE 50 µM. N=8 mice/treatment.

These negative results are probably due to a too low AON dose and the injection protocol. We will perform this experiment injecting a higher dose of AON with an implantable infusion micropump that allows a continuous flux of drug in the selected brain area [86].

4.1.7 LSD1 and neuroLSD1 splicing ratio modulation in the human hippocampus

In the last years the molecular characterization of LSD1 and neuroLSD1 role has been studied predominantly in neuronal primary cultures and in the mouse brain [28,30,34,35,36]. However, no one ever investigated their physiological and pathological relevance in the human brain. To address this question, we decided to analyze LSD1 and neuroLSD1 expression in human cerebral tissues, sampling post-

mortem female and male hippocampal specimens of different ages, ranging from young adults to elderly. We collected 10 female and 23 male hippocampal samples from 20 to 94 years old (table 4).

	Age group			
	20-39 y	40-59 y	60-79 y	≥80 y
Mean age y (± SEM)	31.80 (± 3.72)	51.78 (± 1.56)	70.92 (± 1.58)	88.0 (± 2.32)
Sex	4 males 1 female	7 males 2 females	8 males 4 females	4 males 3 females
Postmortem Interval h (± SEM)	54.60 (± 5.34)	38.56 (± 5.44)	41.63 (± 7.22)	14.57 (± 2.27)
RNA integrity number mean (± SEM)	5.54 (± 0.36)	5.96 (± 0.30)	5.47 (± 0.23)	5.03 (± 0.17)

TABLE 4. Post-mortem female and male hippocampal specimens of different ages. In the table few information are reported according to age groups: mean age (years), sex, post-mortem interval (hours) and RNA integrity number.

RNA extraction was performed starting from frozen tissues within post-mortem intervals ranging 15 to 55 hours to evaluate the presence and relative ratio of LSD1 splicing isoforms. Analyzing the samples with rqfRT-PCR, we found a statistically significant decrease in neuroLSD1 splicing isoforms along with aging in both male and female hippocampi as shown by linear regression analysis and comparing individuals pooled by age ranges with younger group (20-39-year-old) (FIG 41).
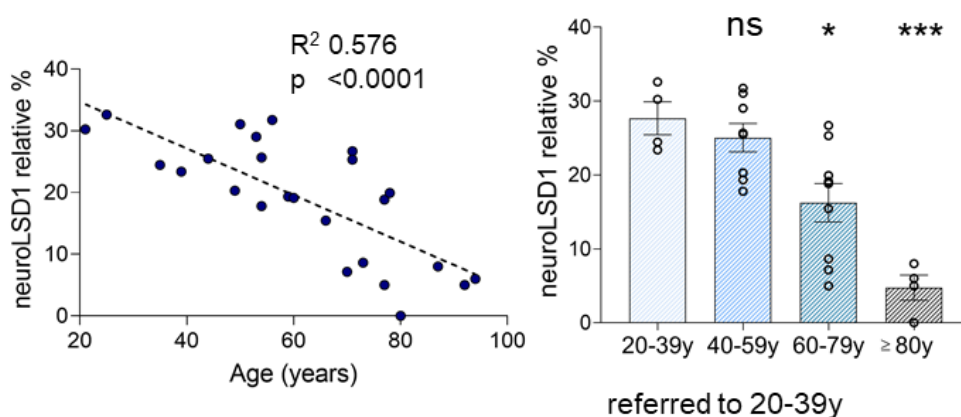
Figure 41. NeuroLSD1 relative expression in the hippocampus of male and female human post-mortem specimens ranging from 20 to 94 years of age. On the left, linear regression analysis of neuroLSD1 relative expression along with aging. **On the right**, rqfRT-PCR data clustered in age ranges. *Refers to the 20-39y group. Data are presented as means ± SEM. *$p < 0.01$, ***$p < 0.0001$, one-way ANOVA coupled to Tukey *post hoc* test.

In parallel we performed qRT-PCR on the same samples and we confirmed neuroLSD1 decrease during aging (FIG 42A). Worth of notice is the fact that above 70

years old, neuroLSD1 relative expression is almost absent. Total LSD1 transcripts levels, which have been measured with primers that do not discriminate the two splicing isoforms, revealed a similar though non-significant trend (FIG 42B). Interestingly, we did not score a gender effect of neuroLSD1 modulation, since the tendency towards a decrease in neuroLSD1 can be seen within male- and female-only clusters in the same way (FIG 42C).
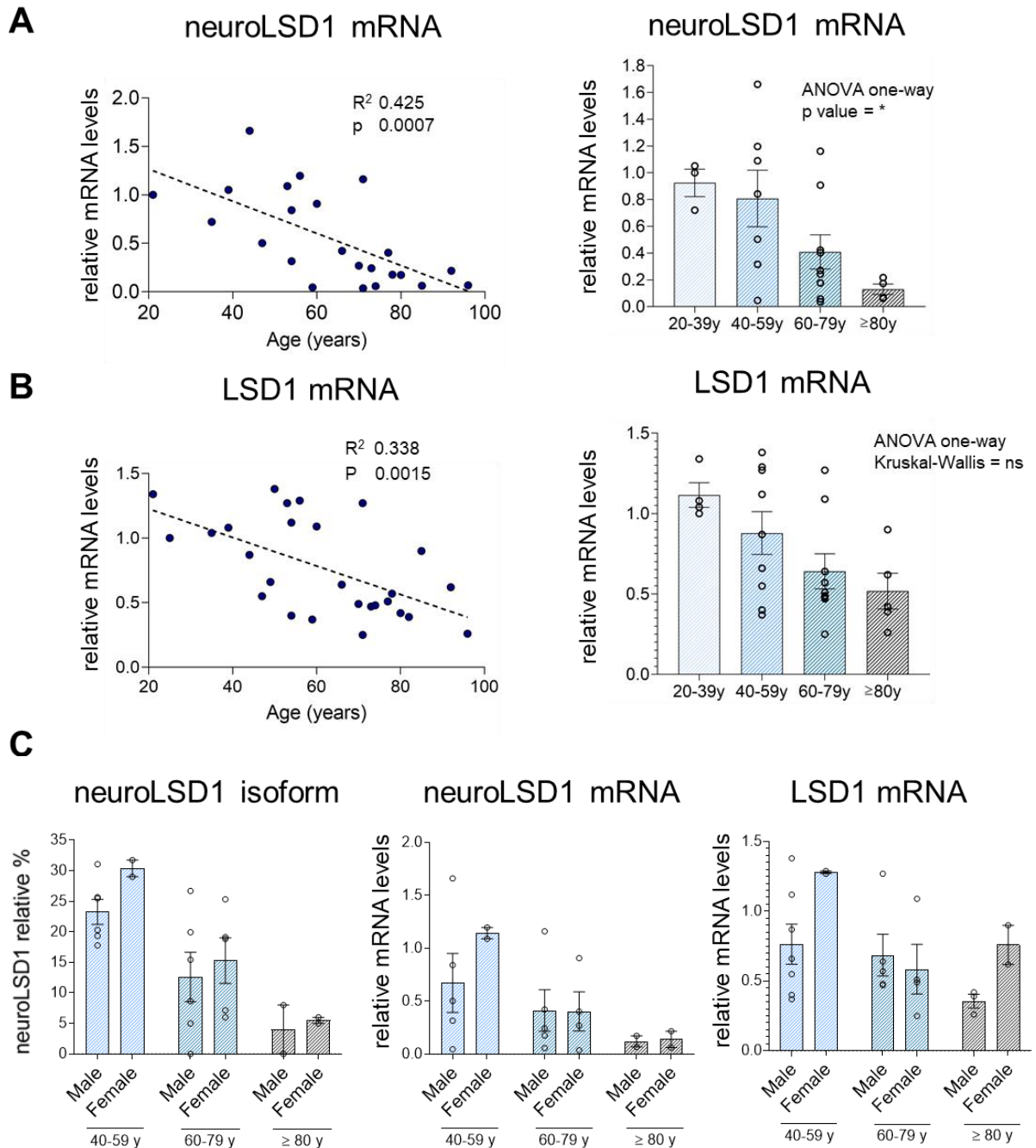
Figure 42. Along with aging, human hippocampi display a sharp neuroLSD1 decrease potentially contributing to the main signs of age including memory loss. (A) On the left, linear regression analysis linking neuroLSD1 expression, evaluated with qRT-PCR using isoform-specific primers, and age. **On the right,** data are

aggregated per age ranges. Data are presented as means $\pm$ SEM. *p<0.01; one-way ANOVA *Refers to the youngest group. **(B) On the left**, linear regression analysis linking total LSD1 isoforms expression, evaluated with qRT-PCR using primers that do not discriminate the different LSD1 splicing isoforms, and age. **On the right,** data are aggregated per age ranges. *Refers to the youngest group. **(C)** Male- and female-specific data aggregation does not show evident gender effects within the analyzed parameters. qRT-PCR data are normalized on RPL13, which we proved to be invariant along with human brain aging (not shown).

These are the first data collected from human samples showing that neuroLSD1 is present in human brains and that the splicing ratio between LSD1 isoforms is dynamic and changes along with aging. These results also seem to suggest that in elderly LSD1 is almost the only isoform present, therefore exerting a strong repressive activity on target genes. Further analyses are needed to investigate whether this event might be either protective or detrimental. Anyway, considering the impoverishment of dendritic spine morphology associated to neuroLSD1$^{-/-}$ mice, a possible stable neuroLSD1 downregulation in the human aging hippocampus well-correlates with known age-related neurostructural decline affecting both cortical and limbic structures, not to mention that neuroLSD1 decrease in the elderly's hippocampus likely contributes to hampering memory consolidation, a core aspect of aging.

4.2 Termination of acute stress response by the endocannabinoid system is regulated through LSD1-mediated transcriptional repression of 2-AG hydrolases ABHD6 and MAGL

4.2.1 Acute social defeat stress negatively regulates the levels of the two 2-AG degradative enzymes ABHD6 and MAGL

It has been demonstrated that acute environmental stress leads to the increase (tens of minutes after the paradigms) of the endocannabinoid 2-AG in the hippocampus [88], mPFC [87] and hypothalamus [89]. Several mechanisms cooperate to this rise for example on demand synthesis at the synapse [39], hormonal glucocorticoid-mediated regulation [90] and probably, transcriptional mechanisms. We focused our attention on the transcriptional processes that might be involved in the regulation of 2-AG upon stress in the murine hippocampus analyzing transcript and protein levels of ABHD6 and MAGL, which are the two main degradative enzymes of this endocannabinoid,

respectively at the post- and pre- synaptic compartments, and other enzymes and receptors involved in its metabolism and actions.

To do so we applied sessions of acute social defeat stress to wild-type male mice of two month since we know that this kind of behavioral paradigm induces the modulation of the ratio between LSD1 and neuroLSD1 isoforms [36]. As shown in FIG 43A, 2 hrs and 7 hrs after the beginning of the stress, neuroLSD1 is downregulated compared to controls. However, if experimental mice go back to their home cage after the 7 hrs session (7 hrs ASDS + 17 hrs resting) and therefore are analyzed 24 hrs from the beginning of the stress, neuroLSD1 levels are comparable to control levels. At these time points we analyzed by qRT-PCR and western blotting transcript and protein levels of ABHD6, MAGL, DAGLα which is the enzyme devoted to the synthesis of 2-AG, and CB1r, the post-synaptic receptor for 2-AG. Concerning Abhd6 and Mgll relative mRNA levels, we observed a decrease in their amount at the 7 hrs time point, concomitant with neuroLSD1 stress-induced downregulation (FIG 43B). Worth of notice is the fact that we did not observe any transcriptional changes after the 2 hrs stress, suggesting that the process requires a longer time interval. After 7 hrs of ASDS we observed a reduction in ABHD6 protein levels, while at this time point, no changes we detected for MAGL protein suggesting a probable higher MAGL protein stability (FIG 43B). Notably, along with recovery (ASDS 7 hr + resting), concomitantly with the splicing ratio between LSD1 isoforms returned to basal levels (FIG 43A), also ABHD6 and MAGL transcript levels go back to control levels (FIG 43B).
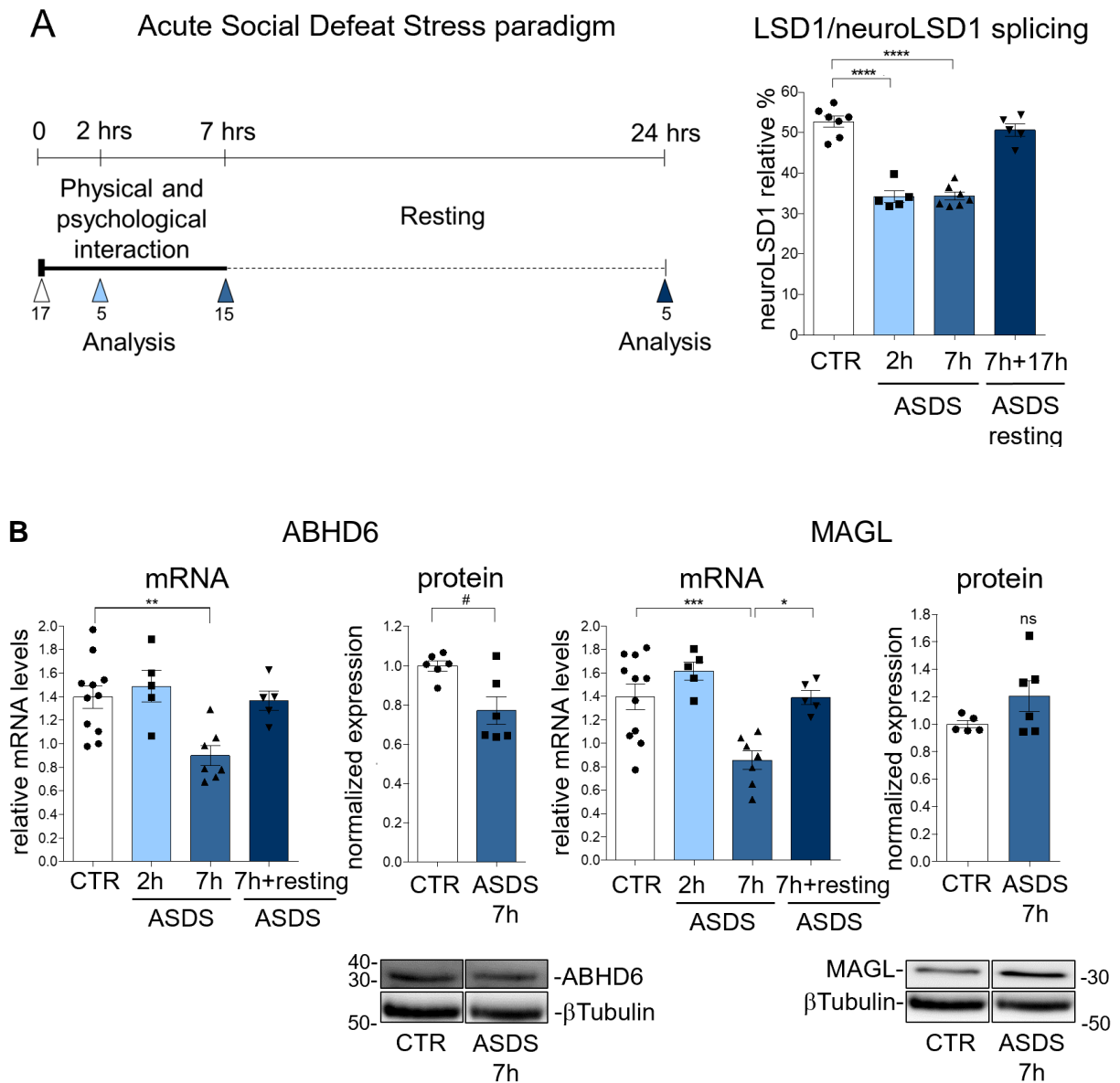
Figure 43. ASDS negatively regulates ABHD6 and MAGL transcript and protein levels. (A) On the left, a schematic representation of ASDS behavioral paradigm. Initial number of animals used for each group is indicated, this number also corresponds to the total number of animals. **On the right**, rqfRT-PCR showing the relative ratio of LSD1 isoforms upon ASDS (2 hrs, 7 hrs, 7 hrs + 17 hrs). **(B) On the left,** relative mRNA levels normalized over RPSA and protein levels normalized over βTubulin together with western blotting densitometry of ABHD6 upon ASDS. **On the right,** relative mRNA levels normalized over RPSA and protein levels normalized over βTubulin together with western blotting densitometry of MAGL upon ASDS. Results are shown as the mean ± SEM. *$p < 0.05$; **$p < 0.01$; ***$p < 0.001$, ****$p < 0.0001$ assessed with one-way ANOVA variance test. Tukey post-hoc test. #$p < 0.05$; assessed by Student t test.

Alongside with the above-mentioned enzymes, we also evaluated possible modifications in DAGLα and CB1R levels. As shown in FIG 44, we did not find any transcriptional alteration. However, we noticed that ASDS leads to other modifications of the ECS at the protein levels that are not related to transcriptional processes.

Indeed, both DAGLα and CB1R proteins are decreased upon ASDS probably through a post-translational mechanism (FIG 44).
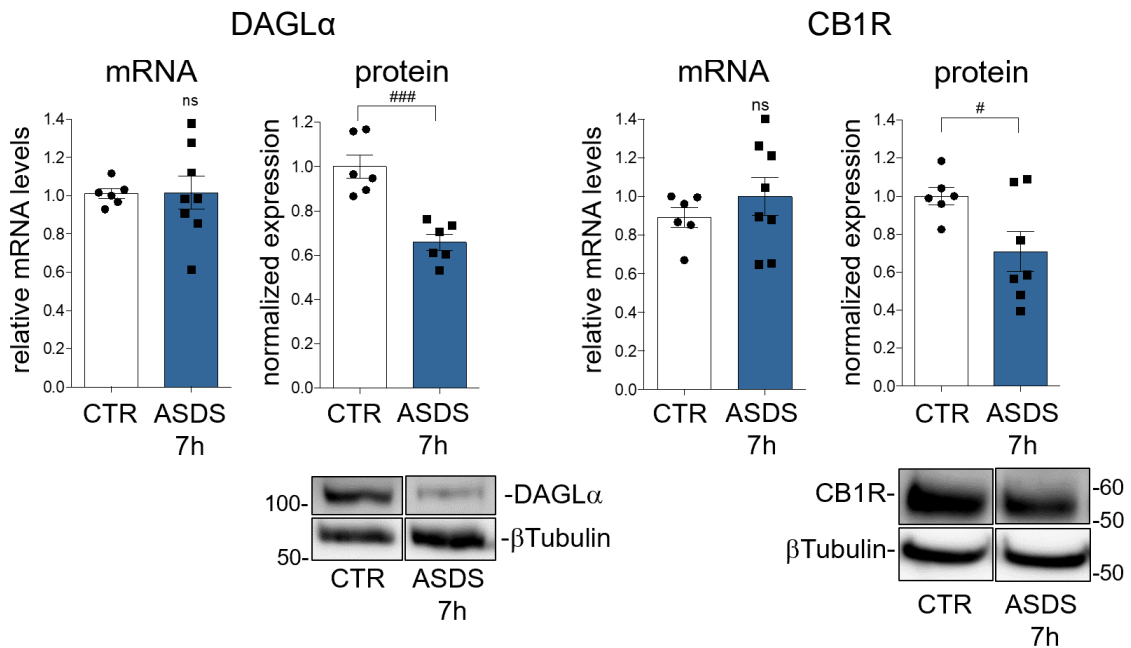
Figure 44. ASDS does not influence transcripts levels of DAGLα and CB1R. On the left, relative mRNA levels normalized over RPSA and protein levels normalized over βTubulin alongside with western blotting densitometry of DAGLα upon ASDS. **On the right,** relative mRNA levels normalized over RPSA and protein levels normalized over βTubulin alongside with western blotting densitometry of CB1R upon ASDS. Results are shown as the mean ± SEM. #$p < 0.05$, ### 0.001, assessed by Student t test.

Since the decrease in relative mRNA levels of the two degradative enzymes of 2-AG ABHD6 and MAGL occur concomitantly with a shift of the balance between LSD1 splicing isoforms in favor of the corepressor LSD1, we speculate that this epigenetic enzyme might play a role in this process.

4.2.2 The transcriptional corepressor LSD1 interacts with the promoter regions of Abhd6 and MgII genes

To further investigate a possible role for LSD1 in the transcriptional regulation of ABHD6 and MAGL, we decided to evaluate the association of this enzyme with the promoter regions of the two degradative enzymes. In order to do that we consulted available data sets from LSD1 ChIP-seq experiments previously performed in primary mouse neuronal cultures, deposited at the Genome Expression Omnibus (GEO) under the subseries entry GSE63271 [35]. Thanks to the analysis of these traces, we could

find an enrichment of LSD1 at the promoter regions of both Abhd6 and Mgll, close to the transcription start site (TSS) (FIG 45). At the same time, we investigated also Daglα and Cnr1 genes and, as expected, since we did not score any modulation upon ASDS, we did not observe any significant residency of LSD1 on their TSS (not shown).

Abhd6

Mgll
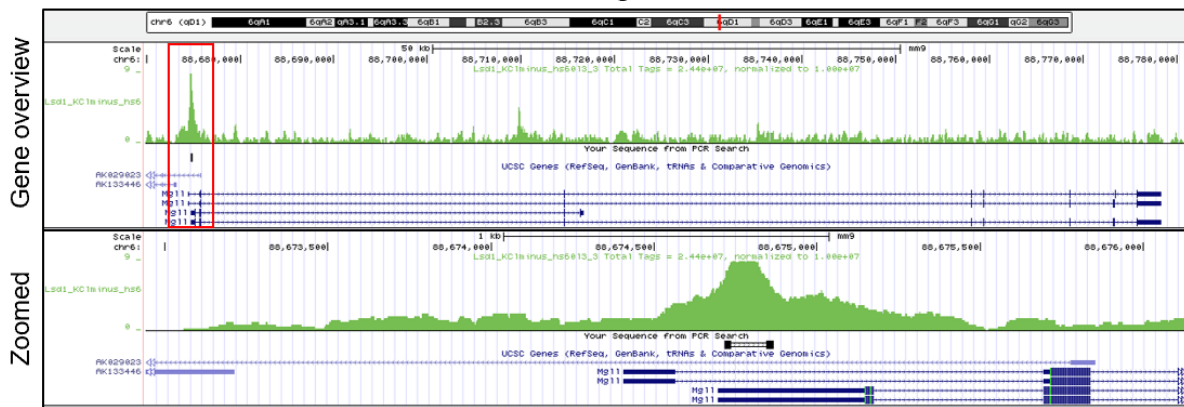
Figure 45. In silico analysis of LSD1 occupancy of Abhd6 and Mgll promoters. Custom LSD1 ChIP-seq tracks loaded on UCSC Genome Browser (Mouse genome, version July 2007, NCBI37 mm9). Wet data were obtained from mouse primary neuronal cultures [35]. **Upper panels** (gene overview), an overview of LSD1 association to Abhd6 and Mgll genes, in green. Boxed in red a detail of TSS flanking genomic regions of interest with LSD1 peaks. **Lower panels** (zoomed), magnification of higher LSD1 association peaks at the promoters. qRT-PCR amplicons used in our "candidate gene" Chromatin Immunoprecipitation (ChIP) analysis are shown.

Starting from these in silico data, we designed the primers to perform a ChIP followed by a qRT-PCR on the hippocampus of two-month-old wild-type mice since we wanted to verify if we could observe a similar association also in vivo. As shown in FIG X we observed a significant enrichment of LSD1 on both Abhd6 and Mgll promoter regions, corroborating the hypothesis that this epigenetic corepressor might play a role in the negative modulation of the degradative enzymes of 2-AG. The transcription factor REST/NRSF is one of the best characterized transcriptional repressors recruiting LSD1/CoREST corepressor complex on chromatin [21]. We checked whether we could

76

find an enrichment for this factor and actually we found a significant increase of REST occupancy in the same area of the promoter of Abhd6 that was used to analyze LSD1 interaction (FIG 46). This result seems to suggest that at least for Abhd6 gene, REST/NRSF might have a role in tethering LSD1 to its site of action at the DNA level.
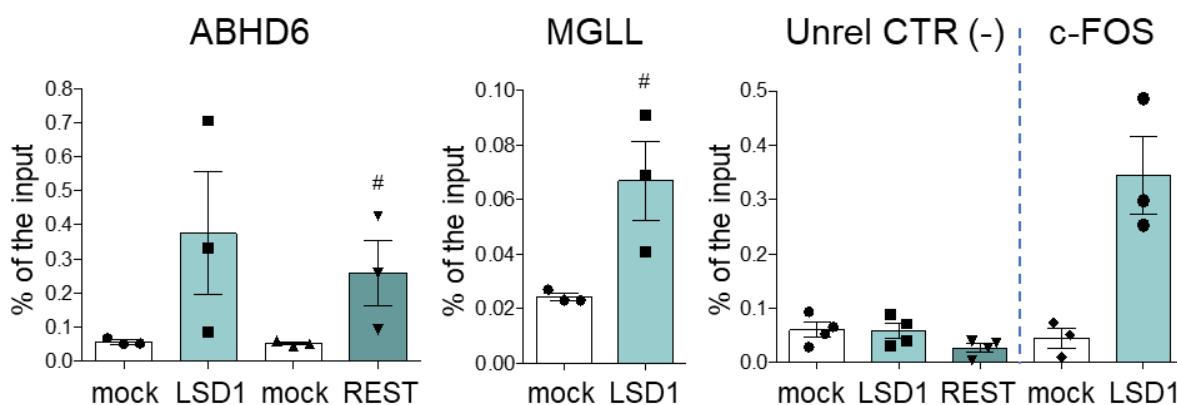
Figure 46. LSD1 interacts with the proximal promoter regions of Abhd6 and Mgll genes in the mouse hippocampus. ChIP followed by a qRT-PCR on Abhd6 and Mgll promoter regions scoring LSD1 and REST/NRSF associations to highlighted genomic regions. Enrichments over the Input condition are shown. Internal unrelated negative control is shown CTR (−) and positive controls taking as probe an already validated LSD1 target, c-fos [36] (n = 3–4 mice per condition). Results are shown as the mean ± SEM. #p < 0.05 assessed by Student's t test.

4.2.3 Lack of neuroLSD1 modulation hinders the transcriptional regulation of ABHD6 and MAGL upon stress

With the previous experiments we provided evidences of the possible involvement of LSD1 and neuroLSD1 in the transcriptional regulation of ABHD6 and MAGL showing that concomitantly to neuroLSD1 decrease (and LSD1 increase) upon ASDS, the mRNA levels of the two pre- and post-synaptic degradative enzymes of 2-AG are reduced. Moreover, we found a significant enrichment of LSD1 on the promoter regions of these two genes. In order to provide a causal relationship between LSD1 isoforms splicing ratio modulation and the alteration in the levels of ABHD6 and MAGL, we exploited neuroLSD1$^{-/-}$ mice, where the lack of neuroLSD1 leads to the impossibility to modulate the splicing since LSD1 is the only isoform present. In resting condition neuroLSD1$^{-/-}$ mice show decreased mRNA levels of both ABHD6 and MAGL, while a negative protein modulation can be found only for ABHD6. Such a discrepancy between mRNA and protein might suggest a compensatory post-translational mechanism restricted to MAGL, present in the genetically modified mouse (FIG 47).

These were the expected results since the pro-repressive isoform LSD1 is the only one present.
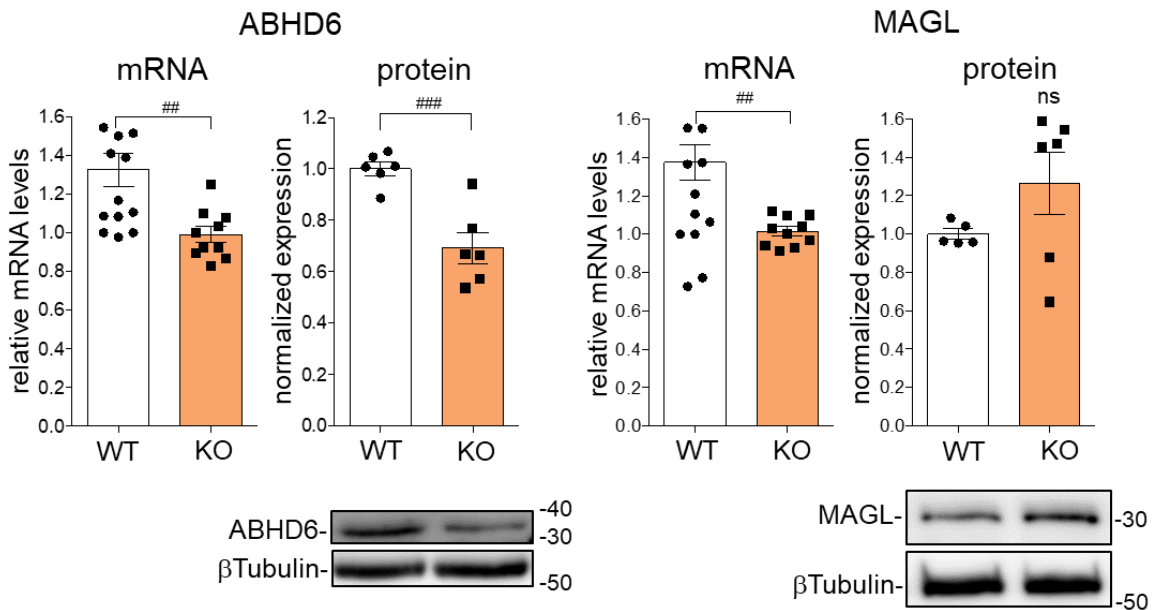
Figure 47. Lack of neuroLSD1 leads to a negative modulation of ABHD6 and MAGL in murine hippocampus in resting condition. Transcripts are expressed as relative mRNA levels, analyzed by qRT-PCR, normalized on RPSA. Protein band densitometry assessed as normalized values over β-tubulin and expressed as fold increase over CTR. 2-month-old male neuroLSD1^{-/-} mice compared to wild type littermates were analyzed (mRNA analyses n = 10–12, protein analyses n = 5–6 mice per condition). Results are shown as the mean ± SEM. ## p < 0.01, ### p < 0.001 assessed by Student's t test.

To strengthen our results, we decided to perform an ASDS in neuroLSD1^{-/-} mice. Upon a 7-hr-long session of social defeat stress we analyzed the expression of ABHD6 and MAGL in the hippocampi of stressed animals and we found that neither of the genes were modulated upon stress both at a transcript and a protein level (FIG 48). We can conclude that the transcriptional regulation that we observe for Abhd6 and Mgll upon ASDS requires splicing modulation of the two LSD1 isoforms. Altogether these data are consistent with a primary role of LSD1 gene function in reducing ABHD6 and MAGL mRNA levels upon stress in the hippocampus of naïve wild-type mice probably with the aim of sustaining eCB responses to the negative experiences.
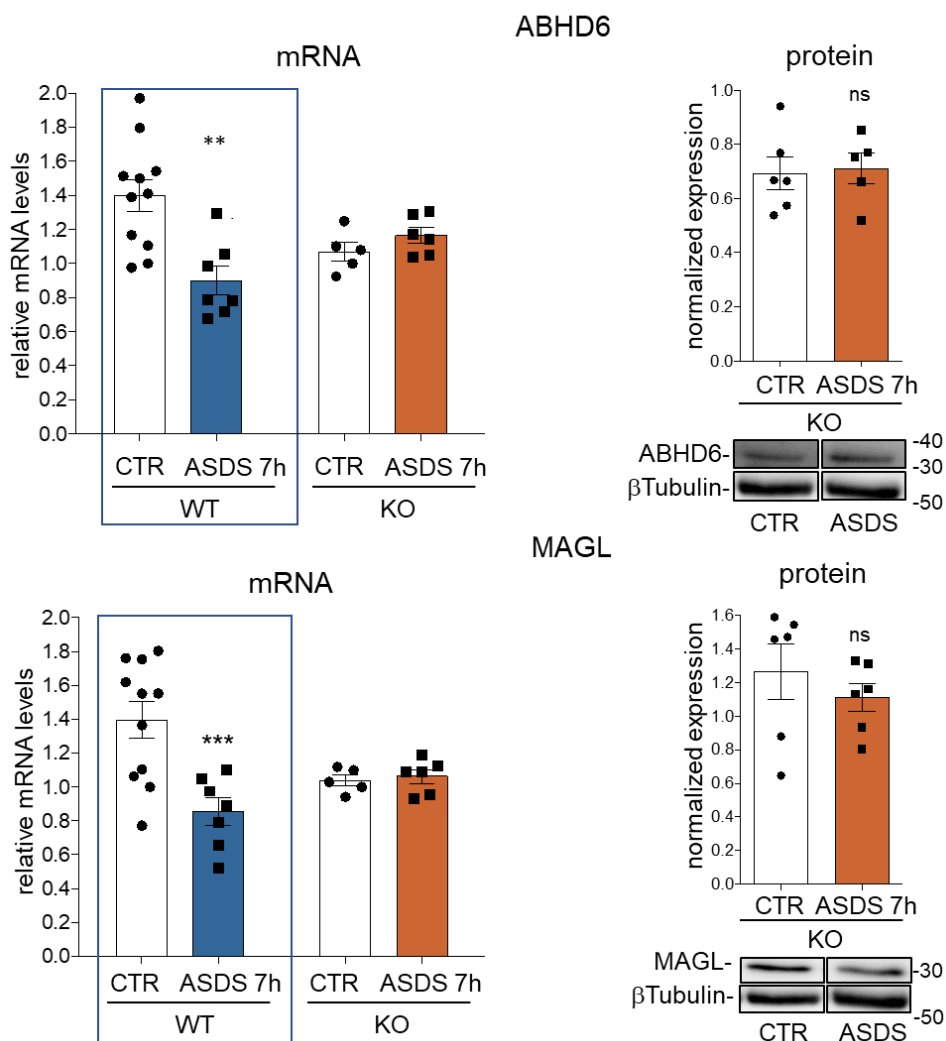
Figure 48. Lack of neuroLSD1 modulation upon stress in neuroLSD1$^{-/-}$ mice leads to the absence of transcriptional control of ABHD6 and MAGL. Comparison of ASDS-induced modulation of Abhd6 and Mgll mRNA levels in neuroLSD1$^{-/-}$ mice. Transcript expressed as relative mRNA levels, analyzed by qRT-PCR, normalized on RPSA. Protein band densitometry assessed as normalized values over β-tubulin and expressed as fold increase over CTR of 2-month-old male neuroLSD1$^{-/-}$ mice compared to wild type littermates; framed data has already been shown in FIG 43, re-plotted here as reference and included in the statistical comparison between WT and neuroLSD1$^{-/-}$ littermates (mRNA analyses n = 5–11 mice per condition) (protein analyses n = 5–6 mice per condition). Results are shown as the mean ± SEM. **p < 0.01 ***p < 0.001 assessed with two-way-ANOVA variance test. Tukey post-hoc test.

In parallel we performed the analyses on wild-type and neuroLSD1$^{-/-}$ mice upon stress also for the other enzymes involved in endocannabinoid metabolism. Notably, this particular stress paradigm seems not to modify expression of synthetic NAPE-PLD (N-acyl-phosphatidylethanolamine-hydrolyzing phospholipase D) and degradative FAAH (fatty acid amide hydrolase) enzymes of the other well-known eCB, anandamide nor

of the synthetic enzyme of 2-AG DAGLα or its presynaptic receptor CB1R as shown in FIG 49.
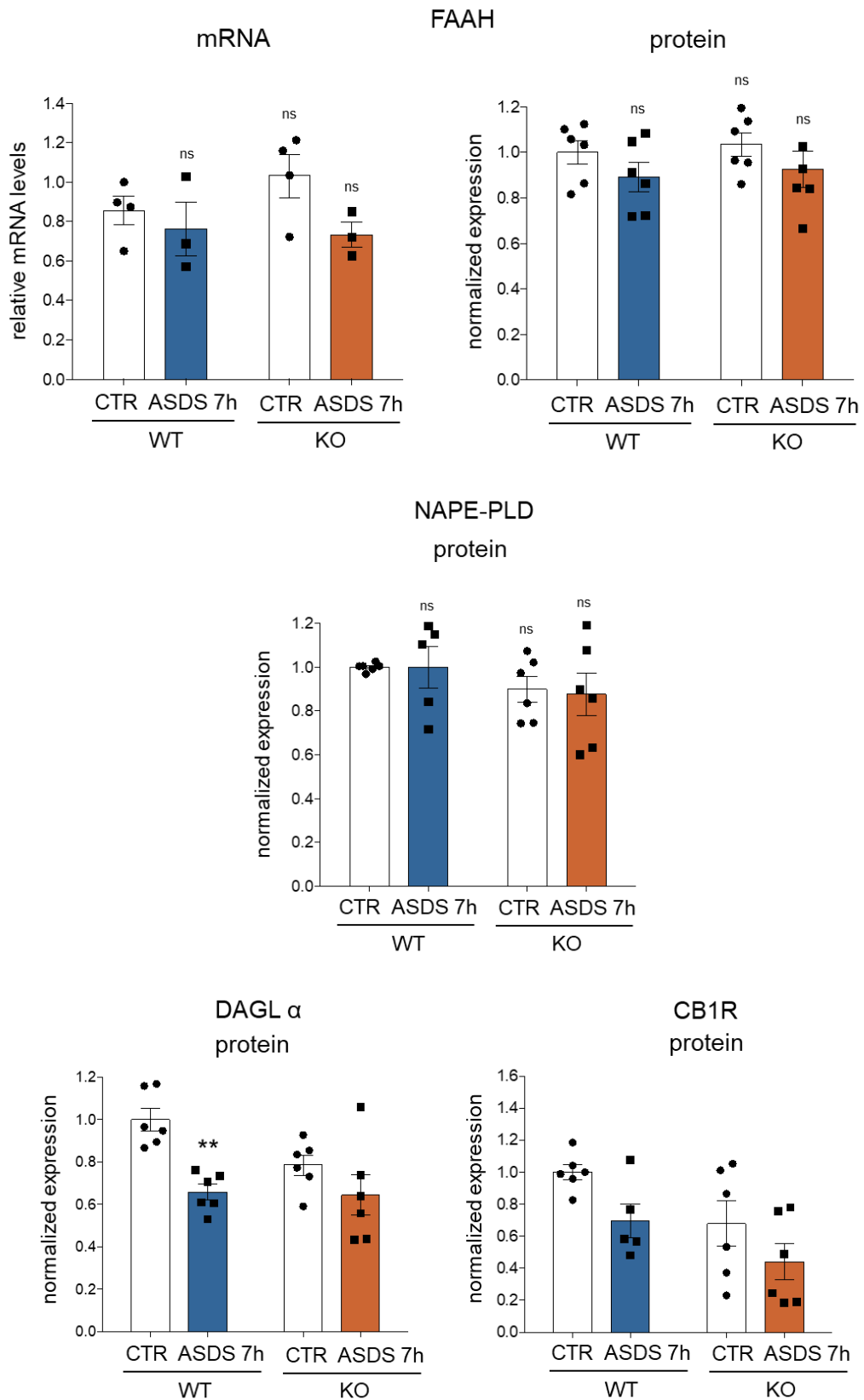
Figure 49. Lack of neuroLSD1 modulation upon stress in neuroLSD1$^{-/-}$ does not influence transcript and protein levels of other ECS enzymes. Comparison of ASDS-induced modulation of FAAH, NAPE-PLD, DAGLα

and CB1R mRNA and protein levels in neuroLSD1^{-/-} mice. Transcript expressed as relative mRNA levels, analyzed by qRT-PCR, normalized on RPSA. Protein band densitometry assessed as normalized values over β-tubulin and expressed as fold increase over CTR of 2-month-old male neuroLSD1^{-/-} mice compared to wild type littermates; (mRNA analyses n = 3-4 mice per condition) (protein analyses n = 5–6 mice per condition). Results are shown as the mean ± SEM. **p < 0.01 assessed with two-way-ANOVA variance test. Tukey post-hoc test.

4.2.4 Chronic social defeat stress less efficiently elicits neuroLSD1 downregulation, hindering transcriptional modulation of ABHD6 and MAGL

In recently published articles from our lab, based on our data and public literature we proposed that the typical adaptive modifications that occur upon acute stress, might be less efficiently elicited upon chronic stress [27,37]. Starting from this hypothesis we decided to perform a chronic social defeat stress (CSDS) and see if LSD1/neuroLSD1 balance is equally shifted towards a repressive layout as it happens upon acute stress. We modified the canonical CSDS in a way that after each daily 7-hour-long stress session, mice returned to their home cage (FIG 50). This resting phase allowed the ratio between LSD1 and neuroLSD1 to recover to control levels (CTR versus ASDS + resting in FIG 43). We observed the same phenomenon after the 9th session (CTR versus CSDS ×9 + resting in FIG 43) with LSD1/neuroLSD1 ratio recovered to resting values. However, after the 10th session of the CSDS protocol, neuroLSD1 downregulation (analyzed after the standard seven hour-long stress) is less efficiently induced. We observed that the ratio is still shifted towards an increase in LSD1 (CSDS ×9 + resting versus CSDS ×10 in FIG 50), but such a change is significantly reduced compared to the one that occurs during the first stress session (CTR versus ASDS in FIG 50).

Chronic Social Defeat Stress paradigm

LSD1/neuroLSD1 splicing
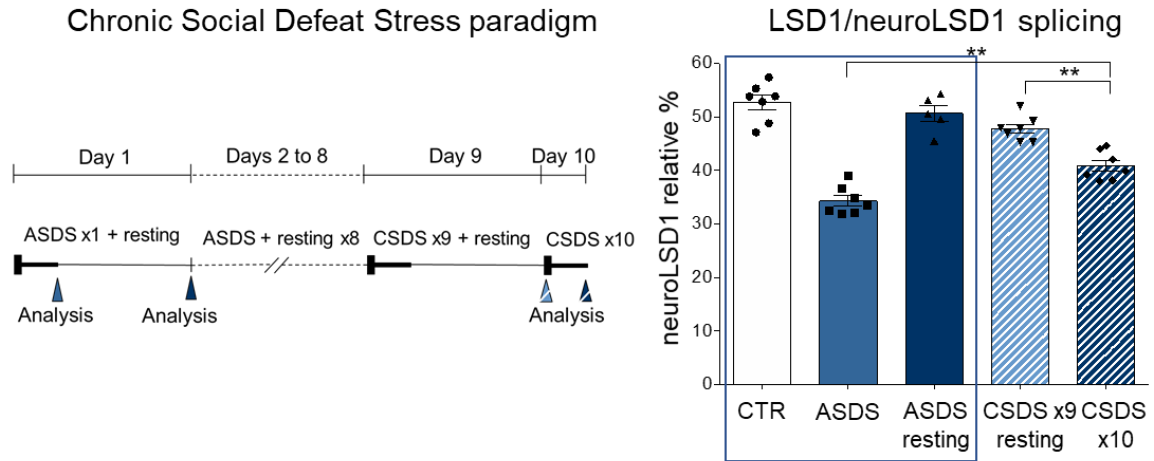
Figure 50. NeuroLSD1 downregulation is less efficiently elicited upon chronic stress. On the left, experimental scheme. **On the right,** rqf-RT-PCR evaluating LSD1 isoforms on hippocampi of acutely and chronically stressed mice. Framed are data relative to controls, 7 hour-long acute social defeat stress (ASDS)-treated mice and recovered from stress (ASDS plus resting) already showed in FIG 43, re-plotted here as reference and included in the statistical comparison (n = 5–7 mice per condition). Results are shown as the mean ± SEM. **p < 0.01; assessed with one-way-ANOVA variance test. Tukey post-hoc test.

Previously we showed that the negative transcriptional modulation of ABHD6 and MAGL that occurs upon ASDS is dependent on neuroLSD1 downregulation. Since the ratio modulation upon CSDS is disrupted we decided to check whether also targets levels might undergo a similar outcome. Consistently with our hypothesis, ABHD6 and MAGL levels do not change in response to the 10th stress session (FIG 51) further supporting a transcriptional causal relationship between LSD1 splicing modulation and eCB regulation.

Abhd6 mRNA

Mgll mRNA

Figure 51. LSD1-mediated transcriptional repression of ABHD6 and MAGL is lost upon chronic stress. Transcriptional evaluation of acute and chronic stress-mediated modulation of ABHD6 and MAGL analyzed with qRT-PCR normalized on RPSA (framed are data relative to controls and 7-hour-long ASDS treated mice, already showed in FIG 43, re-plotted here as reference and included in the statistical analysis) (n = 6–11 mice per condition). Results are shown as the mean ± SEM. **p < .01; assessed with one-way-ANOVA variance test. Tukey post-hoc test.
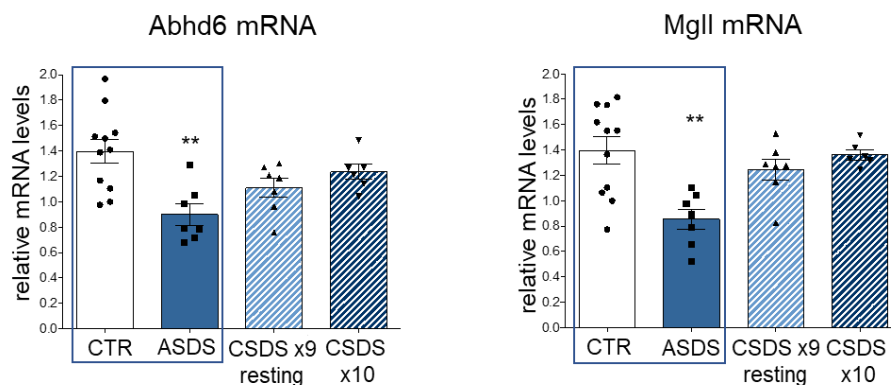
Based on these data, we can speculate two possible scenarios: (1) stress has elicited an adaptive habituation in a way that homeostatic splicing modulation is no longer required; (2) allostatic load associated to stress reiteration has desensitized LSD1-based mechanisms devoted to limiting the toxic effects of stress. Other experiments are needed to identify the functional meaning of this molecular event however, in line with both interpretations, upon CSDS ABHD6 and MAGL lose their tunability, possibly limiting 2-AG contribution to stress termination.

5 DISCUSSION

5.1 LSD1, an environment and aging-sensitive negative modulator of the glutamatergic synapse

According to our results a picture emerges in which upon environmental stress, mechanisms aimed at associating contextual cues to aversive paradigms occur [93,94] but, concomitantly, a protective neurospecific epigenetic homeostatic process is engaged. This is mediated by the decrease of neuroLSD1, an enhancer of neuroplasticity, through a splicing-based event [36,83]. Our in vitro and in vivo data seem to suggest that neuroLSD1 downregulation might have a role in reducing the excitability of glutamatergic synapses via a negative feedback mechanism, since its decrease is directly induced by the activation of NMDA receptors by glutamate. In this light, it is worth noticing that LSD1 isoforms tunability upon stress acts as a coincident detector of synaptic and extrasynaptic NMDAr stimulation [95], indeed bicuculline treatment alone is not able to induce neuroLSD1 downregulation while NMDA bath application can. Therefore the simultaneous stress-induced activation of both subsets of NMDAr leads to neuroLSD1 decrease pushing the system towards an homeostatic synaptic plasticity directed downwards which might be interpreted with an adaptive meaning, in the light of anxiolytic effects of neuroLSD1 deletion in vivo [36,37]. This hypothesis is corroborated by the fact that when neuroLSD1 is absent, neuroplastic processes aimed at increasing neuronal excitatory responses, like LTP, are impaired, as it happens upon acute stress where formation, consolidation, and memory retrieval are temporarily occluded [95,96]. Interestingly neuroLSD1 downregulation and the altered LTP occur concomitantly upon stress in the murine hippocampus [95,36]. Furthermore LTP counterpart, known as LTD, is instead facilitated by an environmental stress, since it requires the activation of both synaptic and extrasynaptic NMDAr [84], as shown also by the induction of chemical LTD in vitro applying an NMDA bath stimulation [79,80].

Human post-mortem data add value to our results since we observe that LSD1 isoforms are present in the hippocampus and that their balance is dynamic along with aging, as it happens in mice. Moreover, this observation might help a deeper comprehension of the functional implications of neuroLSD1 decrease. It is clear that

the progressive downregulation of neuroLSD1 in the aging hippocampus is just one of the many molecular events that take place, however it is worth considering that a hypofunctional drift at the cellular, circuital, and behavioral level, might actually concur to age-related neuropsychiatric disorders like frailty. Nevertheless, it might be that neuroLSD1 decrease/LSD1 increase play a neuroprotective role, hampering neuroplastic processes at the expenses of cognition and flexibility, in order to preserve the system.

Interestingly, another core molecular event of human aging is the upregulation of the transcriptional repressor REST. In recent studies it has been established that REST has a role in preserving neuronal survival and extending lifespan, played more by the increase of its function rather than of its levels [97,98]. In this light REST corepressors, such as LSD1, CoREST and HDAC2, could act enhancing REST repressive activity on synaptic genes promoting a circuitry shift of E/I ratio towards reduced excitability [97,98]. The data here reported that sustain this hypothesis, phenocopied by neuroLSD1 genetic and pharmacological deletion, are also further corroborated by already published results [30].

5.2 Termination of acute stress response by the endocannabinoid system is regulated through LSD1-mediated transcriptional repression of 2-AG hydrolases ABHD6 and MAGL

Upon stress the ratio between LSD1 splicing isoforms is shifted towards a pro-repressive layout [36,23] in hippocampal neurons, in a process aimed at decreasing IEGs activation, and consequent activity-induced plasticity, in a homeostatic fashion [37]. Our results show how that, at the same time, neuroLSD1 downregulation also has an impact on the two main enzymes involved in 2-AG clearance, ABHD6 and MAGL, decreasing their transcriptional levels, in a window in which stress induces the increase of 2-AG [99,100,101]. We hypothesize that the transcriptional control performed by LSD1 on ABHD6 and MAGL in the time window we analyzed (seven hours after the beginning of the behavioral paradigm) allows a fine, mild and continuous modulation of the 2-AG tone in such a way to contribute to enhancing CB1R stimulation upon acute stress.

On the other hand it is known that CB1r incurs in desensitization when 2-AG levels are too high or are increased for a long time [102]. In this light it is interesting to focus on LSD1 isoforms transient modulation upon chronic stress since this might contribute to physiologically limit CB1R desensitization. Another relevant feature is that neuroLSD1 is expressed only in neurons since glial cells express only LSD1 [28]. This means that LSD1/neuroLSD1-mediated modulation of 2-AG skips glial contribution [103], known to be pivotal in degrading 2-AG, supporting the hypothesis of a highly controlled pathway to increase 2-AG concentration. The aforementioned features highlight a role for LSD1/neuroLSD1 as fine tuners of the endocannabinoid system guaranteeing a balance in boosting 2-AG activity while preventing CB1R desensitization.

Our data show for the first time a connection between two pathways involved in buffering stress transduction: a synaptic homeostatic mechanism represented by the ECS, whose main function is guarding the system from excessive stimulation, and a nuclear mechanism, the LSD1 splicing isoforms modulation, known to be implicated in neuroplasticity-related transcriptional homeostasis [23,27,36 37]. With LSD1 ability to regulate the transcription of important ECS genes, we were able to highlight a further role for LSD1 in stress transduction, strengthening the implication of a LSD1-mediated epigenetic regulation in cognitive and emotional brain adaptation to the environment.

Recently the role of 2-AG in ending stress response has been extensively revised [38,39], nevertheless it has been highlighted that this lipidic mediator is also instrumental to stress resiliency. Systemic increase of 2-AG in stress-susceptible mice enhances resiliency while lack of 2-AG and/or CB1r blockade turn resilient mice into susceptible [104]. Importantly, JZL184, a MAGL inhibitor which heightens 2-AG content by preventing its degradation, exerts an acute anxiolytic effect in basal but especially upon stressful behavioral paradigms. However, the chronic administration of this compound leads to a rapid 2-AG-dependent CB1r desensitization and consequent worsening of anxiety, dramatically reducing its therapeutic potential in the treatment of stress-induced psychopathologies [102,105]. A better understanding of 2-AG dynamic modulation during the physiological stress response might open new possibilities to pharmacologically treat stress-induced psychiatric disorders. Concerning this, knowing the molecular mechanisms that regulate ABHD6 and MAGL might be a promising way to design new strategies to exogenously control 2-AG levels in stress susceptible individuals who underwent mental illnesses.

Upon a chronic stress the homeostatic mechanisms devoted to face these stressors can be disrupted due to allostatic load in vulnerable individuals. In this context, upon chronic stress reiteration, the tunability of the ratio between LSD1 and neuroLSD1 is less efficient at the tenth stress session. According to these data the decrease of neuroLSD1 might be accounted among the adaptive molecular events that can be jeopardized and eventually abolished by chronic stress. Actually at the tenth session of social defeat stress, when the relative amount of LSD1 and neuroLSD1 is only weakly modified, the transient negative modulation of transcriptional levels of ABHD6 and MAGL is lost, with the functional perspective of impeding the otherwise adaptive 2-AG up-regulation. Moreover it must be considered that stress can be accounted as one of the most prominent precipitating factors of drug addiction [106], therefore lack of homeostatic mechanisms, including LSD1 role in increasing 2-AG tone, might induce THC seeking as a surrogate of the shortening of endogenous 2-AG. At this point the rupture of LSD1-neuroLSD1 homeostatic rheostat upon chronic stress, that ultimately affects the pro-resiliency rise of 2-AG [38], is likely linked to stress susceptibility and addictive behaviors.

Intriguingly we found that the transcriptional repressor REST/NRSF, that is known to interact with LSD1/CoREST/ HDAC1/2 complex [107], can be found on the promoter region of Abhd6 together with LSD1 in the mouse hippocampus. REST is known to repress neuronal genes in non-neuronal cells, nevertheless this protein has relevant functions also in the brain. Recently, some papers described REST/NRSF involvement in brain protection from detrimental effects of epileptic excitotoxicity [97,108,109]. Environmental stress is able to induce glutamate spillover from dendritic spines of hippocampal pyramidal neurons activating extrasynaptic NMDAr, which resembles the alterations observed in excitotoxic epileptic discharges [94]. Therefore we propose that REST/NRSF in complex with LSD1 might perform an homeostatic activity in response to both epileptic and psychiatric-relevant stimuli. In this light it must be taken into account that epilepsy and neuropsychiatric disorders including anxiety and depression are often comorbid. We could not find the same association to Magl promoter region but this might be due to the fact that REST binding might take place in other sites within gene promoter. Nevertheless LSD1 is able to interact with other transcription factors [110,111], and even directly to target DNA without any mediation [112], justifying the action on functionally convergent pathways of 2-AG degradation.

In the hippocampus, upon acute stress, LSD1 act decreasing the degradative enzymes of 2-AG at the mRNA and protein levels, representing a physiological, innate fine-tuning mechanism to increase 2-AG activity. Taken together, our data indicate that the pharmacological regulation of LSD1 splicing isoforms might represent a new approach to regulate 2-AG without recurring to direct degrading enzymes inhibition. The use of AON-based pharmacological strategies to induce exon skipping are already used in research [113,114] and are a therapeutic option for some diseases such as the Spinal Muscular Atrophy (SMA) [115,116] and Duchenne Muscular Dystrophy (DMD) [117]. However drug intracerebral delivery is a complex and invasive process. In this light the AON-based approach used to decrease neuroLSD1 splicing isoforms might instead considered as a useful tool to validate neuroLSD1 targets. This could lead to the development of specific non-invasive neuroLSD1 inhibitors that could represent a promising opportunity to treat long-term behavioral signs due to chronic stress, simply sustaining a physiological process of stress coping that is susceptible to allostatic load.

6 CONCLUSIONS

During my PhD I was able to show two novel molecular homeostatic mechanisms mediated by LSD1 splicing isoforms that are engaged upon psychosocial stress. Based on our results a picture emerges in which, when a stressful event occurs and glutamatergic neurotransmission is engaged in the hippocampus via activation of the NMDAr, concomitantly, the ratio between LSD1 isoforms is shifted towards a repressive layout with the increase of LSD1 and the decrease of neuroLSD1.

We think that this nuclear event might participate in a complex negative feedback mechanism aimed at decreasing stress-induced glutamatergic signaling in the hippocampus, participating to stress termination and possibly to the buffering of memory consolidation. We hypothesize that this negative feedback mechanism mediated by neuroLSD1 decrease is engaged by the activation of NMDA receptors in the hippocampus and that their downstream signaling reduces neuroLSD1 amount. This hypothesis is supported by in vitro and in vivo experimental data, indeed blockade of the NMDAr with MK-801 hampers neuroLSD1 downregulation (FIG 34D, 35).

A schematic version of our hypothesis is reported in figure 52. In detail, the ability of the AON to induce neuroLSD1 downregulation with a consequent negative modulation of basal glutamatergic transmission in terms of frequency and amplitude of mEPSCs (FIG 39A), a less responsive PSD from a biochemical, electrophysiological and structural point of view in neuroLSD1$^{-/-}$ mice (FIG 26, 30-32), and the decrease of the degradative enzymes of 2-AG upon stress, concur to corroborate the hypothesis that the reduction of neuroLSD1 could be considered as a homeostatic negative feedback mechanism engaged by stress-induced glutamate release aimed at restraining glutamatergic neurotransmission and plasticity.
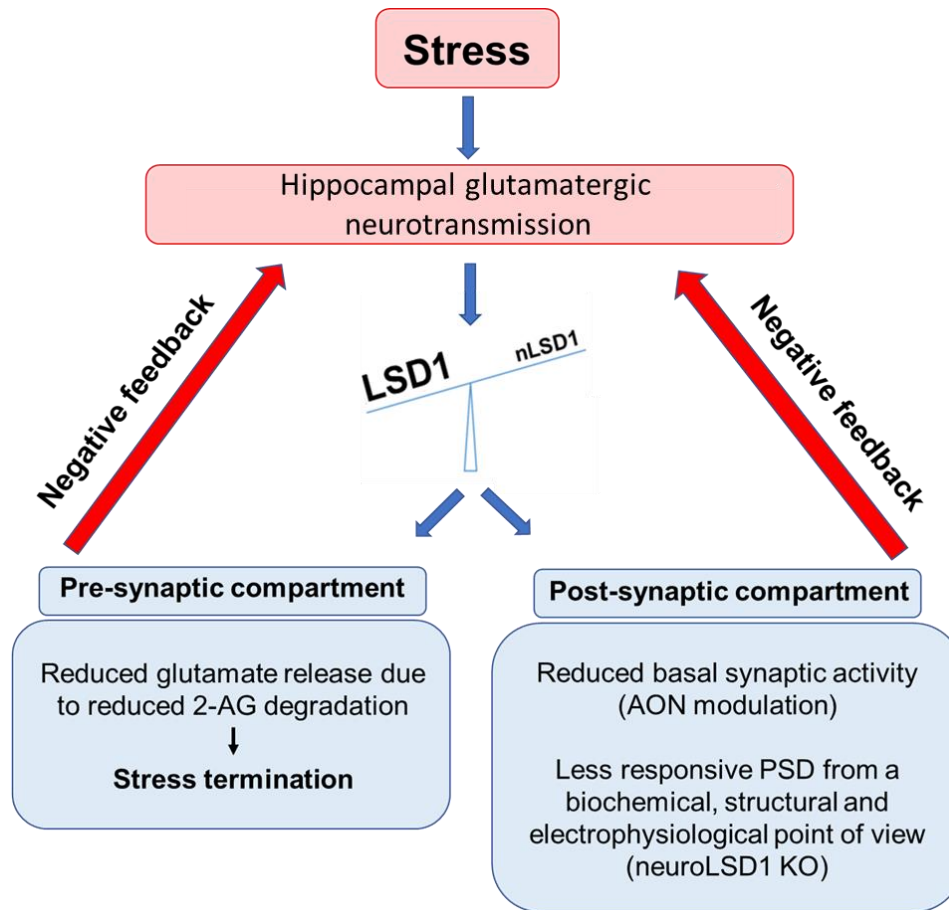
Figure 52. Schematic representation of the project findings. Upon stress, glutamate is released in the hippocampus and NMDAr are engaged. This event leads to neuroLSD1 downregulation affecting the pre-synaptic and post-synaptic compartments in a negative feedback mechanism aimed at buffering glutamatergic neurotransmission

7 REFERENCES

1. Gold PW. The organization of the stress system and its dysregulation in depressive illness. *Mol Psychiatry*. 2015;20(1):32-47. doi:10.1038/mp.2014.163

2. McEwen BS. Neurobiological and Systemic Effects of Chronic Stress. *Chronic Stress (Thousand Oaks)*. 2017;1:2470547017692328. doi:10.1177/2470547017692328

3. Sapolsky RM. Stress and the brain: individual variability and the inverted-U. *Nat Neurosci*. 2015;18(10):1344-1346. doi:10.1038/nn.4109

4. Joëls M, Baram TZ. The neuro-symphony of stress. *Nat Rev Neurosci*. 2009;10(6):459-466. doi:10.1038/nrn2632

5. Italia M, Forastieri C, Longaretti A, Battaglioli E, Rusconi F. Animal models of environmental stress: underlying rationale and relevance to understanding neuropsychiatric disorders. Under submission International Journal of Molecular Sciences

6. Timmermans W, Xiong H, Hoogenraad CC, Krugers HJ. Stress and excitatory synapses: from health to disease. *Neuroscience*. 2013;248:626-636. doi:10.1016/j.neuroscience.2013.05.043

7. Popoli M, Yan Z, McEwen BS, Sanacora G. The stressed synapse: the impact of stress and glucocorticoids on glutamate transmission. *Nat Rev Neurosci*. 2011;13(1):22-37. Published 2011 Nov 30. doi:10.1038/nrn3138

8. Chattarji S, Tomar A, Suvrathan A, Ghosh S, Rahman MM. Neighborhood matters: divergent patterns of stress-induced plasticity across the brain. *Nat Neurosci*. 2015;18(10):1364-1375. doi:10.1038/nn.4115

9. Kim JJ, Diamond DM. The stressed hippocampus, synaptic plasticity and lost memories. *Nat Rev Neurosci*. 2002;3(6):453-462. doi:10.1038/nrn849

10. Christian KM, Miracle AD, Wellman CL, Nakazawa K (2011). Chronic stress-induced hippocampal dendritic retraction requires CA3 NMDA receptors. Neuroscience 174:26–36.

11. McEwen BS, Nasca C, Gray JD. Stress Effects on Neuronal Structure: Hippocampus, Amygdala, and Prefrontal Cortex. *Neuropsychopharmacology.* 2016;41(1):3-23. doi:10.1038/npp.2015.171

12. Cook SC, Wellman CL (2004). Chronic stress alters dendritic morphology in rat medial prefrontal cortex. J Neurobiol 60: 236–248

13. Liston C, Miller MM, Goldwater DS, Radley JJ, Rocher AB et al (2006). Stress-induced alterations in prefrontal cortical dendritic morphology predict selective impairments in perceptual attentional set-shifting. J Neurosci 26: 7870–7874.

14. Radley JJ, Rocher AB, Janssen WGM, Hof PR, McEwen BS, Morrison JH (2005). Reversibility of apical dendritic retraction in the rat medial prefrontal cortex following repeated stress. Exp Neurol 196: 199–203.

15. Radley JJ, Sisti HM, Hao J, Rocher AB, McCall T et al (2004). Chronic behavioral stress induces apical dendritic reorganization in pyramidal neurons of the medial prefrontal cortex. Neuroscience 125:1–6.

16. Bloss EB, Janssen WG, McEwen BS, Morrison JH (2010). Interactive effects of stress and aging on structural plasticity in the prefrontal cortex. J Neurosci 30: 6726–6731.

17. Goldwater DS, Pavlides C, Hunter RG, Bloss EB, Hof PR et al (2009). Structural and functional alterations to rat medial prefrontal cortex following chronic restraint stress and recovery. Neuroscience 164: 798–808.

18. Gray JD, Rubin TG, Hunter RG, McEwen BS (2014). Hippocampal gene expression changes underlying stress sensitization and recovery. Mol Psychiatry 19:1171–1178.

19. Vyas, A., Pillai, A.G. & Chattarji, S. Recovery after chronic stress fails to reverse amygdaloid neuronal hypertrophy and enhanced anxiety-like behavior. Neuroscience 128, 667–673 (2004).

20. Mitra, R., Jadhav, S., McEwen, B.S., Vyas, A. & Chattarji, S. Stress duration modulates the spatiotemporal patterns of spine formation in the basolateral amygdala. Proc. Natl. Acad. Sci. USA 102, 9371–9376 (2005).

21. Shi Y, Lan F, Matson C, et al. Histone demethylation mediated by the nuclear amine oxidase homolog LSD1. *Cell.* 2004;119(7):941-953. doi:10.1016/j.cell.2004.12.012

22. Chen Y, Yang Y, Wang F, et al. Crystal structure of human histone lysine-specific demethylase 1 (LSD1). *Proc Natl Acad Sci U S A.* 2006;103(38):13956-13961. doi:10.1073/pnas.0606381103

23. Rusconi F, Grillo B, Toffolo E, Mattevi A, Battaglioli E. NeuroLSD1: Splicing-Generated Epigenetic Enhancer of Neuroplasticity. *Trends Neurosci.* 2017;40(1):28-38. doi:10.1016/j.tins.2016.11.002

24. Forneris F, Binda C, Battaglioli E, Mattevi A. LSD1: oxidative chemistry for multifaceted functions in chromatin regulation. *Trends Biochem Sci.* 2008;33(4):181-189. doi:10.1016/j.tibs.2008.01.003

25. Forneris F, Binda C, Vanoni MA, Battaglioli E, Mattevi A. Human histone demethylase LSD1 reads the histone code. *J Biol Chem.* 2005;280(50):41360-41365. doi:10.1074/jbc.M509549200

26. Battaglioli E, Andrés ME, Rose DW, et al. REST repression of neuronal genes requires components of the hSWI.SNF complex. *J Biol Chem.* 2002;277(43):41038-41045. doi:10.1074/jbc.M205691200

27. Gerosa L, Grillo B, Forastieri C, et al. SRF and SRFΔ5 Splicing Isoform Recruit Corepressor LSD1/KDM1A Modifying Structural Neuroplasticity and Environmental

Stress Response. *Mol Neurobiol*. 2020;57(1):393-407. doi:10.1007/s12035-019-01720-8

28. Zibetti C, Adamo A, Binda C, et al. Alternative splicing of the histone demethylase LSD1/KDM1 contributes to the modulation of neurite morphogenesis in the mammalian nervous system. *J Neurosci*. 2010;30(7):2521-2532. doi:10.1523/JNEUROSCI.5500-09.2010

29. Toffolo E, Rusconi F, Paganini L, et al. Phosphorylation of neuronal Lysine-Specific Demethylase 1LSD1/KDM1A impairs transcriptional repression by regulating interaction with CoREST and histone deacetylases HDAC1/2. *J Neurochem*. 2014;128(5):603-616. doi:10.1111/jnc.12457

30. Rusconi F, Paganini L, Braida D, et al. LSD1 Neurospecific Alternative Splicing Controls Neuronal Excitability in Mouse Models of Epilepsy. *Cereb Cortex*. 2015;25(9):2729-2740. doi:10.1093/cercor/bhu070

31. Longaretti A, Forastieri C, Toffolo E, Caffino L, Locarno A, Misevičiūtė I, Marchesi E, Battistin M, Ponzoni L, Madaschi L, Cambria C, Bonasoni P, Sala M, Perrone D, Fumagalli F, Bassani S, Antonucci F, Tonini R, Francolini M, Battaglioli E and Rusconi F. LSD1, an environment and aging-sensitive negative modulator of the glutamatergic synapse. Accepted at Neurobiology of Stress. 2020

32. Harris WJ, Huang X, Lynch JT, et al. The histone demethylase KDM1A sustains the oncogenic potential of MLL-AF9 leukemia stem cells [published correction appears in Cancer Cell. 2012 Jun 12;21(6):856]. *Cancer Cell*. 2012;21(4):473-487. doi:10.1016/j.ccr.2012.03.014

33. Whyte WA, Bilodeau S, Orlando DA, et al. Enhancer decommissioning by LSD1 during embryonic stem cell differentiation [published correction appears in Nature. 2018 Oct;562(7728):E24]. *Nature*. 2012;482(7384):221-225. Published 2012 Feb 1. doi:10.1038/nature10805

34. Laurent B, Ruitu L, Murn J, et al. A specific LSD1/KDM1A isoform regulates neuronal differentiation through H3K9 demethylation. *Mol Cell.* 2015;57(6):957-970. doi:10.1016/j.molcel.2015.01.010

35. Wang J, Telese F, Tan Y, et al. LSD1n is an H4K20 demethylase regulating memory formation via transcriptional elongation control. *Nat Neurosci.* 2015;18(9):1256-1264. doi:10.1038/nn.4069

36. Rusconi F, Grillo B, Ponzoni L, et al. LSD1 modulates stress-evoked transcription of immediate early genes and emotional behavior. *Proc Natl Acad Sci U S A.* 2016;113(13):3651-3656. doi:10.1073/pnas.1511974113

37. Rusconi F, Battaglioli E. Acute Stress-Induced Epigenetic Modulations and Their Potential Protective Role Toward Depression. *Front Mol Neurosci.* 2018;11:184. Published 2018 May 31. doi:10.3389/fnmol.2018.00184

38. Morena M, Patel S, Bains JS, Hill MN. Neurobiological Interactions Between Stress and the Endocannabinoid System. *Neuropsychopharmacology.* 2016;41(1):80-102. doi:10.1038/npp.2015.166

39. Lutz B, Marsicano G, Maldonado R, Hillard CJ. The endocannabinoid system in guarding against fear, anxiety and stress. *Nat Rev Neurosci.* 2015;16(12):705-718. doi:10.1038/nrn4036

40. Green B, Kavanagh D, Young R (2003). Being stoned: a review of self-reported cannabis effects. Drug Alcohol Rev 22: 453–460.

41. Bellocchio L, Soria-Gomez E, Quarta C, Metna-Laurent M, Cardinal P, Binder E et al (2013). Activation of the sympathetic nervous system mediates hypophagic and anxiety-like effects of CB(1) receptor blockade. Proc Natl Acad Sci USA 110: 4786–4791

42. Friemel CM, Zimmer A, Schneider M (2014). The CB1 receptor as an important mediator of hedonic reward processing. Neuropsychopharmacology 39:2387–2396.

43. Haller J, Varga B, Ledent C, Freund TF (2004). CB1 cannabinoid receptors mediate anxiolytic effects: convergent genetic and pharmacological evidence with CB1-specific agents. Behav Pharmacol 15: 299–304.

44. Marsicano G, Wotjak CT, Azad SC, Bisogno T, Rammes G, Cascio MG et al (2002). The endogenous cannabinoid system controls extinction of aversive memories. Nature 418: 530–534.

45. Patel S, Roelke CT, Rademacher DJ, Cullinan WE, Hillard CJ (2004). Endo-cannabinoid signaling negatively modulates stress-induced activation of the hypothalamic-pituitary-adrenal axis. Endocrinology 145: 5431–5438.

46. Sanchis-Segura C, Cline BH, Marsicano G, Lutz B, Spanagel R (2004). Reduced sensitivity to reward in CB1 knockout mice. Psychopharmacology (Berl) 176: 223–232.

47. Santucci V, Storme JJ, Soubrie P, Le Fur G (1996). Arousal-enhancing properties of the CB1 cannabinoid receptor antagonist SR 141716A in rats as assessed by electroencephalographic spectral and sleep-waking cycle analysis. Life Sci 58: PL103–PL110.

48. Shonesy BC, Bluett RJ, Ramikie TS, Baldi R, Hermanson DJ, Kingsley PJ et al (2014). Genetic disruption of 2-arachidonoylglycerol synthesis reveals a key role for endocannabinoid signaling in anxiety modulation. Cell Rep 9:1644–1653.

49. Tallett AJ, Blundell JE, Rodgers RJ (2007). Grooming, scratching and feeding: role of response competition in acute anorectic response to rimonabant in male rats. Psychopharmacology (Berl) 195:27–39.

50. Varvel SA, Lichtman AH (2002). Evaluation of CB1 receptor knockout mice in the Morris water maze. J Pharmacol Exp Ther 301: 915–924

51. Hill MN, McLaughlin RJ, Pan B, Fitzgerald ML, Roberts CJ, Lee TT et al (2011). Recruitment of prefrontal cortical endocannabinoid signaling by glucocorticoids contributes to termination of the stress response. J Neurosci 31: 10506–10515.

52. Wang M, Hill MN, Zhang L, Gorzalka BB, Hillard CJ, Alger BE (2012). Acute restraint stress enhances hippocampal endocannabinoid function via glucocorticoid receptor activation. J Psychopharmacol 26:56–70.

53. Evanson NK, Tasker JG, Hill MN, Hillard CJ, Herman JP (2010). Fast feedback inhibition of the HPA axis by glucocorticoids is mediated by endocannabinoid signaling. Endocrinology 151: 4811–4819.

54. Haller J, Bakos N, Szirmay M, Ledent C, Freund TF. The effects of genetic and pharmacological blockade of the CB1 cannabinoid receptor on anxiety. *Eur J Neurosci.* 2002;16(7):1395-1398. doi:10.1046/j.1460-9568.2002.02192.x

55. Hill MN, Hillard CJ, McEwen BS. Alterations in corticolimbic dendritic morphology and emotional behavior in cannabinoid CB1 receptor-deficient mice parallel the effects of chronic stress. *Cereb Cortex.* 2011;21(9):2056-2064. doi:10.1093/cercor/bhq280

56. Martin M, Ledent C, Parmentier M, Maldonado R, Valverde O. Involvement of CB1 cannabinoid receptors in emotional behaviour. *Psychopharmacology (Berl).* 2002;159(4):379-387. doi:10.1007/s00213-001-0946-5

57. Mikics E, Vas J, Aliczki M, Halasz J, Haller J. Interactions between the anxiogenic effects of CB1 gene disruption and 5-HT3 neurotransmission. *Behav Pharmacol.* 2009;20(3):265-272. doi:10.1097/FBP.0b013e32832c70b1

58. Urigüen L, Pérez-Rial S, Ledent C, Palomo T, Manzanares J. Impaired action of anxiolytic drugs in mice deficient in cannabinoid CB1 receptors. *Neuropharmacology.* 2004;46(7):966-973. doi:10.1016/j.neuropharm.2004.01.003

59. Plendl W, Wotjak CT. Dissociation of within- and between-session extinction of conditioned fear. *J Neurosci.* 2010;30(14):4990-4998. doi:10.1523/JNEUROSCI.6038-09.2010

60. Jenniches I, Ternes S, Albayram O, et al. Anxiety, Stress, and Fear Response in Mice With Reduced Endocannabinoid Levels. *Biol Psychiatry.* 2016;79(10):858-868. doi:10.1016/j.biopsych.2015.03.033

61. Atsak P, Hauer D, Campolongo P, Schelling G, McGaugh JL, Roozendaal B. Glucocorticoids interact with the hippocampal endocannabinoid system in impairing retrieval of contextual fear memory. *Proc Natl Acad Sci U S A.* 2012;109(9):3504-3509. doi:10.1073/pnas.1200742109

62. Colombo G, Rusconi F, Rubino T, et al. Transcriptomic and proteomic analyses of mouse cerebellum reveal alterations in RasGRF1 expression following in vivo chronic treatment with delta 9-tetrahydrocannabinol. *J Mol Neurosci.* 2009;37(2):111-122. doi:10.1007/s12031-008-9114-2

63. Spreafico M, Grillo B, Rusconi F, Battaglioli E, Venturin M. Multiple Layers of *CDK5R1* Regulation in Alzheimer's Disease Implicate Long Non-Coding RNAs. *Int J Mol Sci.* 2018;19(7):2022. Published 2018 Jul 11. doi:10.3390/ijms19072022

64. Zapata J, Moretto E, Hannan S, et al. Epilepsy and intellectual disability linked protein Shrm4 interaction with GABA$_B$Rs shapes inhibitory neurotransmission. *Nat Commun.* 2017;8:14536. Published 2017 Mar 6. doi:10.1038/ncomms14536

65. Folci A, Murru L, Vezzoli E, et al. Myosin IXa Binds AMPAR and Regulates Synaptic Structure, LTP, and Cognitive Function. *Front Mol Neurosci.* 2016;9:1. Published 2016 Jan 20. doi:10.3389/fnmol.2016.00001

66. Caffino L, Piva A, Giannotti G, et al. Ketamine Self-Administration Reduces the Homeostasis of the Glutamate Synapse in the Rat Brain. *Mol Neurobiol.* 2017;54(9):7186-7193. doi:10.1007/s12035-016-0231-6

67. Zamberletti E, Gabaglio M, Piscitelli F, et al. Cannabidivarin completely rescues cognitive deficits and delays neurological and motor defects in male *Mecp2* mutant mice. *J Psychopharmacol.* 2019;33(7):894-907. doi:10.1177/0269881119844184

68. Wang J, Telese F, Tan Y, et al. LSD1n is an H4K20 demethylase regulating memory formation via transcriptional elongation control. *Nat Neurosci.* 2015;18(9):1256-1264. doi:10.1038/nn.4069

69. Rimessi P, Sabatelli P, Fabris M, Braghetta P, Bassi E, Spitali P, et al. Cationic PMMA nanoparticles bind and deliver antisense oligoribonucleotides allowing restoration of dystrophin expression in the mdx mouse. Mol Ther. 2009;17(5):820-7. doi: 10.1038/mt.2009.8.

70. Capobianco ML, Barbarella G, Manetto A. Oligothiophenes as fluorescent markers for biological applications. Molecules. 2012;17(1):910-33. doi: 10.3390/molecules17010910.

71. Baralle D, Baralle M. Splicing in action: assessing disease causing sequence changes. J Med Genet. 2005;42(10):737-48. doi: 10.1136/jmg.2004.029538

72. Golden SA, Covington HE 3rd, Berton O, Russo SJ. A standardized protocol for repeated social defeat stress in mice [published correction appears in Nat Protoc. 2015 Apr;10(4):643]. *Nat Protoc.* 2011;6(8):1183-1191. Published 2011 Jul 21. doi:10.1038/nprot.2011.361

73. Leonzino M, Ponzoni L, Braida D, et al. Impaired approach to novelty and striatal alterations in the oxytocin receptor deficient mouse model of autism. *Horm Behav.* 2019;114:104543. doi:10.1016/j.yhbeh.2019.06.007

74. Pitsikas N, Rigamonti AE, Cella SG, Locatelli V, Sala M, Muller EE. Effects of molsidomine on scopolamine-induced amnesia and hypermotility in the rat. *Eur J Pharmacol.* 2001;426(3):193-200. doi:10.1016/s0014-2999(01)01164-5

75. Le François et al. A Novel Alternative Splicing Mechanism That Enhances Human 5-HT1A Receptor RNA Stability Is Altered in Major Depression. J. Neurosci. 2018. 38(38):8200–8210

76. Pfaffl MW, Tichopad A, Prgomet C, Neuvians TP. Determination of stable housekeeping genes, differentially regulated target genes and sample integrity: BestKeeper--Excel-based tool using pairwise correlations. Biotechnol Lett. 2004;26(6):509-15. doi: 10.1023/b:bile.0000019559.84305.47

77. Borczyk, M., Śliwińska, M.A., Caly, A., Bernas, T., and Radwanska, K. (2019). Neuronal plasticity affects correlation between the size of dendritic spine and its postsynaptic density. Sci Rep *9*, 1693.

78. Malenka, R.C., and Bear, M.F. (2004). LTP and LTD: an embarrassment of riches. Neuron *44*, 5-21.

79. Sheng, M., and Ertürk, A. (2014). Long-term depression: a cell biological view. Philos Trans R Soc Lond B Biol Sci *369*, 20130138.

80. Li, Z., Jo, J., Jia, J.M., Lo, S.C., Whitcomb, D.J., Jiao, S., Cho, K., and Sheng, M. (2010). Caspase-3 activation via mitochondria is required for long-term depression and AMPA receptor internalization. Cell *141*, 859-871.

81. Howland JG, Harrison RA, Hannesson DK, Phillips AG. Ventral hippocampal involvement in temporal order, but not recognition, memory for spatial information. *Hippocampus*. 2008;18(3):251-257. doi:10.1002/hipo.20396

82. Hardingham GE, Fukunaga Y, Bading H. Extrasynaptic NMDARs oppose synaptic NMDARs by triggering CREB shut-off and cell death pathways. Nat Neurosci. 2002;5(5):405-14. doi: 10.1038/nn835.

83. Longaretti A, Forastieri C, Gabaglio M, Rubino T, Battaglioli E, Rusconi F. Termination of acute stress response by the endocannabinoid system is regulated through lysine-specific demethylase 1-mediated transcriptional repression of 2-AG

hydrolases ABHD6 and MAGL [published online ahead of print, 2020 Mar 5]. *J Neurochem.* 2020;10.1111/jnc.15000. doi:10.1111/jnc.15000

84. Papouin T, Ladépêche L, Ruel J, Sacchi S, Labasque M, Hanini M, et al. Synaptic and extrasynaptic NMDA receptors are gated by different endogenous coagonists. Cell. 2012;150(3):633-46. doi: 10.1016/j.cell.2012.06.029.

85. Xu, X., and Pozzo-Miller, L. (2017). EEA1 restores homeostatic synaptic plasticity in hippocampal neurons from Rett syndrome mice. J Physiol *595*, 5699-5712.

86. Sztainberg Y, Chen HM, Swann JW, et al. Reversal of phenotypes in MECP2 duplication mice using genetic rescue or antisense oligonucleotides. *Nature.* 2015;528(7580):123-126. doi:10.1038/nature16159

87. Hill, M. N., McLaughlin, R. J., Pan, B., Fitzgerald, M. L., Roberts, C. J., Lee, T.-T.-Y., … Hillard, C. J. (2011). Recruitment of prefrontal cortical endocannabinoid signaling by glucocorticoids contributes to termination of the stress response. Journal of Neuroscience, 31, 10506– 10515. https://doi.org/10.1523/JNEUR OSCI.0496-11.2011

88. Wang, M., Hill, M. N., Zhang, L., Gorzalka, B. B., Hillard, C. J., & Alger, B. E. (2012). Acute restraint stress enhances hippocampal endocannabinoid function via glucocorticoid receptor activation. Journal of Psychopharmacology, 26, 56–70. https://doi.org/10.1177/02698 81111 409606

89. Evanson, N. K., Tasker, J. G., Hill, M. N., Hillard, C. J., & Herman, J. P. (2010). Fast feedback inhibition of the HPA axis by glucocorticoids is mediated by endocannabinoid signaling. Endocrinology, 151, 4811– 4819. https://doi.org/10.1210/en.2010-0285

90. Atsak, P., Hauer, D., Campolongo, P., Schelling, G., McGaugh, J. L., & Roozendaal, B. (2012). Glucocorticoids interact with the hippocampal endocannabinoid system in impairing retrieval of contextual fear memory. Proceedings of the National Academy

of Sciences of the United States of America, 109, 3504–3509. https://doi.org/10.1073/ pnas.12007 42109

91. Shi, Y., Lan, F., Matson, C., Mulligan, P., Whetstine, J. R., Cole, P. A., … Shi, Y. (2004). Histone demethylation mediated by the nuclear amine oxidase homolog LSD1. Cell, 119, 941–953. https://doi.org/10.1016/j. cell.2004.12.012

92. Gupta S, Kim SY, Artis S, et al. Histone methylation regulates memory formation. *J Neurosci*. 2010;30(10):3589-3599. doi:10.1523/JNEUROSCI.3732-09.2010

93. Alarcón JM, Malleret G, Touzani K, et al. Chromatin acetylation, memory, and LTP are impaired in CBP+/- mice: a model for the cognitive deficit in Rubinstein-Taybi syndrome and its amelioration. *Neuron*. 2004;42(6):947-959. doi:10.1016/j.neuron.2004.05.021

94. Yang CH, Huang CC, Hsu KS. Behavioral stress enhances hippocampal CA1 long-term depression through the blockade of the glutamate uptake. *J Neurosci*. 2005;25(17):4288-4293. doi:10.1523/JNEUROSCI.0406-05.2005

95. Diamond DM, Campbell AM, Park CR, Halonen J, Zoladz PR. The temporal dynamics model of emotional memory processing: a synthesis on the neurobiological basis of stress-induced amnesia, flashbulb and traumatic memories, and the Yerkes-Dodson law. *Neural Plast*. 2007;2007:60803. doi:10.1155/2007/60803

96. Zoladz PR, Campbell AM, Park CR, Schaefer D, Danysz W, Diamond DM. Enhancement of long-term spatial memory in adult rats by the noncompetitive NMDA receptor antagonists, memantine and neramexane. *Pharmacol Biochem Behav*. 2006;85(2):298-306. doi:10.1016/j.pbb.2006.08.011

97. Zullo JM, Drake D, Aron L, et al. Regulation of lifespan by neural excitation and REST. *Nature*. 2019;574(7778):359-364. doi:10.1038/s41586-019-1647-8

98. Lu T, Aron L, Zullo J, et al. Addendum: REST and stress resistance in ageing and Alzheimer's disease. *Nature*. 2016;540(7633):470. doi:10.1038/nature20579

99. Evanson NK, Tasker JG, Hill MN, Hillard CJ, Herman JP. Fast feedback inhibition of the HPA axis by glucocorticoids is mediated by endocannabinoid signaling. *Endocrinology*. 2010;151(10):4811-4819. doi:10.1210/en.2010-0285

100. Hill MN, McLaughlin RJ, Pan B, et al. Recruitment of prefrontal cortical endocannabinoid signaling by glucocorticoids contributes to termination of the stress response. *J Neurosci*. 2011;31(29):10506-10515. doi:10.1523/JNEUROSCI.0496-11.2011

101. Wang M, Hill MN, Zhang L, Gorzalka BB, Hillard CJ, Alger BE. Acute restraint stress enhances hippocampal endocannabinoid function via glucocorticoid receptor activation. *J Psychopharmacol*. 2012;26(1):56-70. doi:10.1177/0269881111409606

102. Schlosburg JE, Blankman JL, Long JZ, et al. Chronic monoacylglycerol lipase blockade causes functional antagonism of the endocannabinoid system. *Nat Neurosci*. 2010;13(9):1113-1119. doi:10.1038/nn.2616

103. Savinainen JR, Saario SM, Laitinen JT. The serine hydrolases MAGL, ABHD6 and ABHD12 as guardians of 2-arachidonoylglycerol signalling through cannabinoid receptors [published correction appears in Acta Physiol (Oxf). 2012 Mar;204(3):460]. *Acta Physiol (Oxf)*. 2012;204(2):267-276. doi:10.1111/j.1748-1716.2011.02280.x

104. Patel S, Shonesy BC, Bluett RJ, Winder DG, Colbran RJ. The Anxiolytic Actions of 2-Arachidonoylglycerol: Converging Evidence From Two Recent Genetic Endocannabinoid Deficiency Models. *Biol Psychiatry*. 2016;79(10):e78-e79. doi:10.1016/j.biopsych.2015.04.028

105. Long JZ, Li W, Booker L, et al. Selective blockade of 2-arachidonoylglycerol hydrolysis produces cannabinoid behavioral effects. *Nat Chem Biol*. 2009;5(1):37-44. doi:10.1038/nchembio.129

106. Peña CJ, Bagot RC, Labonté B, Nestler EJ. Epigenetic signaling in psychiatric disorders. *J Mol Biol*. 2014;426(20):3389-3412. doi:10.1016/j.jmb.2014.03.016

107. Ballas N, Battaglioli E, Atouf F, et al. Regulation of neuronal traits by a novel transcriptional complex. *Neuron*. 2001;31(3):353-365. doi:10.1016/s0896-6273(01)00371-3

108. Hu XL, Cheng X, Cai L, et al. Conditional deletion of NRSF in forebrain neurons accelerates epileptogenesis in the kindling model. *Cereb Cortex*. 2011;21(9):2158-2165. doi:10.1093/cercor/bhq284

109. McClelland S, Brennan GP, Dubé C, et al. The transcription factor NRSF contributes to epileptogenesis by selective repression of a subset of target genes. *Elife*. 2014;3:e01267. Published 2014 Aug 12. doi:10.7554/eLife.01267

110. Adamo A, Atashpaz S, Germain PL, et al. 7q11.23 dosage-dependent dysregulation in human pluripotent stem cells affects transcriptional programs in disease-relevant lineages. *Nat Genet*. 2015;47(2):132-141. doi:10.1038/ng.3169

111. Sun G, Alzayady K, Stewart R, et al. Histone demethylase LSD1 regulates neural stem cell proliferation. *Mol Cell Biol*. 2010;30(8):1997-2005. doi:10.1128/MCB.01116-09

112. Pilotto S, Speranzini V, Tortorici M, et al. Interplay among nucleosomal DNA, histone tails, and corepressor CoREST underlies LSD1-mediated H3 demethylation. *Proc Natl Acad Sci U S A*. 2015;112(9):2752-2757. doi:10.1073/pnas.1419468112

113. Hua Y, Sahashi K, Hung G, et al. Antisense correction of SMN2 splicing in the CNS rescues necrosis in a type III SMA mouse model. *Genes Dev*. 2010;24(15):1634-1644. doi:10.1101/gad.1941310

114. Hua Y, Sahashi K, Rigo F, et al. Peripheral SMN restoration is essential for long-term rescue of a severe spinal muscular atrophy mouse model. *Nature*. 2011;478(7367):123-126. Published 2011 Oct 5. doi:10.1038/nature10485

115. Finkel RS, Mercuri E, Darras BT, et al. Nusinersen versus Sham Control in Infantile-Onset Spinal Muscular Atrophy. *N Engl J Med.* 2017;377(18):1723-1732. doi:10.1056/NEJMoa1702752

116. Mercuri E, Darras BT, Chiriboga CA, et al. Nusinersen versus Sham Control in Later-Onset Spinal Muscular Atrophy. *N Engl J Med.* 2018;378(7):625-635. doi:10.1056/NEJMoa1710504

117. Rodrigues M, Yokota T. An Overview of Recent Advances and Clinical Applications of Exon Skipping and Splice Modulation for Muscular Dystrophy and Various Genetic Diseases. *Methods Mol Biol.* 2018;1828:31-55. doi:10.1007/978-1-4939-8651-4_2